Optimization of the Cathode Catalyst Layer Composition of a PEM Fuel Cell Using a Novel 2-Step Preparation Method

by

Roland Friedmann

Submitted to the graduate degree program in Chemical and Petroleum Engineering and the Graduate Faculty of the University of Kansas School of Engineering in partial fulfillment of the requirements for the degree of Master of Science.

The Thesis Committee for Roland Friedmann certifies that this is the approved Version of the following thesis:

Optimization of the Cathode Catalyst Layer Composition of a PEM Fuel Cell Using a Novel 2-Step Preparation Method

by

Roland Friedmann

Pre-Diploma, University of Stuttgart, Stuttgart, Germany, 2005

_____

Professor in charge

_____

_____

Committee Members

_____

Date thesis accepted

An Abstract of the Thesis

Roland Friedmann for the degree of Master of Science in Chemical Engineering presented on January 28, 2008.

Title: Optimization of the Cathode Catalyst Layer Composition of a PEM Fuel Cell Using a Novel 2-Step Preparation Method

For good performance and high durability PEM fuel cells run at high water saturation levels. However, excess liquid water generated by the oxygen reduction reaction at the cathode can block pores in the catalyst layer so that reactant gases can't access the active catalyst sites. Thus, to prevent electrode flooding, the optimal catalyst layer structure has to provide channels for gas and liquid water transport, while maintaining high ionic and electronic conductivity at the same time. In detail the catalyst layer contained Nafion® as the ionic component to extend the three-dimensional reaction zone of the electrode, and needed Teflon® to provide continuous hydrophobic pathways for reactant gas transport. A simple intermixing process of the components doesn't allow optimal placement of Nafion® and Teflon® within the catalyst layer leading to coverage of active catalyst sites by Teflon®. By means of a two-step process the formation of the catalyst ink was separated into two parts. In the first step, a mixture of Nafion® ionomer and catalyst particles was annealed to form ionomer coated catalyst particles. In the second step, these ionomer coated catalyst particles were mixed with nano-sized Teflon® particles and additional Nafion® ionomer, which was needed to crosslink the ionomer coated catalyst agglomerates. Since the catalyst particles have been covered by Nafion® ionomer before Teflon® was added, active sites were not blocked by Teflon®, which could be placed into void spaces between the catalyst clusters to form continuous hydrophobic pathways for gas transport. To determine the optimal composition for the catalyst ink in the two-step process, a matrix study with 16 different catalyst compositions was developed, and electrodes prepared from this matrix were tested in a fuel cell using the operating conditions chosen from this study. From this test two regions of catalyst composition

that resulted in electrodes with good fuel cell performance were identified. The best performing fuel cells with peak powers of >0.5 W/cm² were obtained with cathode catalyst layer with a composition of Nafion®:Teflon®:C of 1.375:0.375:1 and 0.875:0.875:1, respectively. A comparison study of a two-step and one-step prepared catalyst was also done to characterize the effect of air flow rates with the different catalyst layer structures.

This catalyst composition study for the two-step process resulted in the following understandings. First, an adequate amount of Nafion® is needed to provide ionic conduction within the catalyst layer and extend the 3-D reaction zone. Too little Nafion® resulted in poor ionic conductivity and too much Nafion® led to high liquid water entrapment, because of its high hydrophilicity, and poor oxygen diffusion. Second, an adequate amount of Teflon® was needed to provide continuous hydrophobic pathways within the catalyst layer for gas transport. The amount of Teflon® depended greatly on the Nafion® content, which determined the void volume available. While too little Teflon® didn't result in continuous hydrophobic pathways, too much Teflon® resulted in separation and isolation of reactive particles agglomerates and poor electronic conductivity. In general the two-step approach led to better performing catalyst layers which were less sensitive to liquid water flooding. This was even more evident at lower air flow rates where liquid water flooding is more severe. The better performance was attributed to the more ordered catalyst layer structure. Future work should confirm this finding in the whole composition range and have a closer look on the annealed catalyst particles and the final micro-structure of the catalyst layer.

Acknowledgements

First of all I would like to thank Dr. Trung Nguyen for being a great advisor and for introducing me to the field of fuel cells. His excellent lectures and discussions, but also his support, guidance and strong belief in me made it possible for me to finish this work. I would also like to thank Dr. Kyle Camarda, Dr. Marylee Southard, Dr. Laurence Weatherley and the whole staff of the CPE Department and the ISSS, who made it possible for me to be a KU graduate student. For helpful discussions, constant help and support whenever needed I also want to thank my colleagues Xuhai Wang and Pau Ying Chong. A big thank you goes to my thesis committee as well, consisting of Dr. Laurence Weatherley and Dr. Javier Guzman.

Many thanks go to my family in Germany for their help and support. I would like to thank my parents and grandparents for their constant support and giving me the opportunity of studying at the University of Kansas. Thanks go to my second family in Lawrence, Rene Sandigo, Nando and Celeste Yaluk. The most special thanks go to my wife Viviana Yaluk. She was always on my side and with her love and encouragement I was able to get where I am now and to live the life I have always dreamed of.

TABLE OF CONTENTS

List of Figures

List of Tables

Table Page

Nomenclature

E = Cell Potential [V]

E^{θ} = Open circuit potential [V]

F = Faraday's number [= 96485 $\frac{C}{mol\ e^{-}}$]

ΔH = Reaction Enthalpy [J/mol]

η_{Carnot} = Carnot efficiency

η_{th} = Thermal efficiency

NFP® = Nafion weight percentage parameter

P_{in} = Inlet pressure of gases [psi]

Pt/C = Platinum supported by carbon catalyst, i.e. Vulcan XC-72

Q_{in} = Heat entering the system [J/mol]

RHC = Relative humidity cathode

RHA = Relative humidity anode

T_{cell} = Cell Temperature [°C]

$T_{humidification}$ = Humidification temperature or gases [°C]

W_{cell} = Work in a cell [J/mol]

z_e = Number of transferred electrons

Optimization of the Cathode Catalyst Layer Composition of a PEM Fuel Cell Using a Novel 2-Step Preparation Method

Chapter 1

Introduction

1.1 History of Fuel Cells

In the 21st century environmental issues became of prime importance in the world's politics and industry and can't be glossed over any longer. The key factor leading to a more polluted environment is clearly the population growth. Being at 2.5 billion people in 1950 it took less than 50 years to double the amount of people on earth. Currently the total size of the world population is 6.7 billion and will increase to 9.2 billion people by 2050 [1]. The huge growth in population has resulted in an increasing demand on resources and energy, and simultaneously to more and more waste causing gigantic costs to both the people and the environment. Among those waste materials a major group is represented by gaseous species, especially the so-called greenhouse gases, which lead to global warming. In detail, carbon dioxide contributes about 50% to global warming, and its emission has become an extremely significant issue [2]. Thus we all have to make an effort to reduce both the amount of carbon dioxide which is present now and which will be emitted in the future. The lowering of CO_2 and its methods go hand in hand with a change in the energy and its resources respectively. Eighty-four percent of emitted carbon dioxide is produced by industry, transportation and electricity generation, with the latter being the highest contributing sector [3]. A step towards a solution of this problem is the use of fuel cells. A fuel cell is a so-called zero-emission engine, using hydrogen as fuel and having water as its only product. The first fuel cell was invented by William R. Groove in 1839 and was called a "gaseous voltaic battery". Platinum, known to be a good catalyst for hydrogen/oxygen reactions, was used as electrode material and sulfuric acid served as an electrolyte [4]. Further development of different electrodes

and electrolytes in the 19th and 20th century has been made to give better performance and more energy. Fuel cells are now classified by their electrolyte. The debut practical application of a fuel cell was the Gemini space mission in 1962, using an ion-exchange membrane fuel cell, i.e. a solid polymer fuel cell, developed at General Electric in 1960, to power the two-man Gemini vehicle. In 1965 for the Apollo space mission, an alkaline fuel cell was used to provide the crew with electricity and water during the two-week mission to the moon. After this extraordinary mission, fuel cells started to flourish and experienced a big focus by the market. In today's research on alternative energies, fuel cells are one of the big players for a variety of applications with stationary power generation; portable applications, like notebooks, cell phones, PDAs; and the automotive sector as the most important ones [5].

1.2 General principle of Fuel Cells

Fuel cells are electrochemical devices converting chemical energy of a fuel directly into electrical energy. More precisely they are galvanic cells, consisting of an anode, a cathode and an electrolyte. Unlike batteries, fuel cells are open energy conversion systems where the reactants that are consumed are fed into the systems from an external storage. In theory a fuel cell can run continuously as long as it is supplied with the necessary fuels. The fuel and oxidant reactions in a fuel cell vary with the type of electrolyte used [6]. Some examples of different fuel/oxidant combinations are given in Table 1.2-1.

Fuel Cell	Anode Reaction	Cathode Reaction
Alkaline Fuel Cell	$H_2 + 2\ OH^- \rightarrow 2\ H_2O + 2\ e^-$	$1/2\ O_2 + H_2O + 2\ e^- \rightarrow 2\ OH^-$
Polymer Electrolyte Fuel Cell	$H_2 \rightarrow 2\ H^+ + 2\ e^-$	$1/2\ O_2 + 2\ H^+ + 2\ e^- \rightarrow H_2O$
Phosphoric Acid Fuel Cell	$H_2 \rightarrow 2\ H^+ + 2\ e^-$	$1/2\ O_2 + 2\ H^+ + 2\ e^- \rightarrow H_2O$
Molten Carbonate Fuel Cell	$H_2 + CO_3^{2-} \rightarrow H_2O + CO_2 + 2\ e^-$	$1/2\ O_2 + CO_2 + 2\ e^- \rightarrow CO_3^{2-}$
Solide Oxide Fuel Cell	$H_2 + O^{2-} \rightarrow H_2O + 2\ e^-$	$1/2\ O_2 + 2\ e^- \rightarrow O^{2-}$

Table 1.2-1. Typical Electrochemical Reactions in Fuel Cells

For the remainder of this chapter, the focus will be on the hydrogen/oxygen based Polymer Electrolyte Membrane Fuel Cell commonly known as Proton Exchange Membrane Fuel Cell (PEMFC).

1.3 Operating principles

The basic fuel cell reactions in a PEMFC at 25°C are

Anode	$2\ H_{2\,(g)} \rightarrow 4\ H^+ + 4\ e^-$	$E^\theta = 0V$	(1.3-1)
Cathode	$O_{2\,(g)} + 4\ H^+ + 4\ e^- \rightarrow 2\ H_2O_{(l)}$	$E^\theta = 1.229V$	(1.3-2)
Overall	$2\ H_{2\,(g)} + O_{2\,(g)} \rightarrow 2\ H_2O_{(l)}$	$\Delta E^\theta = 1.229\ V$	(1.3-3)

At about 80 °C, the typical operating temperature of a PEMFC, oxidation of hydrogen (fuel) on the anode side and reduction of oxygen (oxidant) on the cathode side yield to liquid water, the main by-product of the reactions. The water is generally ejected into the oxygen stream and carried out of the fuel cell. To assure for good proton transport the membrane needs to be well-hydrated. Thus, hydrogen and/or oxygen are humidified before they enter the cell. A detailed schematic of the processes occurring in a PEMFC is shown in Figure 1.3-1.

The reactant gases diffuse through a porous gas diffusion layer (GDL), made of carbon fibers, to reach the catalyst layer (CL), which is in contact with the membrane. An assembly consisting of a cathode GDL, a cathode CL, membrane, an anode CL and an anode GDL is called a membrane and electrode assembly (MEA). A fuel cell consisting of the MEA sandwiched by the gaskets and gas distributors is presented in Figure 1.3-3.

On the anode side of the fuel cell the protons generated by the hydrogen oxidation reaction react with water to form hydrated hydronium ions as shown below.

$$H^+ + H_2O \leftrightarrow H_3O^+ \text{ (aq.)} \qquad (1.3\text{-}4)$$

These hydrated hydronium ions pass through the ionically conducting, but electronically insulating, membrane while the generated electrons pass through an external circuit to reach the cathode. There the electrons complete the oxygen reduction reaction (ORR). Hence the membrane actually acts as a separator of electrons, fuel and oxidant, and at the same time as an ionic conduction path between anode and cathode. The most suitable membrane material for PEM fuel cells, which has been developed so far, is Nafion®.

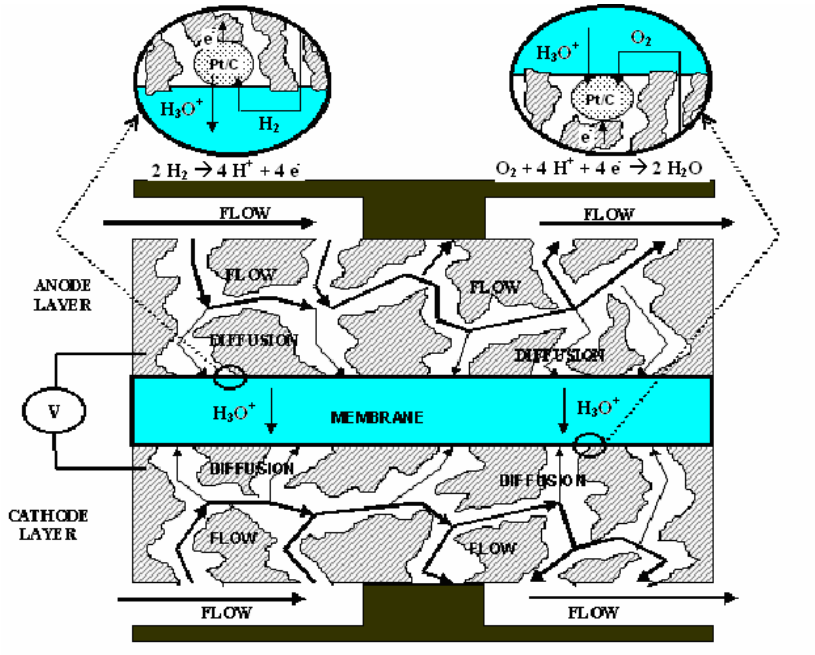

Figure 1.3-1. Schematic of reactions in a PEMFC [7]

Even at 80 °C both the hydrogen oxidation reaction (HOR) and the ORR can't occur at a useful rate. Thus a catalyst is needed. The best-working catalyst to-date is

platinum. To have high active surface area, platinum supported on high surface area carbon is used. To achieve high catalyst utilization an ionic polymer phase is added to the catalyst to extend the 3-D reaction zone in the catalyst layer. The catalyst layers are either coated directly on both sides of the membrane or on the GDLs that are then attached to the membrane. The maximum (theoretical) efficiency of a PEMFC is calculated in Chapter 1.4.

To prevent gas leakage and income of unwanted species, the electrodes are sealed with an electronically insulating Teflon® gasket. The incoming reactant gases are then directed by gas-distributors with special flow fields designed to provide a good distribution of reactant gases over the whole electrode area. In this work a so-called interdigitated flow field was used [8] on both the anode and the cathode side. The design of this flow field is shown in Figure 1.3-2. The dead ends force the gas to penetrate deeper into the GDL and thus the diffusion path of reactant gases is shortened. Figure 1.3-1 visualizes the effect of such a flow field. With conventional flow fields, e.g. serpentine shaped, gases flowing over the GDL would have to reach the CL and the active catalyst sites mainly by diffusion.

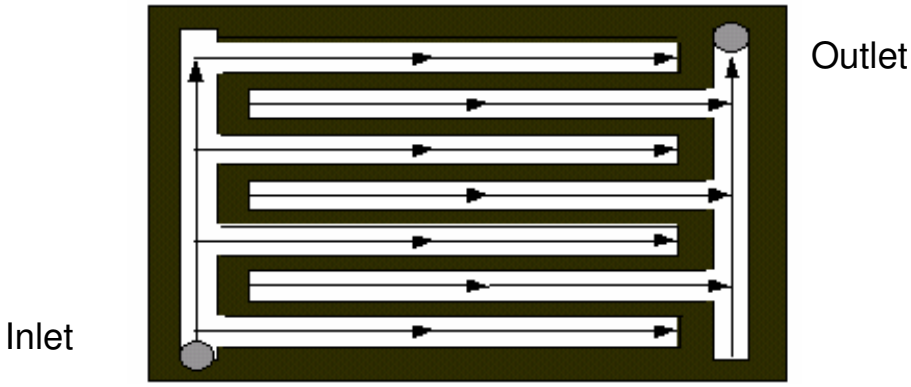

Figure 1.3-2. Design of an interdigitated flow field [7]

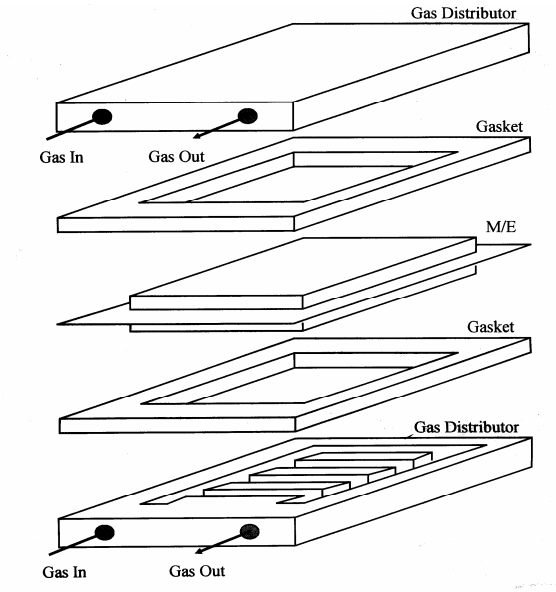

Figure 1.3-3. Schematic of a PEMFC assembly [7]

1.4 Thermal Efficiency of a Fuel Cell

Contrary to a heat engine (e.g. combustion engine), which converts chemical energy indirectly to electrical energy by first converting it to heat, then to mechanical energy and finally to electrical energy, fuel cells do this conversion directly in a single step. Fuel cells don't share any characteristics with a heat engine, whose maximum efficiency can be calculated by a reversible Carnot Cycle.

$$\eta_{Carnot} = \frac{T_{hot} - T_{cold}}{T_{cold}} < 1 \qquad (1.4\text{-}1)$$

Energy conversion of real processes will be even lower than the Carnot efficiency. These restraints don't apply to fuel cells, since the process is isothermal and the chemical energy is not used to heat up any products, but is converted directly to electrical energy.

Hence the maximum work $W_{\max,cell}$ obtained by an electrochemical cell corresponds to Gibbs free energy of the reaction.

$$W_{\max,cell} = -\Delta G \tag{1.4-2}$$

The actual work in a cell W_{cell} is done by electron movement through an electrical potential difference. In equation (1.4-3) z_e stands for the number of electrons transferred by one mole of gas, F for Faraday's number ($F = 96485 \frac{C}{mol\ e^-}$) and ΔE for the electrochemical potential difference of the fuel cell reactions.

$$W_{cell} = z_e F \Delta E \tag{1.4-3}$$

The general expression for the thermal efficiency is defined as

$$\eta_{th} = \frac{W_{cell}}{Q_{in}} \tag{1.4-4}$$

In case of a fuel cell, the net work is the actual work in a cell W_{cell}, and Q_{in} is replaced by the reaction enthalpy (ΔH). Hence equation (1.4-4) becomes

$$\eta_{th,fuel\ cell} = \frac{W_{cell}}{\Delta H} = \frac{z_e F \Delta E}{\Delta H} \tag{1.4-5}$$

The maximum theoretical efficiency of a fuel cell is obviously at open circuit conditions with $\Delta E = \Delta E^0 = 1.23V$ with a value of $\eta_{th,\max} = 0.83$ for a hydrogen-oxygen fuel cell at 1 atm and 25°C. For an equivalent Carnot efficiency the heat engine would have to run at a temperature of $T_{hot} = 1480°C$ with $T_{cold} = 25°C$ [9]. Carnot efficiencies of practical applications lie within a range of $\eta_{Carnot} = 0.25$ - 0.4, while fuel cell efficiencies are $\eta_{fuel\ cell} = 0.5 - 0.9$ [10].

1.5 Details of components and their role in a PEMFC

1.5.1 Electrode

The electrode of a PEMFC is the region where the actual electrochemical reactions take place. To give high performance the active surface area has to be maximized both per mass of the catalyst and per area of the electrode. Further the restraints on the transport rates of the reactant gases to the catalyst, which is distributed on the electrode material, have to be as low as possible. Obviously the overall performance of a good electrode has to be constant with respect to time and the cell's operation conditions, i.e. the materials have to be extremely stable and reliable.

The key factor of achieving these goals is a perfect catalyst distribution over the electrode. The catalyst particles have to assure for ionic conduction for hydronium ions, hydrophobic pathways for gas transport, hydrophilic pathways for the removal of liquid water, and most importantly for good contact to the external electrical circuit, where electrons are transported from the anode to the cathode in order to complete the cell reaction. To be able to match these requirements one has to select specific materials for the different parts of a MEA.

1.5.2 Membrane

The membrane in a PEMFC consists of a solid polymer electrolyte and is placed between the two electrodes of the fuel cell. To achieve high performance both electrodes have to be provided with their reactants in high concentrations, and protected from unwanted species and pollutants. The hindrance of pollutants and the transport of hydrated hydronium ions from anode to cathode while keeping both electrodes electronically insulated are the main tasks of the membrane. Thus the membrane has to have high ionic, low electronic conductivity and low permeability

of reactant gases. To enable fast transport of hydronium ions from anode to cathode the membrane has to be well hydrated. Finally, the membrane has to show high mechanical, thermal and chemical stability to enable a long-lasting, durable fuel cell.

In the early history of fuel cells hydrocarbon-type polymers, like polystyrene divinylbenzene sulfonic acids or sulfonated phenolformaldehyde, were used as membrane materials. Due to the lack of stability caused by C-H bond cleavage, further research has been done, and in the 1960s Du Pont developed Nafion® as a new membrane material. Nafion® contains a polymerized tetrafluorethylene (PTFE or Teflon®) backbone with sulfonic acid groups as side-chains. The sulfonic acid groups are attached to the polymer, but once being hydrated their protons are free to move throughout the electrolyte. A detailed picture of Nafion® is shown in Figure 1.5.2-1.

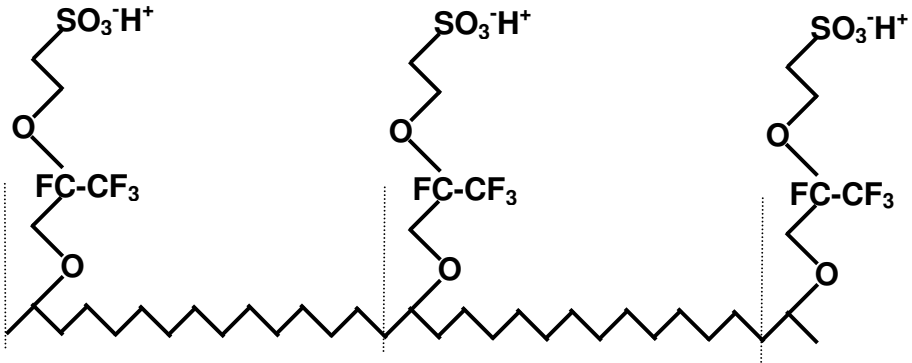

Nafion® 1100

$$-(CF_2CF_2)_6-(CFCF_2)-$$
$$|$$
$$O-CF_2CF(CF_3)-O-CF_2CF_2SO_3H$$

Figure 1.5.2-1. Structure and formula of Nafion® [11]

Depending on the thickness of the Nafion® membrane, the performance of the fuel cell may vary a lot. According to Kordesch et al. thinner membranes at open circuit conditions showed a lower voltage than thicker ones, due to higher crossover rate of hydrogen resulting in decreasing fuel utilization. On the other hand Kocha

reported significant performance improvements of thinner membranes at high current densities caused by lower iR losses and better hydration of the membrane. With thicker membranes one would expect to observe less reactant crossover due to lower permeability and increased durability leading to better performance at low current densities. However, thicker membranes have a higher resistance to protons resulting in lower power densities [12, 13]. There is still a lot of research going on in the membrane design to balance the advantages associated with thick and thin membranes to achieve optimal properties at the desired operating ranges. In this study a solution cast Nafion® NRE 212 membrane by Ion Power was used.

1.5.3 Catalyst

In a PEMFC the ongoing reactions are taking place in presence of a heterogeneous catalyst, which has to show certain requirements for giving high performance:

- electrical conductivity
- good interplay with the ionomer
- accessible for reactant gases
- stable while in contact with reactant gases, products and membrane electrolyte
- reactions on both the anode and the cathode side have to occur as close as possible to the thermodynamic potential

As mentioned before, the most commonly used catalyst for the reactions in a PEMFC is platinum. It shows all the required characteristics above and is highly active and stable.

Since the reaction takes place at the surface of the catalyst its active surface area has to be as high as possible. One way of increasing the active surface area of the platinum catalyst is reducing the particle size. In addition the particles have to be

dispersed on an inert material, matching the same requirements as platinum itself. Carbon black is the most commonly used support. It shows good electrical and thermal conductivity, low thermal expansion and a large porosity to ensure for reactant gas and liquid water transport [12, 14]. Hence the ratio of Pt/C will play a significant role in the catalyst utilization. For the experiments in this study a catalyst by Tanaka with Pt/C of 46.2 wt-% and 48.9 wt-% of Pt was used.

1.5.4 Gas Diffusion Layer

A GDL functions as a distributor of reactant gases to the catalyst layers and as a liquid water evacuator on the cathode side of a PEM fuel cell. Further the GDL has to collect the produced current, be thermally conductive and provide mechanical support to the CL. Typical GDLs are made of thin porous layers of carbon fibers [12]. A problem that a GDL might face is that it may accumulate water in it and thus hinder the gas flow. Thus almost all GDLs are wet-proofed, i.e. PTFE has been added to the GDL [15, 11, 16, 17]. PTFE creates hydrophobic channels in the GDL where water can not penetrate through. Those pores are then available for reactant gas transport. A further improvement of the standard GDL is a so-called micro-porous layer (MPL), which is further discussed later. A MPL is made of carbon and PTFE applied on the top of the GDL. In this study the 35 BC material (with MPL) by SGL Carbon was used as the gas diffusion material.

1.6 Polarization curve

In order to characterize the performance of a fuel cell and visualize voltage losses a so-called polarization curve is plotted. This 2-dimensional plot shows the cell voltage over the current density of the cell. The current density is simply the actual current divided by the electrode area.

A typical polarization curve is presented in Figure 1.6-1 and typical voltage loss sources are discussed in the following.

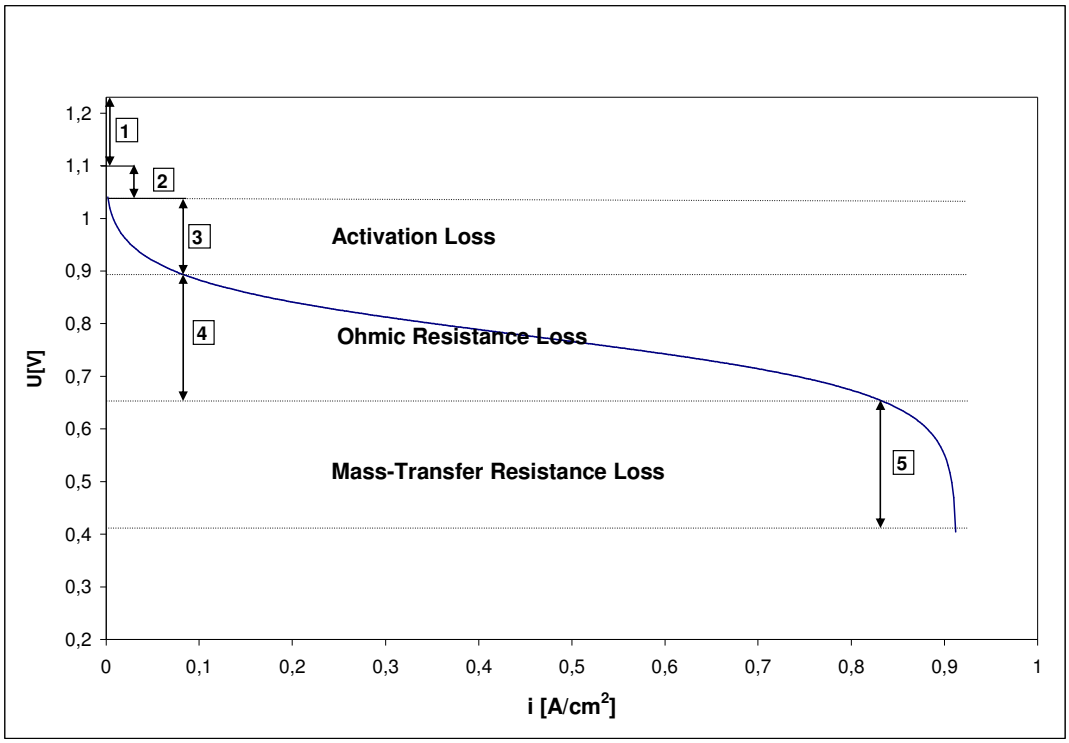

Figure 1.6-1. Polarization curve of a PEMFC

1) Non-standard operating conditions: The thermodynamic open circuit voltage (OCV) of E = 1.229V is practically unachievable. At atmospheric pressure and an operating temperature of T_{cell} = 60°C the theoretical value of the OCV is E = 1.1V.
2) Hydrogen crossover: The drop below E = 1.1V is due to fuel crossover through the membrane. Since hydrogen molecules are extremely small (less than 3Å) they diffuse through the membrane to the cathode side of the cell. Hydrogen at the cathode side will cause a mixed potential due to competition of ORR and hydrogen oxidation resulting in a lower OCV.
3) At low current densities most of the voltage loss is attributed to the activation or kinetic resistance of the electrode reactions. Most of this loss is attributed to the slow kinetics of the ORR on the cathode side, which are about 5 orders of

magnitude slower than the hydrogen oxidation rate on the anode side [16].

4) Ohmic resistance loss: In this region the voltage loss is due to electric resistance to the e^- - flow through CLs, MPLs, GDLs, gas distributors, current collectors, and apart from that the membrane resistance to ionic transport of protons. By Ohm's Law the voltage is proportional to the actual current density with the combined resistance of all materials mentioned as the proportional coefficient.
5) Mass transfer resistance loss: At high current densities the diffusion rate of the reactants can't keep up with the rate of reaction. Again the limiting side is the cathode, since the diffusivity of oxygen through the GDL and the MPL is about 5 times less than the diffusivity of hydrogen and so the concentration of oxygen on the cathode is also lower. This loss is also often described as concentration loss.

1.7 The catalyst layer of a PEM Fuel Cell

1.7.1 Literature review

Even though a lot of research in the field of PEMFCs has been carried out in the last few decades, there are still some major issues to be solved. Low catalyst utilization and thus low energy efficiency keep the costs of PEMFCs still too high to be ready for an average consumer. Advances in both materials and structure of the CL have helped to partly overcome that problem. Nafion® has been incorporated into the CL trying to connect the ionomer network of the membrane with the CL [18, 19]. By means of impregnation of the electrode with Nafion® Srinivasan et al. observed an extension of the three-dimensional reaction zone and a significant improvement of the cell performance [18]. Wilson and Gottesfeld found out that impregnation doesn't provide sufficient ionomer contact within the CL and thus it was suggested to use a direct intermixing method, where Nafion® solution was added directly into the

catalyst ink [20]. The same group found the best results with the CL as dense and thin as possible, because at high current densities the active region of the CL narrowed. Pt loading of the electrode could be lowered to 0.15 mg Pt/cm².

The results of Wilson and Gottesfeld [19] were later reproduced by Passalacqua et al. in their experiments [23]. It was verified that direct intermixing of Nafion® to the catalyst ink instead of impregnating yielded to a higher Pt activity [23]. Another study on Nafion® impregnation was done by Lee et al. who suggested an optimal ratio of C:Nafion® = 1:1.19 for O_2 and C:Nafion® = 1:0.375 for air. They noticed for increasing Nafion® content at low current densities decreasing charge transfer resistance and increasing electrochemical active surface area. In the ohmic region effects on ionic and diffusional resistance due to increasing film thickness around the agglomerates were found. Mass transfer losses showed the highest significance. The overall diffusional resistance increased due to a thicker Nafion® film combined with higher penetration depth. In general, pore volume distributions narrowed with increasing Nafion® caused by shrinking pore sizes [24].

Antolini et al. came up with a Nafion® weight percentage parameter (NFP), which is the ratio of the mass of Nafion® (dry) to the total weight of Nafion® (dry), Pt and C [26]. Optimized ratios were found to be at NFP = 0.33 to 0.4 [22, 26, 27, 28] for Nafion® intermixed and NFP = 0.27 [21] for Nafion® impregnation. Whether air or oxygen was used didn't affect the results significantly. Higher Nafion® contents resulted in decreasing performance throughout all groups due to mass transport limitations, even though Gode et al. measured high Pt utilization and good electronic conductivity up to NFP = 0.7 [29]. Shin et al. continued research of an approach called the "colloid method" of using normal butyl acetate (NBA) instead of iso-propyl alcohol (IPA) as a solvent [30]. In this method the ink was dripped into the solvent, while the conventional so-called "solution method" suspended the ink fully in the IPA [31]. With the colloid method the formed agglomerates were a lot bigger, the catalyst layers thicker and in general the solution was more dispersed and dense (verified by TEM). Further the colloids didn't penetrate into the primary pores (<0.07 μm) but

only in the larger pores (0.07 μm - 1 μm). Therefore the porosity of the agglomerates was bigger which resulted in a better mass transport and higher Pt utilization, while keeping the ionomer network on the outside of the agglomerate conductive [31]. Later on research began focusing on computer models which should predict the catalyst layer behavior and performance, and give ideas for a better catalyst layer structure. An electrode with a 3-phase structure was suggested by Wang et al. [32]. By computer model [33] and experiment [34] it was shown that a gradually distributed Nafion® content lead to less pore blockage, better water removal, ionomer contact and thus proton transport. An optimum NFP of 0.35 was distributed linearly from 0.3 (close to GDL for less blockage and better water removal) to 0.4 (close to membrane for better contact and proton transport) [33, 34]. Song et al. used a double variable model with Pt and Nafion® as parameters. They showed that it was sufficient to consider only Nafion® as a single variable. Their optimal NFP gradient was also linear but from 0.21 to 0.46 [35]. Another mathematical model by Song et al. [36] obtained an ideal NFP of 0.32 and verified Qi and Kaufman's data [28]. Recently Cheng et al. developed a three-dimensional model for numerical simulations of Nafion® loadings which was in good accordance with their experimental data [37]. Since water management problems in a fuel cell became a more severe topic, Eikerling developed a model to find an optimal wetting state of the fuel cell [38]. A local equilibrium between the gas and liquid phase in the primary pore (3-10 nm) and the secondary pores (20-40 nm) open for gas transport of reactants and products showed the best performance [38].

The idea of adding Teflon® as a hydrophobic component for gas transport was rejected, because it may block active catalyst sites [19]. Further it was proposed to catalyze the membrane instead of the GDL for good ionomer conductivity and better water transport at the membrane-CL interface [20]. In the same year Poltarzewksi et al. took a closer look at how Nafion® fills up the pores of a catalyst ink containing 40 wt-% PTFE [21]. By SEM studies it was shown that Nafion® fills up the micro pores and macro pores first, before it starts covering the surface of the catalytic layer

forming a film. Adding more Nafion® resulted in a constant pore volume, but larger film thickness and thus higher ionic resistance. Small variations in film thickness caused large variations in the ionic conductivity [21]. Uchida et al. showed that increasing ionomer solution would affect the whole current density range, while increasing Teflon® content played only a role at high current densities [22]. Unlike other groups, Flemion instead of Nafion® was used as a perfluorosulfonate ionomer (PFSI). PFSI was adsorbed on both PTFE and Pt/C particles and increased the continuity of the ionomer network significantly. Teflon® was recognized as duct for gases and drain water, but a too high amount resulted in thicker CL and thus lower Pt utilization or even complete dryout [22].

Cheng et al. showed that a catalyst layer containing Teflon and impregnated Nafion® yielded to 77.8% of Pt utilization comparing to 45.4% of a catalyst prepared with the intermixing thin film method [25]. Nafion® didn't block e^--conduction and Teflon® caused only little blockage of the active surface area, although being too close to the catalyst decreased the Nafion® humidity and the proton conductivity. Hence there was a need for a more optimized catalyst layer structure [25]. Nguyen et al. developed a new 2-step preparation method for the catalyst ink where it was possible for the first time to control the Teflon distribution in the CL [39]. This method serves as a basis for this work.

Besides research within the CL for better water management there have also been investigations on active water management with an external electro osmotic pump [40] or by means of an MPL, which enhanced water back diffusion from the cathode through the membrane to anode as well as water removal from the CL and thus the fuel cell performance [41]. That the MPL managed to push liquid water back from the cathode to the anode also indicated that the cathode side of the fuel cell is likely to be saturated with liquid water. Another effect of the MPL due to its structural characteristics was increased oxygen transport rates and less ohmic resistance [41].

1.7.2 Problems in the catalyst layer of a fuel cell and research objective

Low catalyst utilization resulting in low fuel cell efficiency and high costs is still one of the main obstacles impeding the deployment of PEMFCs. However, additionally to achieving higher catalyst utilization, proper liquid water production and removal within a fuel cell is another key factor to increase fuel cell efficiencies. On one hand low water saturation levels may dehydrate the membrane and shorten the lifetime of the fuel cell tremendously, and on the other hand excess liquid water may lead to cell starvation due to reduced gas accessibility to the CL caused by flooding of open pores. Flooding occurs at the cathode side of a PEM fuel cell when the removal rate of water is lower than the combined rate of water transport by electro-osmotic drag from anode to cathode and of liquid water generation by the oxygen reduction reaction. Air-filled pores in the GDL and the CL are then occupied by liquid water and oxygen can not reach the active catalyst sites fast enough. These active catalyst sites are covered by water themselves and oxygen has to diffuse through a second water film to reach the reaction zone. Both effects combined, pore blocking and a water film on the active catalyst sites, will lead to insufficient oxygen concentration and thus low fuel cell performance [42]. A schematic of the water transport process within a fuel cell is shown in Figure 1.7.2-1.

Hence to achieve both high catalyst utilization and good water management, the CL has to have excellent conductivity (both electronic and ionic), and pathways for gas and water transport where liquid water doesn’t block active catalyst sites.

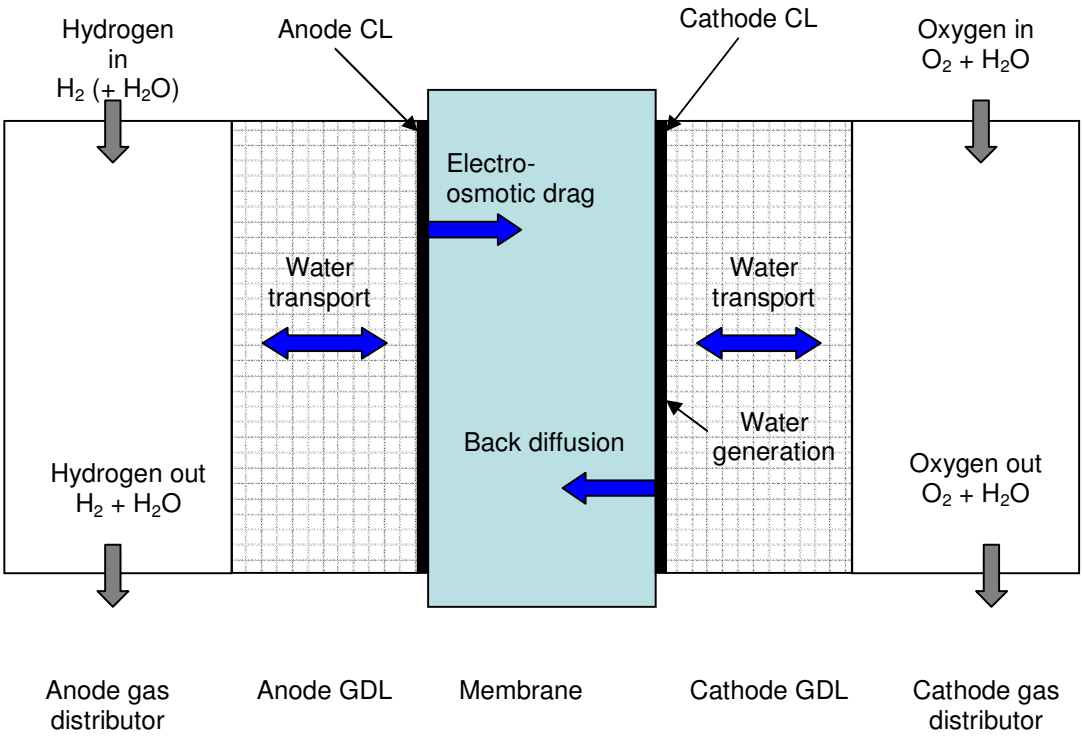

Figure 1.7.2-1. Water transport in a PEM fuel cell

In this thesis a 2-step preparation method of the CL for achieving a controllable structure of the CL including Nafion® for high ionic conductivity and Teflon® for hydrophobic paths while keeping catalytic activity as high as possible is presented [39]. This method serves as a basis for optimizing the cathode catalyst layer composition by a matrix-study.

1.8 Approach

As mentioned earlier flooding usually takes place at the cathode side of a PEM fuel cell, because liquid water is generated by the ORR. Hence this study focuses on the cathode catalyst layer. The anode was a fixed electrode manufactured by TVN Systems, consisting of catalyst layer applied directly onto a SGL 35 BC GDL by the SGL Carbon Group.

A simple schematic of a region inside of the cathode catalyst consisting only of Nafion® and catalyst material and no Teflon® is shown in Figure 1.8-1.

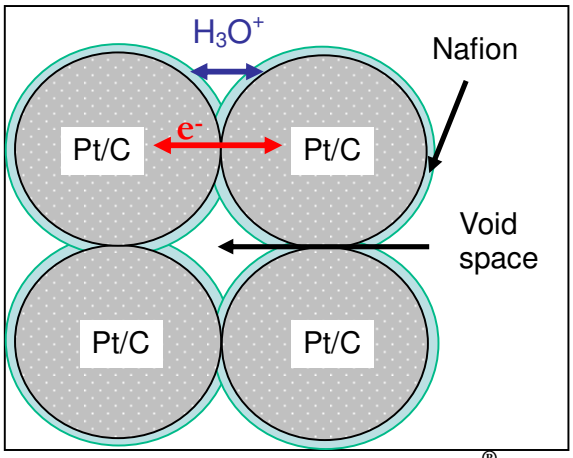

Figure 1.8-1. CL with no Teflon®

A continuous network of both ionic and electronic paths assures good conductivity for protons and electrons. Active catalyst sites can be reached by oxygen by means of diffusion through the catalyst layer network pores and through the ionomer. However, generated liquid water will first occupy the void space created by this structure, so that oxygen can not be transported there anymore. It would have to diffuse through water as an additional barrier and at high current densities the oxygen diffusion rate could not keep up with the reaction rate and the resulting water accumulation. The fuel cell will eventually starve. An improvement of this conventional CL layer is to add nano-particles of Teflon® to the catalyst ink. Teflon® creates hydrophobic regions which would not be occupied by generated liquid water and are thus available for gas transport. Next to the Teflon® particles close to the hydrophilic ionomer liquid water can be drained. The biggest problem of this approach is illustrated in Figure 1.8-2.

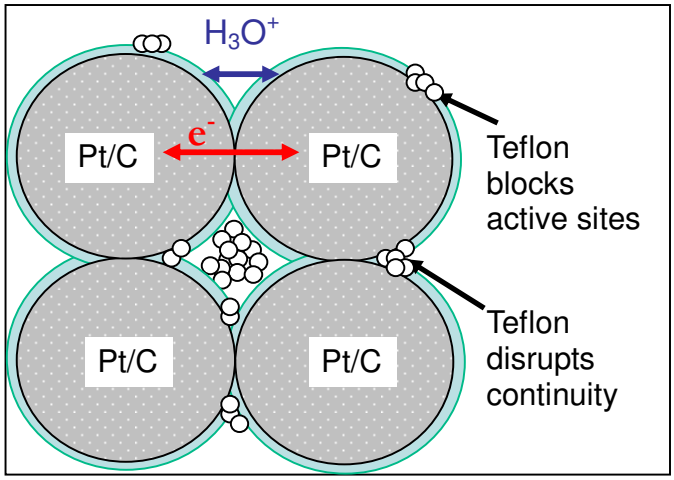

Figure 1.8-2. Problems of the conventional catalyst ink preparation method when adding Teflon®

Teflon which is added to the catalyst ink is competing with Nafion® for structuring the CL. By simple mixing of Nafion® and Teflon® to the catalyst ink one is unable to control where Nafion® and Teflon® are placing itself in the CL, and the CL structure will form randomly. The first problem is that Teflon® might block active catalyst sites and the ionomer won't be able to reach them. In that case the active catalyst area is unused and wasted. The second problem that may occur combined with catalyst blocking is that Teflon® might place itself between catalyst agglomerates that are already covered by Nafion® and then disrupt the ionomer network. The benefit of adding Nafion® to extend the three-dimensional reaction zone by building up a continuous ionomer network would be lost. However, as mentioned earlier Teflon® as a hydrophobic component providing pathways for gas transport is very important and has to be incorporated into the CL somehow.

A desirable structure of a CL containing both Nafion® and Teflon® is presented in Figure 1.8-3. In this structure it is assured that only Nafion® coats the catalytic particles. The nano-sized Teflon® particles do not disrupt the ionomer network or block any active catalyst sites, but rather place itself into the empty void space to create a hydrophobic channel for gas transport. Next to the particle cluster of Teflon® water can be transported because of the hydrophilic properties of the ionomer

film. Such a CL structure would address both the problem of low catalyst utilization and water transport [42].

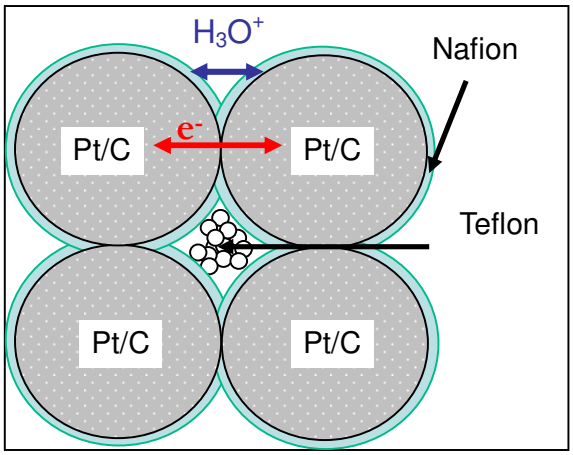

Figure 1.8-3. Optimal CL structure achieved by a 2-step preparation method

To achieve such a structure our group proposed a 2-step preparation method for the catalyst ink [39]. In the first step a catalyst ink consisting of Pt/C powder and Nafion® is prepared and by heat treatment above the glass transition temperature of Nafion® (≈110°C) the ionomer phase is polymerized onto the catalyst particles [42]. Hence it is assured that the catalyst particles are covered by ionomer and there are no free active sites left that can be covered by Teflon® later. In the second step one has to add additional ionomer solution to crosslink the Nafion®-covered agglomerates in order to create a continuous ionomer network. Further the nano-particles of Teflon® are added in the second step. Since part of the ionomer has already been polymerized onto the catalyst particles Teflon® can not block any active catalyst sites anymore, but places itself into the voids [39, 42].

Besides creating this novel structure, composition of the catalyst ink is very important. Both Nafion® and Teflon® are electronically insulating and a too large amount of solid, either Nafion® or Teflon® or both combined, would decrease the fuel cell performance, because the electronic network would be disrupted by one or the other. Too little Nafion® would not cover the whole catalyst surface and not be able to

crosslink the covered catalyst particles and build up a continuous ionomer network. Too much ionomer would increase the film thickness around the catalyst particles and thus increase the diffusion barrier for oxygen or even disrupt the electronically conductive network. Teflon®, when being too little, might not provide enough continuous hydrophobic regions for good gas transport. Too much Teflon® might disrupt the ionomer and eventually even the electronic network [42].

Hence the main goal of this study was to find an optimal cathode catalyst ink composition by using a 2-step preparation method leading to a novel CL structure.

Chapter 2

Experiment

2.1 Catalyst ink preparation

For the catalyst ink preparation platinum on carbon support catalyst from Tanaka Pt/C with 46.2 wt-% and 48.9 wt-% of Pt was used as catalyst material. Further Liqion-1000 Nafion® 15 wt-% 950 EW Solution by Ion Power Inc., and a Teflon® dispersion of 60 wt-% by DuPont diluted with distilled water to 10 wt-% were used for the catalyst ink preparation. The annealing of the catalyst under a steam-containing environment was performed with a Valueklave™ 1730 by Tuttnauer. As a scale a SA120 (accuracy 0.0001g) by Scientech was used.

The steps to prepare a catalyst ink with the 2-step process are as follows:

1) Add Pt/C in a dry glass vial
2) Add water
3) Add first half of Nafion®
4) Add 2 magnetic stirrers
5) Seal container with wax paper and aluminum foil
6) Place sealed catalyst ink in a water bath at room temperature and stir for 24 hours
7) Open glass vial, place it in the autoclave and sterilize from a cold start for 20 minutes at T = 134°C. Dry annealed catalyst for 20 minutes at T = 75°C and let it cool down to room temperature in the autoclave
8) Place annealed catalyst in a mortar and grind to powder
9) Add grinded catalyst in a dry glass vial
10) Determine weight loss during grinding to adjust ingredient masses
11) Add water

12) Add second half of Nafion®
13) Add Teflon®
14) Place the vial in an inert gas environment
15) Add IPA/water mixture (80 wt-% IPA)
16) Repeat 4) - 6)

For the conventional single-step process one goes from 3) directly to 12) neglecting 14) having added the desired amount of Teflon®.

In order to achieve best coating results later on, the ratio $R1 = \frac{IPA/water}{catalyst\ powder} \approx \frac{5-10}{1}$ was determined experimentally. The viscosity of the ink should be similar to oil. The vial was stored in a cool and dry location to avoid evaporation. If the catalyst gets too dry one has to add IPA/water mixture and stir for approximately 1 hour.

It was experimentally verified that 7) leads to complete polymerization of the Nafion® by means of pH measurements. It was also observed that the annealed catalyst showed a very strong hydrophobic character, i.e. after adding water in step 11) the annealed catalyst and water formed 2 phases with the catalyst powder floating on the water surface. It was not possible anymore to wet the catalyst with water to prevent it from burning when adding IPA/water in 15). However, adding additional IPA becomes unavoidable after the annealing, because it is needed to form a consistent solution of annealed catalyst and liquid. Since the Nafion® solution added in 12) contains a liquid mixture of 80 wt-% water and 20 wt-% IPA and didn't show any macroscopic catalyst burning after adding, it was concluded that at this ratio it was safe to add IPA/water to the catalyst. However, in order to prepare the catalyst ink and achieving a good viscosity for brush-coating the best water to IPA content in the final catalyst ink solution was found to be $R2 = \frac{water}{IPA} \approx \frac{1.3}{1}$. An IPA/water mixture with only 20 wt-% IPA would not yield to both ratios R1 and R2. Therefore

an IPA/water mixture with 80 wt-% IPA was prepared to be added in 15). Since severe catalyst burning was observed by adding the latter mixture, the last step was performed under an inert-gas environment (see 14)). In this study Argon was used to prevent air contact with the annealed catalyst. A complete calculation of one catalyst ink sample is shown in Appendix [A].

It is important to mention that the samples prepared for this work were very small so that a precise composition was not achieved. However, the discussion of the CL will always base on the composition which was tried to be achieved. The exact composition of each CL can be found in Appendix [C].

2.2 Coating of the catalyst layer

For the coating of the catalyst layer a 35 BC GDL by SGL Carbon was used. Per catalyst ink 2 GDLs were coated. The steps of the coating procedure are as follows:

1) Cut GDL to (2.7 x 5.2) cm^2
2) Heat it heated up on a clean glass plate to 40°C for 5 minutes
3) Determine the dry-weight
4) Place GDL onto the warm glass plate with the MPL facing upwards and attach the tips of the 4 corners by Scotch tape
5) Dust the MPL off with a dry brush
6) Place open vial with the catalyst ink into a beaker of cold water to prevent evaporation of the solvent
7) Dip a brush with (width ≈ 1.5cm) into the ink and wipe excess ink off on the side of vial
8) Sweep the brush slowly from the left to the right starting at the top of the GDL with a light pressure. One has to make sure that there are no lumps of catalyst ink on the CL surface, because they could puncture the membrane during

hotpressing or assembling.

9) Let coating dry
10) Rotate glass plate 90° and repeat 7) – 9) until the glass plate was completely rotated, i.e. 4 coatings
11) Determine weight of the GDL to calculate loading
12) Brush some more catalyst ink onto the GDL if needed
13) Let coating dry and weigh GDL.

12) and 13) are repeated until the desired loading is achieved. Depending on the viscosity of the ink a coating cycle could also be 2 coatings, having rotated the glass plate 180°. For a high-viscosity ink the loading might be too high otherwise. A calculation of the loading of one sample can be found in Appendix [A]. After coating the GDL was dried 10 minutes on the glass plate at 40°C and then overnight at room temperature in a tray which used a Kimwipe as a cover to prevent contamination. On the next day 2 pieces of (2.3 x 2.3) cm² were cut off the coated GDL with a scalpel and weighed to determine the exact loading. After that each electrode was stored in a Ziploc bag. The anode GDL with a CL by TVN Systems was cut and stored likewise. For cutting the GDL was put on a clean piece of paper with the MPL and CL facing down. Both the ruler and the scalpel were thoroughly cleaned with IPA before being used.

One has to mention that the desired loading of 0.5 mg Pt/cm² (see Table 2.6.4-1) can not be achieved very precisely with the brush coating method. Thus all CL loadings vary both upwards and downwards.

2.3 MEA preparation

For the MEA preparation the self-prepared catalyst coated on a SGL 35 BC GDL (thickness 325 µm) was used as the cathode and an electrode by TVN Systems with a loading of 0.35 mg Pt/cm² was used as the anode side of the PEMFC. As

membrane a solution cast Nafion® membrane NRE 212 by IonPower was used. Scalpel and ruler were always cleaned with IPA and for the whole preparation process lab gloves have been used. A schematic of the hotpress is shown in Figure 2.3-1 and a detailed schematic of the MEA in Figure 2.3-2. The geometries are not true to scale. The following is a step-by-step procedure how the MEA was prepared.

1) Heat up hotpress to 135°C
2) Clean 2 carbon plates with IPA
3) Cut a (2.3 x 2.3) cm² of anode electrode
4) Cut (5 x 5) cm² of membrane
5) Place cathode in the center of one carbon plate
6) Place membrane centered on top of the cathode
7) Place anode centered on top of the cathode/membrane
8) Put the other carbon plate on top of the MEA
9) Hotpress with 33lb/cm² electrode at 135°C for 5 minutes
10) Remove from hotpress and allow to cool down to room temperature
11) Store the MEA in a Ziploc bag with a humid Kimwipe.

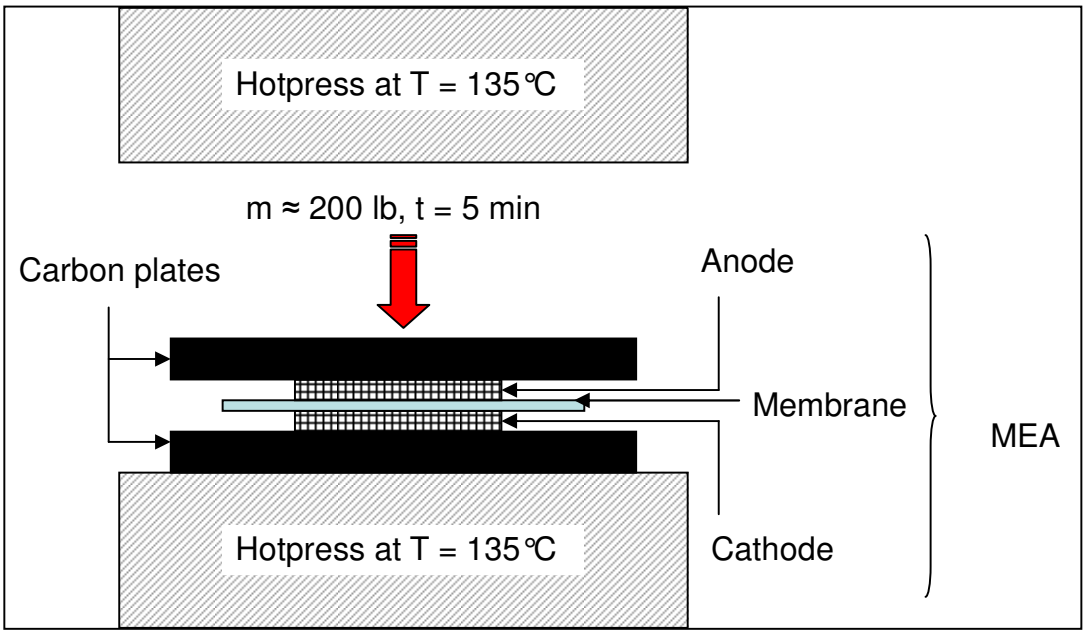

Figure 2.3-1. Hotpressing of the membrane electrode assembly

The hotpressing procedure above the glass transition temperature of Nafion® causes the ionic polymer phase to flow, polymerizes and provides good contact between the CLs and the membrane [42]. Further it is very important that the cathode and anode electrodes align exactly to maximize electrode area utilization. For hotpressing a pressure of 33 lb/cm² electrode, i.e. 2.3 x 2.3 x 33 = 175lb was used. In general this pressure can not be too low on one hand, because there wouldn't be sufficient contact between CL and membrane. On the other hand a too high pressure might cause a collapse of the porous GDL material [42, 43]. Putting a humid Kimwipe into the Ziploc bag together with the MEA is essential to keep the membrane hydrated. However, too much water could penetrate through the electrodes and swell the membrane which could lead to separation from the electrodes.

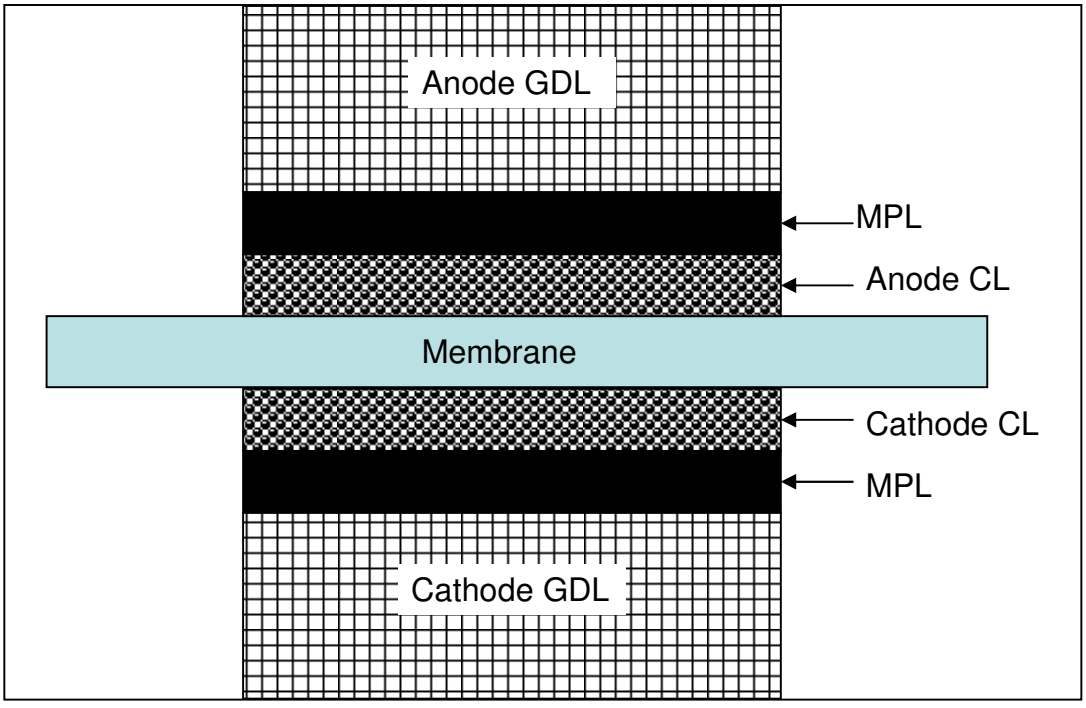

Figure 2.3-2. Detailed view of the MEA

2.4 Assembly of the PEM fuel cell

To assemble the actual fuel cell 2 gas distributors plates made out of carbon with an interdigitated flow-field design were used. As mentioned in Section 1.3 the interdigitated flow-field assures for good transport characteristics at high current densities [8]. Further 2 gaskets were cut out of expanded PTFE membranes by Donaldson Inc. to prevent gas leakage (see Figure 1.3-3). The thickness of the gaskets was 10 mils and the dimensions of the gaskets are the same as the gas distributors itself, except the center square in the middle is slightly larger than the electrode size to avoid placing the GDL on the gasket when assembling the cell. However, the gap between the GDL and the gasket can not be too big, because reactant gases might channel through, flowing directly from the gas inlet to the outlet without penetrating through the electrode. When the gasket is compressed, most of the gap is filled. Figure 2.4-1 shows the dimensions of the cathode gas distributor and Figure 2.4-2 a top view on the MEA and the gasket.

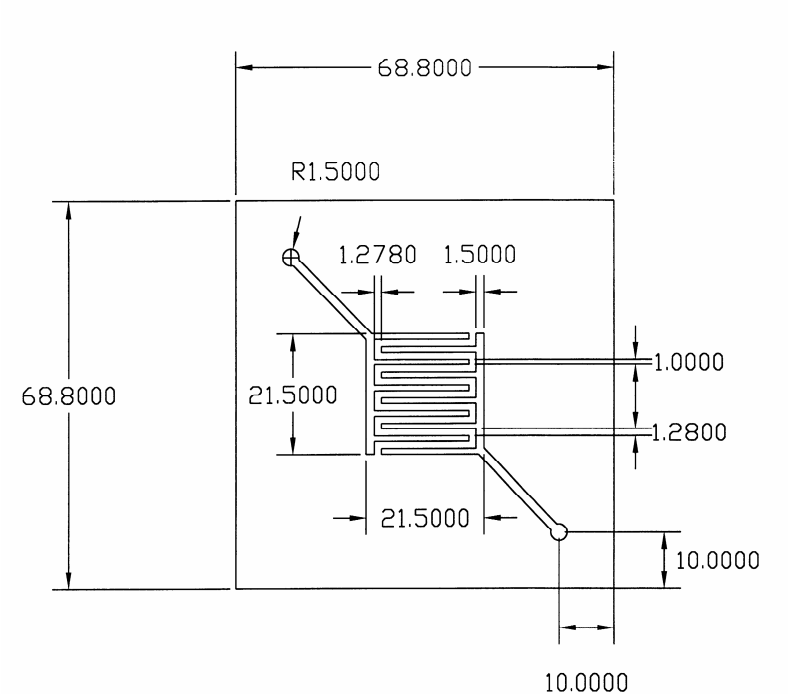

Figure 2.4-1. Dimensions of the interdigitated flow field in mm

The anode gas distributor has exactly the same geometries but two more holes for gas inlet on the lower left and top right corner at the same distance to the border of the plate. The dimensions of the flow-field ((2.15 x 2.15) cm²) are slightly smaller than the electrodes ((2.3 x 2.3) cm² to prevent gas channeling from the edges.

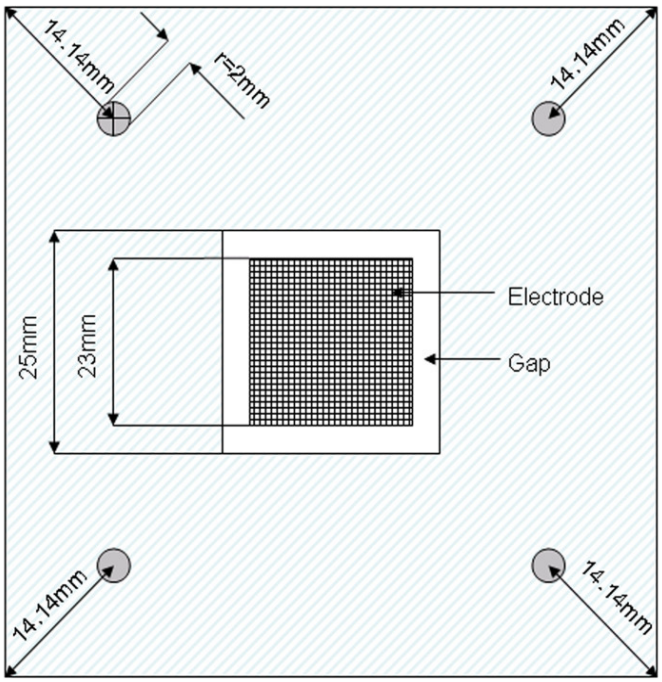

Figure 2.4-2. Teflon gasket with MEA

Copper plates are used as current collectors on the anode and cathode side, because of their high electric conductivity. While the control wires from the testing station were directly connected to the current collectors the voltmeter was in contact with the gas distributors to minimize ohmic voltage loss from the carbon gas distributors to the copper current collectors. To control the temperature of the fuel cell a heating rod controlled by a Watlow™ temperature controller was inserted into a stainless steel heating plate. For a symmetrical temperature gradient the heating rod was centered. As a support the fuel cell was compressed by stainless steel compression plates. To prevent electrical shortage the cell was insulated from the metal endplates by Teflon® sheets on both sites. For optimal contact the compression

plates were compressed and held in place by 8 steel rods with bolts. The steel rods were insulated with a shrinking tube to prevent an electrical short-circuit. The compression force of the whole assembly plays a very important role in the testing procedure. While a too weakly compressed cell lacks good contact between the gas distributors and the GDL or lead to gas leakage, a too high compression force could destroy the GDL, i.e. the porous network would collapse and the reactant gases could not penetrate to the CL fast enough. The worst case that could happen is that the membrane gets punctured by a lump on a CL surface. The optimal compression force clearly depends on the thickness of the gaskets and the GDLs being used in the fuel cell. For the 10 mil gaskets and the SGL 35 BC GDLs a compression force of 58 lb/cm² gasket, i.e. approximately 2500 lb, was used.

A schematic of the flow through the gas distributors is shown in Figure 2.4-3 and an assembled fuel cell in Figure 2.4-4.

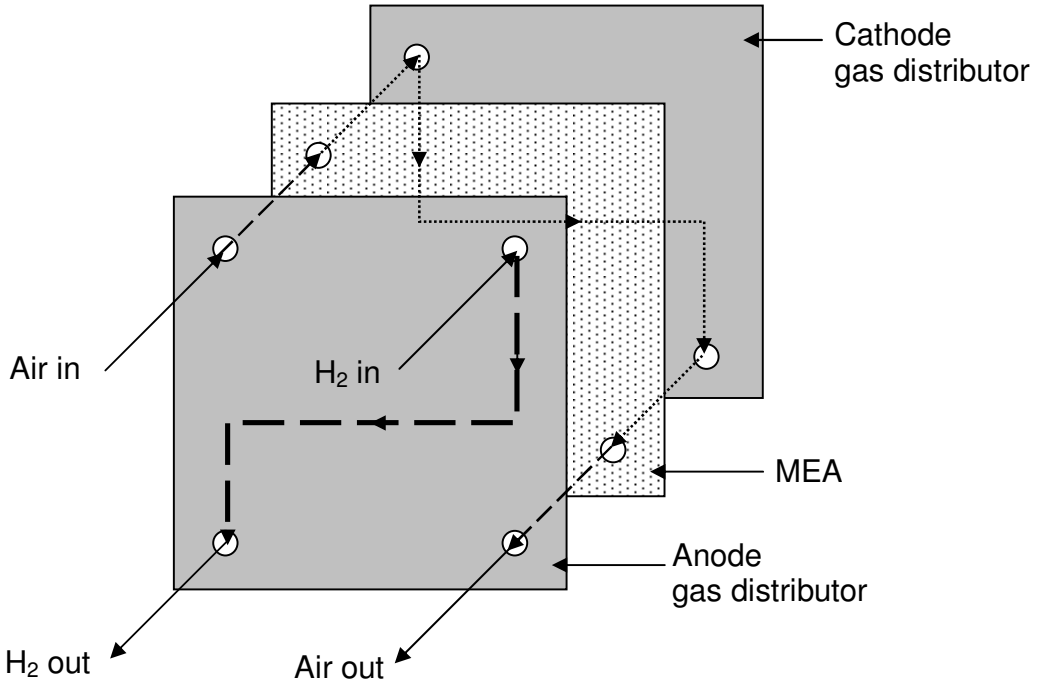

Figure 2.4-3. Schematic of the gas flow through a PEMFC

The upper compression plate has 4 gas inlet and outlet holes, which are matching with the ones on the anode gas distributor. Those are not shown in Figure 2.4-4.

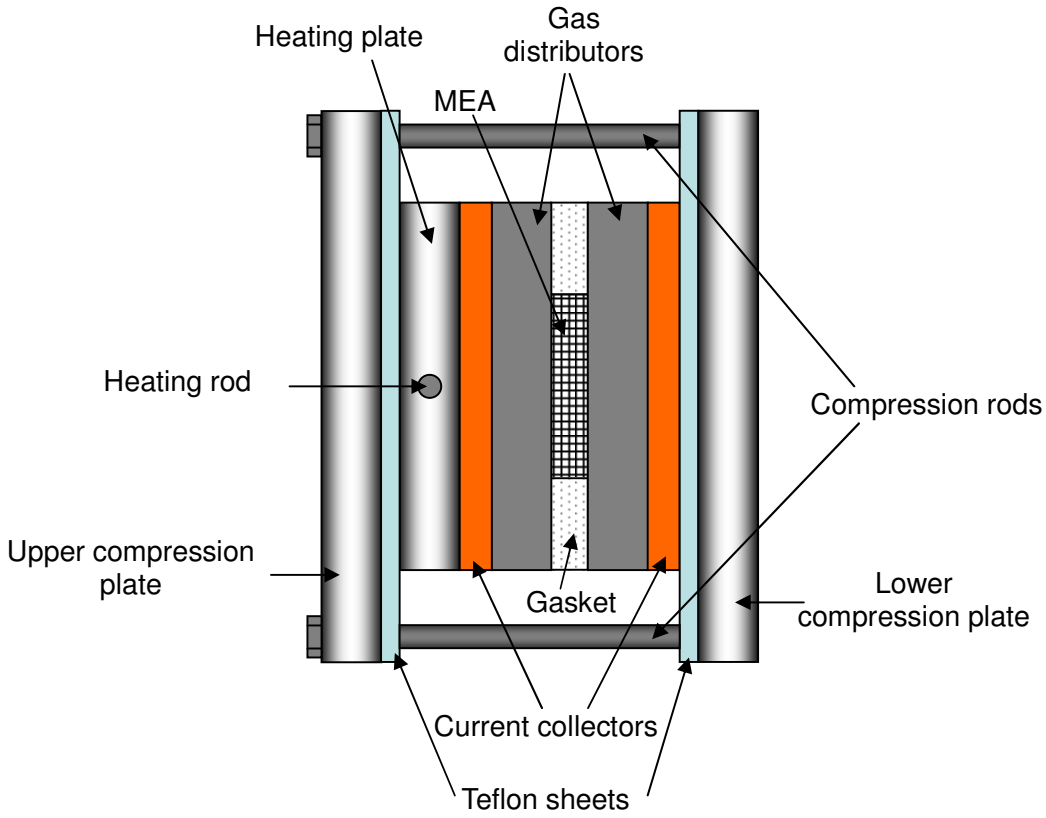

Figure 2.4-4. Schematic of an assembled PEMFC

2.5 Experimental setup

The experimental setup of the fuel cell test stand is illustrated in Figure 2.5-1. Both dry hydrogen and dry air are fed through a humidifier, which is simply a sparging bottle, heated by a heating jacket and filled with deionized water. The dry gases are dispersed into the water by a porous metal rod and the bubbles pick up

moisture and leave the bottle carrying water vapor. The tubing system after the humidifiers is completely insulated to prevent condensation of the water at the walls of the tubes. For the gas humidifiers as well as for the fuel cell itself Watlow™ temperature controllers were used. The hydrogen flow rate was controlled by a rotometer and the air flow rate by a more precise mass flow controller FMA-2406 by Omega. Further a Honeywell 26PC (0-5 psi) pressure transducer measured the pressure drop between the air entering and leaving the system. This pressure drop can give important information about the water content in the fuel cell [44], as well as explain effects like increased performance due to high gas pressures/concentrations [45]. For potential and current control a potentiostat BT-2043 by Arbin Instruments with MITS'97 as testing software was used. This system can run both as a current controlled system (galvanostatic mode) and a voltage controlled system (potentiostatic mode). With MITS'97 all data such as temperatures, voltage and current were recorded every 10 seconds and later analyzed with MS Excel.

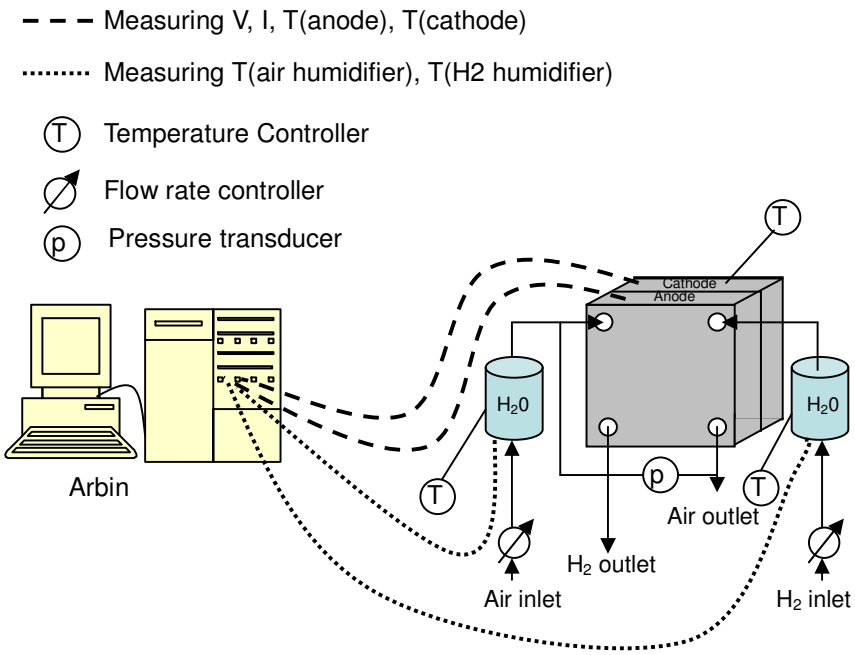

Figure 2.5-1. Experimental setup of the fuel cell test stand

2.6 Fuel cell testing procedure

Before the actual test of the fuel cell several pre-tests have to be done to assure for functioning test equipment and cell. The pre-tests are run in the following order.

2.6.1 Checking gas flow, cross-over and leakage

To check whether the gases enter and exit the fuel cell system properly air is connected to the air inlet at 20 psi while the hydrogen inlet and outlet holes are closed. The end of a tube, which is connected to the air outlet, is held into a beaker of water and bubbles should show the air flow. The same procedure is done with the hydrogen side also using air as the testing gas.

For checking for gas crossover from anode to cathode or vice versa air is again connected to the air inlet at 10 psi, while closing the air outlet and hydrogen inlet. The end of a tube, which is connected to the hydrogen outlet, is held into a beaker of water. The same check is done for the hydrogen side. Air bubbles would represent air crossing over from cathode to anode for the first case and for the second case crossing over from anode to cathode. This could have several reasons, assuming the MEA is correctly centered on the flow fields and covers them completely. The first reason would be an insufficient compression force, so that the gas channels between the gaskets and the membrane to the other side. Applying 100 lb more pressure stepwise might solve that problem. The second reason could be a hole in the membrane, so that the MEA has to be discarded.

By adding water on the edges of the gas distributors gas leakage is checked. If there are air bubbles appearing, the compression plates are not compressed enough. One has to apply stepwise 100 lb more of pressure until the leakage is gone. However, the cell can not be compressed too much, because the GDL pores might be crushed. If the leakage can not be fixed the gaskets should be replaced.

2.6.2 Checking for electrical short-circuit

The fuel cell system further has to be checked for an electrical short-circuit. As illustrated in Figure 2.4-4 the Teflon sheets between the current collector or heating plate and the compression plates prevent any electrical short. Also the insulating shrinking tubes around the compression rods make sure that there is no short if the rods happen to touch any extraneous conductive material.

To test the fuel cell system for electrical short-circuits a voltmeter is switched to ohm-mode and each probe is contacted with one current collector. The ohmmeter should show a fluctuating value in the range of kilo-ohms which would be typical for the electrolyte membrane. What is actually measured is the impedance of the membrane since it can only conduct protons and not electrons. If one observes a low stable reading on the ohmmeter there is a short between the anode and cathode side. That means that the current collectors or the gas distributors or in the worst case the CL are contacting each other. For the first problem checking the compression rods for direct contact with the current collectors and fixing the shrinking tube might help. The second problem can be fixed by changing the gaskets. The most severe problem, a direct contact of both CLs would mean a hole in the membrane and a too high compression force. The MEA would have to be discarded.

For the second test for shortage one probe of the ohmmeter is connected to a current collector and the other one to a compression plate. The ohmmeter should show an infinite value or be in the order of mega-ohms. The same procedure will be done for both current collectors and both compression plates, i.e. four testing procedures. However, if the ohmmeter shows a low resistance value there is a short and the Teflon sheets have to be checked for holes or insufficient coverage of the current collectors and the shrinking tube of the compression rods have to be checked for scratches.

All fuel cells in the study passed the pre-tests and did not show any malfunction.

2.6.3 Membrane massaging

Before a polarization curve is obtained from a fuel cell, it is necessary to assure that the membrane is fully hydrated. For best performance the membrane should absorb as much water as possible without resulting in flooding in the GDLs and gas distributors. In this study a self-developed standard “massaging” procedure was applied to every single cell be before the actual test runs were made. The cell was assembled as described above and heated up to 60°C. The air humidifier was heated to 80°C, so that air entered the fuel cell totally saturated. Also the air flow rate was fixed to a stoich of 3.5. The hydrogen entered the fuel cell at room temperature at a stoichiometric flow rate of 2. A calculation of the stoichiometric flow rates of both gases can be found in Appendix [B]. The fuel cell was run for one hour at a constant voltage of 0.3V while the flow rates were adjusted due to the current. The low voltage was used to assure that impurities, such as carbon monoxide, were removed from the CL and secondly that a high current, which corresponds to a high reaction rate, i.e. high water production, was drawn. After that the cell was run for another 3 hours at a constant voltage of 0.5V. The massaging procedure was then finished and the test stand was shut off and the fuel cell was sealed overnight to let the membrane relax.

2.6.4 Actual fuel cell test

Contrary to the massaging step, the actual test run was current controlled (galvanostatic mode), i.e. the current was set and the voltage measured. The basic operating conditions are the same as in the massaging step and can be found summarized in Table 2.6.4-1. The procedure for the actual fuel cell test run is presented in the following:

1) Before the actual fuel cell test massage the cell for half an hour at 0.3 V
2) Run the cell at open circuit voltage (OCV) for 5 minutes to let membrane

relax

3) Adjust the flow rates depending on the current that will be drawn next in order to have sufficient reactants available and the cell doesn't run in reverse mode
4) Set the current to 0.2A and hold it for 10 minutes to reach equilibrium and record data at equilibrium
5) Adjust flow rates
6) Set the current to 0.4A and hold it for 10 minutes to reach equilibrium and record data at equilibrium
7) Adjust flow rates
8) Increase current by 0.4A and hold it for 10 minutes to reach equilibrium and record data at equilibrium
9) Repeat 7) and 8) until the cell fails to maintain a stable voltage.

For more precise data some samples were also cycled, i.e. at the highest possible current the current was decreased in 0.4A steps, held for 10 minutes and recorded data at equilibrium until OCV was reached. The upward and downward cycle should both yield to the same polarization curve although there can be slight differences due to different flooding conditions.

T,cell [°C] (cathode/anode)	60
T,humidification for hydrogen [°C]	23 (room)
T,humidification for air [°C]	80
Stoichiometry (hydrogen)	2
Stoichiometry (air)	3.5
P,in(hydrogen) [psi]	20
P,in(air) [psi]	20
Flow field type	Interdigitated
Electrode size	2.2cm x 2.2cm
Desired catalyst loading [mg Pt/cm²]	0.5

Table 2.6.4-1. Basic operating conditions

2.7 Summary of objectives

The objective of this work was finding an optimized composition for the cathode catalyst layer for a PEMFC. The anode side used the same GDL material and had a fixed composition and was manufactured by TVN Systems. The ratio Pt:C was fixed by the catalyst powder and the ratio Nafion®:C was varied from 0.75 to 1.5 in 0.25-steps holding Teflon® constant. Likewise Teflon®:C was varied from 0.25 to 1 in 0.25-steps holding Nafion® constant. By hypothesis a fuel cell using a cathode CL with a composition in an optimized region should yield to good fuel cell performance.

Besides finding an optimal CL composition optimizing the operating conditions, particularly cell and humidification temperatures, for best fuel cell performance and reproducibility was also a goal of this study.

Last but not least the influences of the heat treatment of the catalyst ink and the benefits of the new CL structure and composition being prepared with the novel 2-step method had to be understood and explained.

Chapter 3

Results and Discussion

3.1 Operating conditions

3.1.1 Literature review

The operating conditions of a PEMFC play a very important role in the power output of a fuel cell system. The cell temperature for example influences the rate of reaction and the rate of water evaporation. While the hydrogen oxidation on the anode side occurs at very high reaction rates, the oxygen reduction reaction is very slow and thus the rate determining step. At higher temperatures the oxygen reduction reaction rate increases and so the power output. Higher cell temperatures cause faster evaporation within the fuel cell system, which means the humidifier temperatures might have to be adjusted [42]. Studies on operating conditions showed that the temperatures of both humidifiers (air and hydrogen) have a big influence on the water and heat management within the fuel cell and thus also on the direct fuel cell performance output [46, 47, 48]. Nguyen and White found out in their model that the rate of back diffusion from cathode to anode was insufficient to keep the membrane hydrated and thus proposed to humidify the incoming gas on the anode side [46]. By water balance experiments Yan et al. showed that dry oxygen would cause the membrane to dry out [47]. Humidified oxygen on the cathode side would keep the membrane sufficiently hydrated, while hydrogen on the anode could enter the fuel cell dry. In general a decrease of the relative humidity on the cathode side (RHC) had a more detrimental effect than the relative humidity on the anode side (RHA) [47]. Saleh et al. explored the effect of symmetrical and asymmetrical temperature profiles of the humidifiers on the fuel cell performance [48]. In general the impacts of the relative humidity of the gas humidifiers were strongly dependent on the fuel cell

temperature. The higher the cell temperature the higher the humidifier temperatures were needed. Again it was shown that with a RHC = 27% - 100%, the RHA could be zero, but on the other hand with RHC = 0% the RHA had to be at 100% for sufficient membrane hydration [48].

3.1.2 Testing of stoichiometric flow rates and temperatures

The first study of this work serves as the basis for later fuel cell test runs. Stoichiometric flow rates and the temperatures of the fuel cell and the humidifiers and were examined and the best working setup, i.e. best performance and reproducibility, was then picked as the standard operating conditions for all fuel cell test runs.

Initially sample C11, a catalyst with a composition of C:Pt:Nafion®:Teflon® = 1:0.86:1:0.25, is used and Figure 3.1.2-1 shows the results of a higher stoichiometric air flow rate while keeping the hydrogen stoich constant. The test was run in between 0.4V and 0.6V since the peak power of the cell occurs at approximately 0.5V [42].

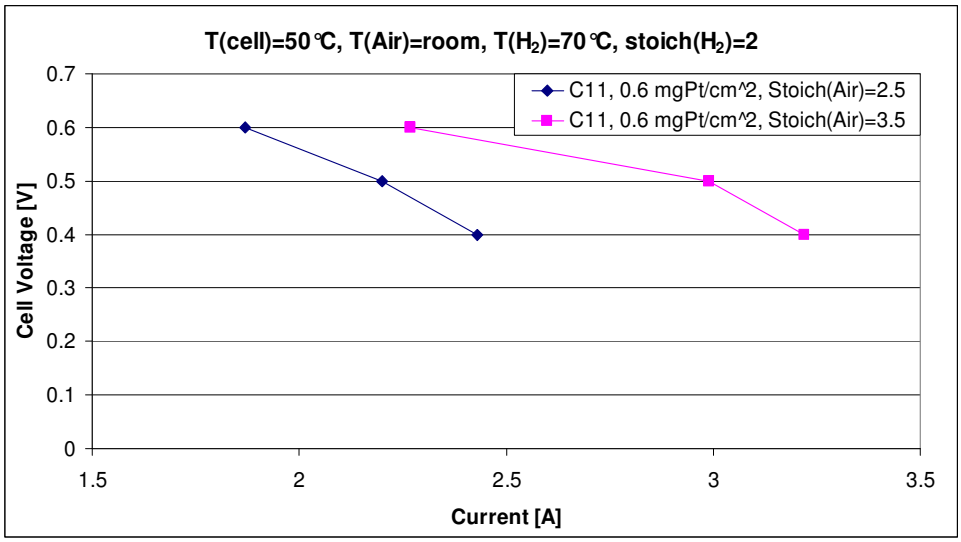

Figure 3.1.2-1. Varying stoichiometric air flow rate at composition C:Pt:Nafion®:Teflon® = 1:0.86:1:0.25

One can clearly observe an increasing performance of almost 50% caused by a higher stoichiometric air flow rate. The higher air flow rate forces more air to the active catalyst sites and thus the reaction rate increases. This is also called pressure or concentration effect, since the higher flow rate combined with the interdigitated flow field yields to a very high pressure drop from the gas inlet to the outlet [8]. Besides forcing more air into the cell, the higher air flow rate showed also benefits related to water management. Liquid water that was generated on the cathode side could be pushed out more easily of the pores of the CL and the GDL. At the exit one could observe more water droplets exiting at higher stoichiometric flow rates than at lower. Hence the diffusion resistance of air was lowered and a combination of both aspects led to higher current densities. Exact pressure measurements and more details on those effects on the fuel cell performance will be discussed later. The stoichiometric flow rate of 3.5 for air and 2 for hydrogen were chosen as the basic stoichiometric flow rates for the fuel cell test runs.

For finding the optimal temperature settings several runs at different catalyst compositions have been made. In general, the combined effects of cell temperature and humidifiers affect the overall fuel cell performance. The effects of loading and compositions are excluded from the following the discussion since this part of the study only focuses on the operating conditions independently of loading or composition. Again sample C11 has been used for first observations and the polarization curves in between 0.4V and 0.6V of different humidifier temperature settings at a cell temperature of 50°C are shown in Figure 3.1.2-2.

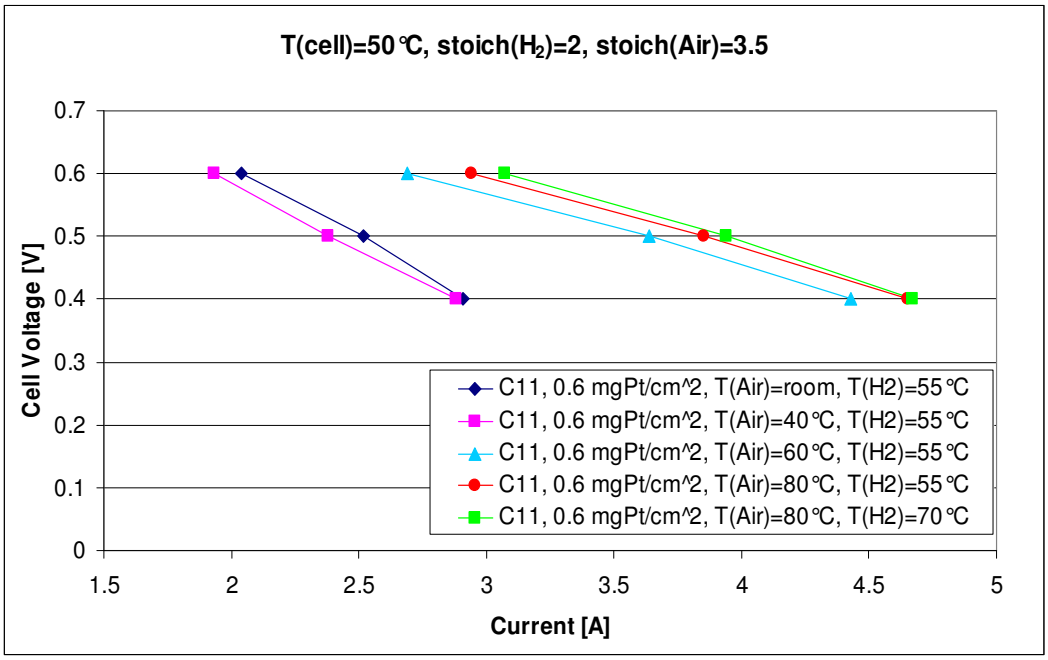

Figure 3.1.2-2. Varying temperature settings at composition C:Pt:Nafion®:Teflon® = 1:0.86:1:0.25

In Figure 3.1.2-3 one can see the polarization curves of sample C25 with C:Pt:Nafion®:Teflon® = 1:0.86:1.5:0.25 and C28 with C:Pt:Nafion®:Teflon® = 1:0.86:0.75:0.5 at an increased cell temperature of 60°C. Since the normal operating temperature of a PEMFC is close to 80°C, 60°C was fixed as the standard cell temperature [42].

All three compositions show best performance at an air temperature of 80°C, i.e. higher than the cell temperature, so that air enters the cell totally saturated. As seen in both figures it doesn't matter whether the hydrogen humidifier is at higher temperature than the cell or at room temperature, which is in accordance to the findings of Yan et al. [47]. Running the cell with dry air, the steep slope indicates insufficient membrane hydration. Especially at high current densities back diffusion rates can't keep up with water transport across the membrane by electro-osmotic drag, so the membrane becomes dehydrated. Nguyen and White proposed higher anode humidification temperatures to counteract this effect and show that at high current densities higher anode humidification leads to better membrane hydration [46].

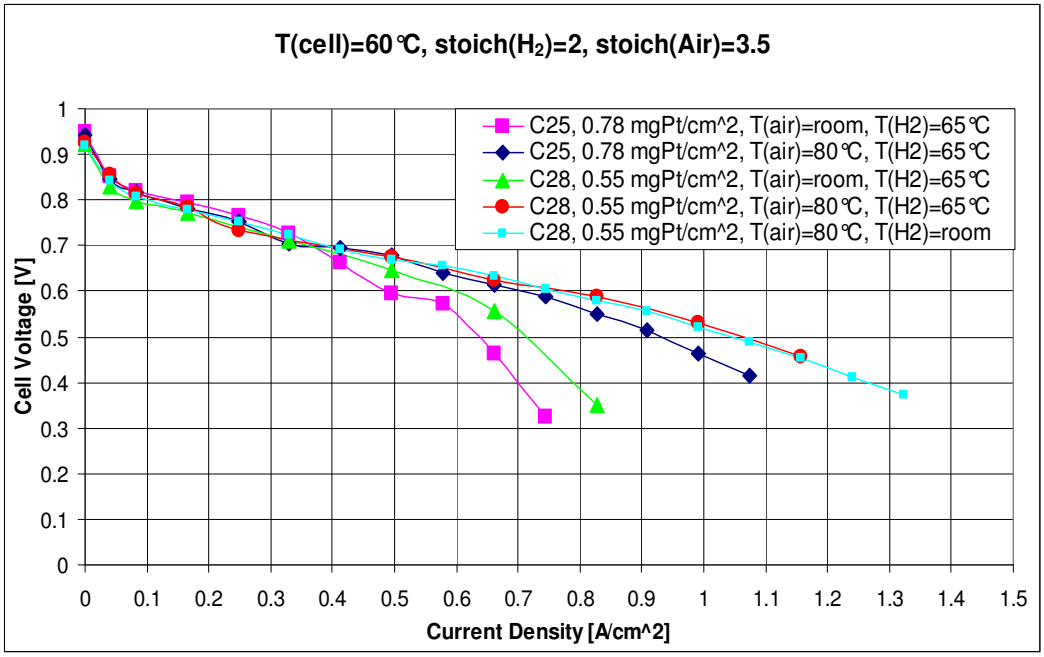

Figure 3.1.2-3. Varying temperature settings at composition C25: C:Pt:Nafion®:Teflon® = 1:0.86:1.5:0.25 and C28: C:Pt:Nafion®:Teflon® = 1:0.86:0.75:0.5

However, both Figure 3.1.2-2 and Figure 3.1.2-3 show that dry air and saturated hydrogen cause a steeper slope and worse performance. This is the case, because while air enters the system unsaturated at a high flow rate even a saturated anode side doesn't provide enough water to keep the membrane hydrated at first place and the back diffusion rate of the generated water is too low or there is not enough liquid water being generated. Thus it makes sense that the cell performance increases with increasing air saturation.

The slope in the ohmic regions flattens the more the air becomes saturated, and thus one can conclude that a saturated air stream would guarantee a well hydrated membrane and thus high proton conductivity. The back diffusion rate of water from the cathode to the anode is high enough, so that the anode doesn't need to be humidified at all. Since both the anode and the cathode sides include a MPL it is very likely that the liquid water is kept in between the two electrodes and thus in the CL and the membrane.

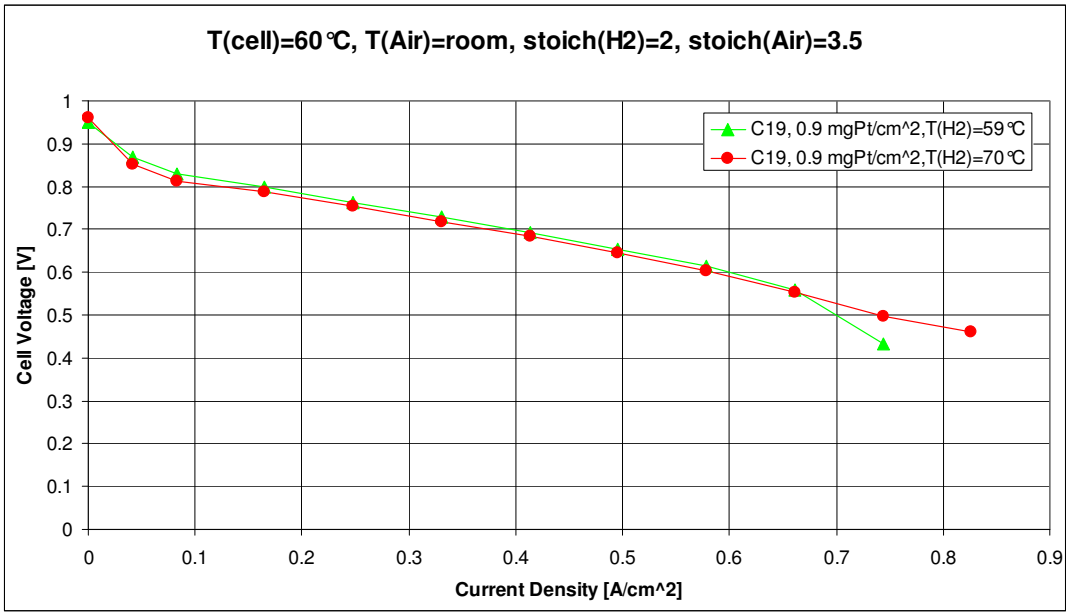

Figure 3.1.2-4. Increasing hydrogen humidifier temperature at composition C19: C:Pt:Nafion®:Teflon® = 1:0.86:1:0.5

A complete set of data for all catalyst samples at different operating conditions can be found in Appendix [C].

3.2 Experimental findings with the 2-step preparation method

After annealing the first half of Nafion® onto the catalyst particles in the first step and it was observed that those floated on water because their outer surface had become highly hydrophobic. By means of pH measurements it was verified that the ionomer phase did not get into solution again when adding a solvent, but stuck to the catalyst particles. Hence those steam-annealed catalyst particles could not adsorb water anymore, which was necessary to prevent burning-off the carbon support from the platinum when adding IPA in the second step of the preparation procedure. IPA was required to bring the catalyst particles back into solution and therefore the extra IPA in the second step had to be added under an inert gas environment. One might question whether the catalyst particles were totally covered by annealed ionomer

solution, but if there were any open sites left, water would have immediately covered those sites, just like the original catalyst powder. Hence the whole surface of catalyst was covered by annealed ionomer and the burning occurred, because oxygen diffusion rates though the polymerized ionomer film were high enough to reach the active catalyst sites.

3.3 Optimizing the cathode catalyst layer composition with a 2-step preparation method

In this section the results of the CL composition studies are presented in the form of polarization curves and power density curves. The raw data for the catalyst samples as well as power density data and pressure measurements can be found in Appendix [C].

3.3.1 Nafion®:C = 0.75:1

As starting basis of the optimization a composition of Nafion®:C = 0.75 was picked. Figure 3.3.1-1 shows the polarization curves and power density curves obtained by increasing the Teflon® content while holding the Nafion® content constant at Nafion®:C = 0.75.

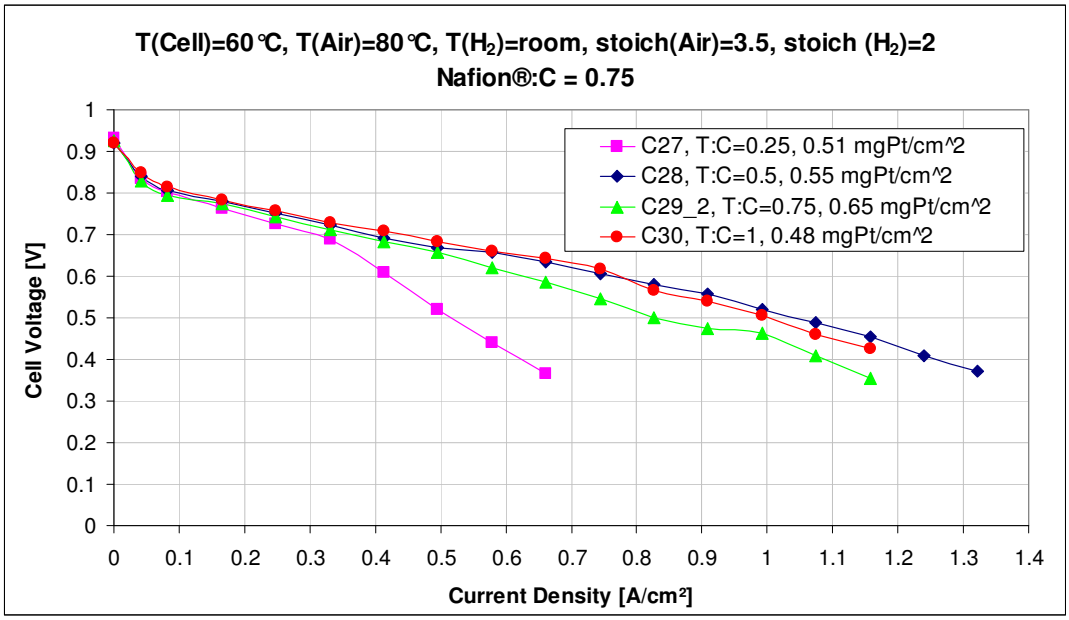

Figure 3.3.1-1. Polarization curves of varying Teflon® content at Nafion®:C = 0.75

The sample C27, having the lowest Teflon® content, shows the worst performance. Mass transfer resistances play the dominant role, so that the polarization curve starts to drop even at very low current densities. This is expected since the very low Nafion® content creates large void volumes between the ionomer-covered catalyst agglomerates. This void is partly filled with Teflon® to provide hydrophobic regions for gas transport and water removal ways. However, the few Teflon® particles can not create a continuous hydrophobic path within the large voids. Hence the main part of them still remains hydrophilic due to the ionomer. The major part of the void volume between the ionomer-covered catalyst agglomerates is occupied by air, so that generated liquid water gets into the voids and blocks them. Accordingly samples C28, C29_2 and C30 with higher Teflon® contents all show a drastic improvement of the cell performance, sample C28 with Teflon®:C = 0.5 as the best. For sample C28 the mass transfer limitations occur at extremely high current densities (>1.2 A/cm²) and the peak power is about 0.52 W/cm² at around 0.5V. More Teflon in the void spaces creates the desired hydrophobic channels and flooding occurs at high current densities. The flat slope of the polarization curve indicates that the membrane is in a

well-hydrated state and the higher Teflon content doesn't lead to complete water removal and membrane dryout. Figure 3.3.1-1 and Figure 3.3.1-2 both show that a further increase of Teflon® leads to decreasing performance of the fuel cell, meaning that at Nafion®:C = 0.75 the maximum Teflon® content needed to fill up the void volumes is reached with sample C28 Teflon®:C = 0.5. Additional Teflon® would not place itself within the empty voids but could settle within the ionomer network and may disrupt the continuity of the ionomer network or even the electronic network. Sample C29_2 performs slightly poorer than samples C28 and C30. This can be explained by the higher loading of sample C29_2. A higher loading means a thicker CL and so the diffusion resistance for the reacting gases increases. Air can not reach the active catalyst sites fast enough and the concentration of air at the active catalyst sites is lower than with using thinner catalyst layers. Also access of air might not be steady, which can be clearly seen in the power density curve of sample C29_2. The discontinuity in the power density at around 0.47V indicates that there might be liquid water build-up or entrapment followed by a sudden removal. Hence a too thick CL, i.e. a too high loading, is not desirable.

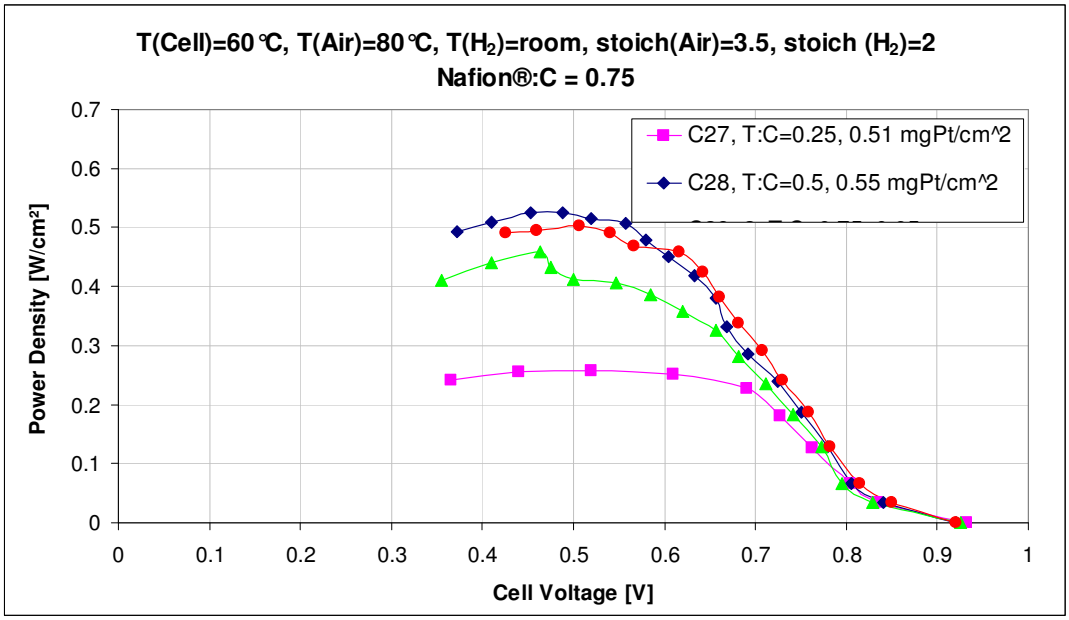

Figure 3.3.1-2. Power density curves of varying Teflon® content at Nafion®:C = 0.75

However, that even at very high Teflon® loadings the fuel cells show good performance indicates that at a Nafion® loading of Nafion®:C = 0.75 adding Teflon® up to Teflon®:C = 1 does not block active catalyst sites and the ionic and electronic networks remain continuous to a high degree. The void volume created by the catalyst agglomerates is sufficient to incorporate a wide range of Teflon® and a high peak power at high Teflon® loadings is not surprising. By the reasoning of above the impact of additional Teflon® should be observed at lower Teflon® contents when increasing Nafion®, i.e. because the more Nafion® is in the CL the less Teflon® is needed to fill up the voids.

3.3.2 Nafion®:C = 1:1

The polarization curves of Nafion®:C = 1 with varying Teflon® content are graphed in Figure 3.3.2-1 and the power density curves in Figure 3.3.2-2.

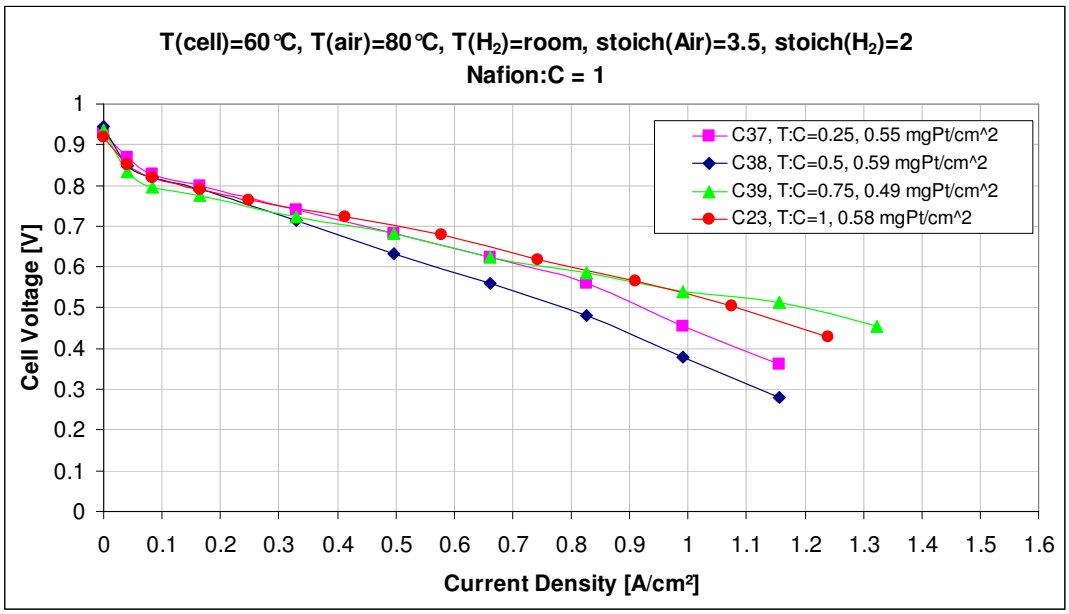

Figure 3.3.2-1. Polarization curves of varying Teflon® content at Nafion®:C = 1

At the fixed ratio Nafion®:C = 1 one can observe that the slope of the polarization curve becomes steeper at first by increasing the Teflon® content from

Teflon®:C = 0.25 to 0.5 and from then on the slope becomes flatter with increasing Teflon® and the mass transfer limitation region is pushed to higher current densities. This upward trend continues until a certain limit of Teflon® and then the performance starts to drop down again. Sample C39 with a Teflon content of Teflon®:C = 0.75 shows the best performance. The same trend as in the polarization curves can also be found in the power density curves in Figure 3.3.2-2. The first drop from sample C37 to sample C38 is then followed by increasing peak powers with higher Teflon® contents and a downward trend after reaching a performance peak. Figure 3.3.2-2 also shows that, as mentioned before, the peak power of a PEMFC under these running conditions occurs at around 0.5V.

Compared to the Nafion®:C = 0.75 samples, one needs more Teflon® to achieve high power densities which is contrary to the expectation from before. However, as expected, sample C39 shows better performance than both samples C37 and C38.

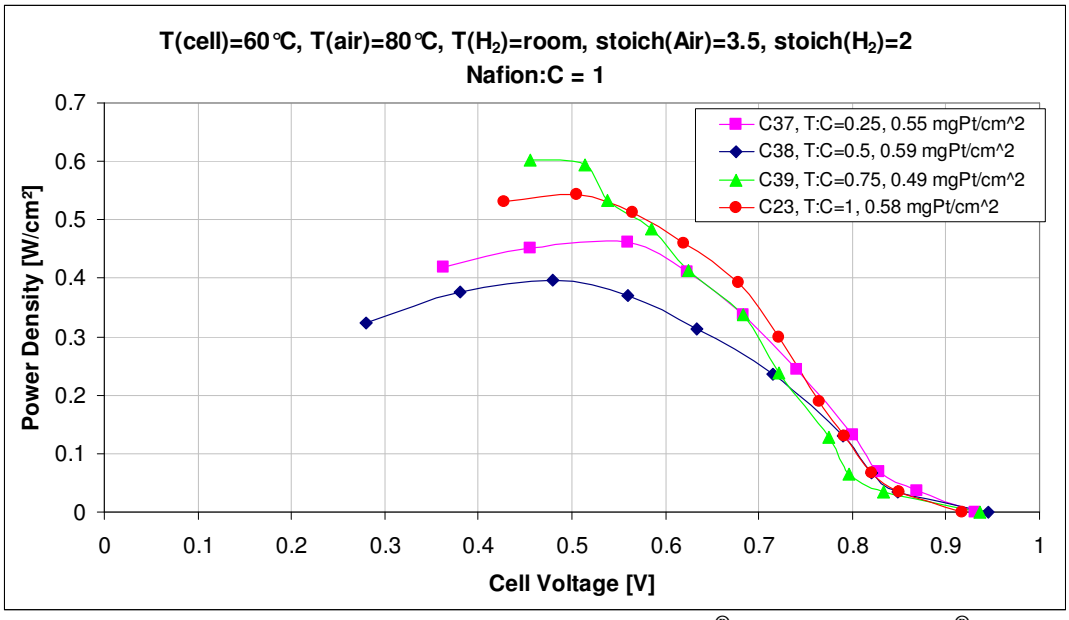

Figure 3.3.2-2. Power density curves of varying Teflon® content at Nafion®:C = 1

The latter two compositions lack Teflon®, so that liquid water flooding leads to mass transfer limitations at lower current densities. Also both the polarization and

the power density curves show that the performance of a cell increases up to certain level (samples C37→C39) and then starts dropping down with higher Teflon® content (sample C23). Again sufficient Teflon® successfully fills up the voids to create hydrophobic pathways for gas transport and removal of liquid water close to the hydrophilic surface. Hence consistently good fuel cell performance could be obtained. The unexpected drop of sample C38 can not be explained by this argumentation and has to be considered as an outlier. A random structure formation that occurred during the coating or hotpressing might have led to a bad CL network. It might also be the case that the void volume is big compared to the amount of Teflon® to fill it up, Teflon® might place itself randomly, providing a continuous path or not. However, sample C38 is excluded from the discussion and would have to be repeated.

The peak powers of this set of data are shifted to higher values, what indicates a better behavior in a wide region of the ohmic resistance losses, i.e. a flatter slope of the polarization curve. The higher Nafion® content provides a more developed ionomer network and thus faster proton transport across the CL and the membrane. Also since more Nafion® is annealed onto the catalyst particles the danger of blocking active catalyst sites is further reduced, because it is less probable that there are any free active catalyst sites available after the annealing process. This could be indicated by the first 3 points of the polarization curves of this set, which show a lower activation loss compared to the Nafion®:C = 0.75 –set.

Increasing the Nafion® content even more should lead to both a better ionomer network and the Teflon® content needed to fill up void spaces should be decrease, as expected before.

3.3.3 Nafion®:C = 1.25

The polarization curves of Nafion®:C = 1.25 with varying Teflon® content are plotted in Figure 3.3.3-1 and the power density curves in Figure 3.3.3-2.

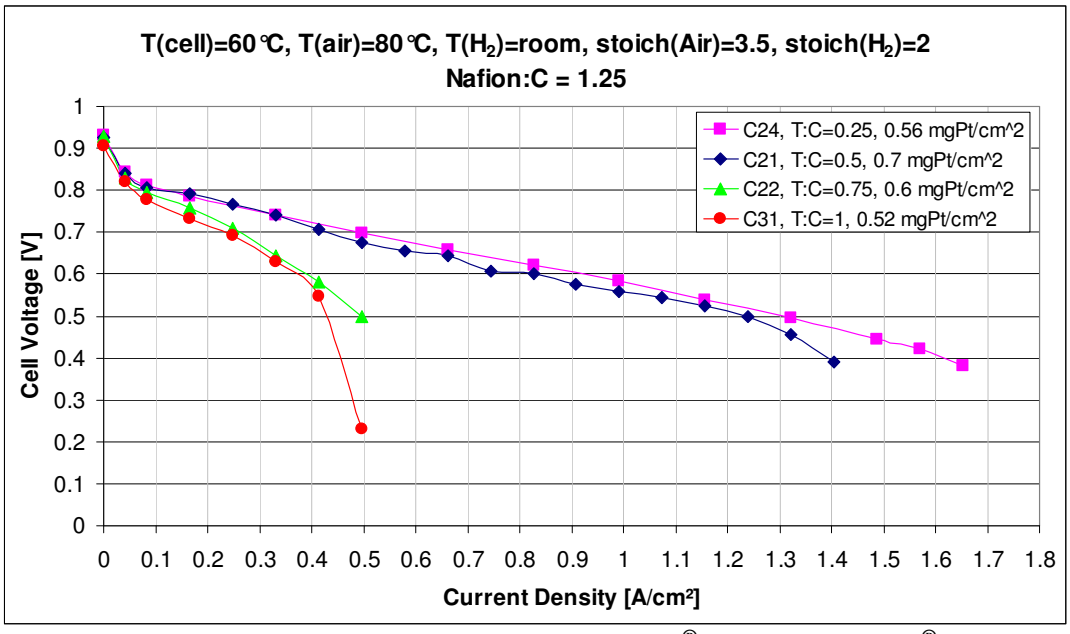

Figure 3.3.3-1. Polarization curves of varying Teflon® content at Nafion®:C = 1.25

This set of data showed again that the best performance is already obtained at very low Teflon loadings followed by a decrease with increasing Teflon® content.

The best performance was observed with sample C24, with a composition of Teflon®:C = 0.25::1. Compared to the set of Nafion®:C = 1 the best performing catalyst contains less Teflon® (sample C24 at 0.75 vs. sample C39 at 0.25).

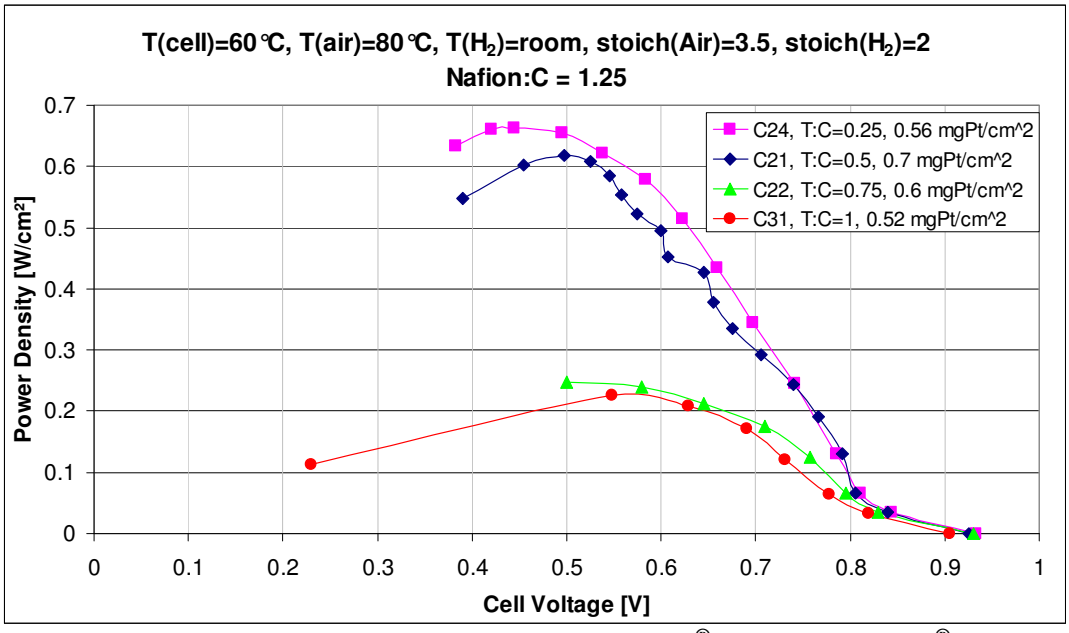

Figure 3.3.3-2. Power density curves of varying Teflon® content at Nafion®:C = 1.25

This clearly supports the idea of needing less Teflon® at higher Nafion® contents to fill up the created void volumes. One can further notice that at this Nafion® content higher Teflon® loadings lead to bad performance. Since at a Nafion® loading of Nafion®:C = 1.25 the void volume is very small, only a slight amount of Teflon® will occupy these void spaces. Additional Teflon® has no chance of being placed elsewhere but between the ionomer clusters. This leads to a stretching of the catalyst agglomerate network, so that clusters move farther apart from each other and become discontinuous. The CL is then not able to conduct protons fast enough and many pathways are getting disrupted so there are only a few ways for protons to flow. The same thing might happen for the electronic conducting pathways. Teflon® and Nafion® are therefore competing for positive effects in the catalyst layer. There is a trade-off between hydrophobic channels and continuity of the electronic and ionomer network. While at lower Teflon® contents the continuity of the electronic and ionomer networks and the incorporation of Teflon® particles in void volumes are highly developed, the negative stretching effect of additional Teflon® occurs at higher Teflon® loadings combined with high Nafion® contents. Thus raising Teflon® even

more will eventually lead to zero proton and electron conductivity of the fuel cell. This trend can be observed with samples C22 and C31, which both show a huge drop in performance compared to sample C24. This means that for Nafion®:C = 1.25 one needs only a Teflon® loading of Teflon®:C = 0.25 to fill up the void volumes and to create a continuous gas pathway and after that additional Teflon® starts to occupying regions outside the void volumes within the ionomer network or causes particle separation and isolation which leads to unutilized catalyst and poor electrical conduction.

3.3.4 Nafion®:C = 1.5

Figure 3.3.4-1 shows the polarization curves and Figure 3.3.4-2 the power density curves obtained by increasing the Teflon® content while holding the Nafion® content constant at Nafion®:C = 1.5.

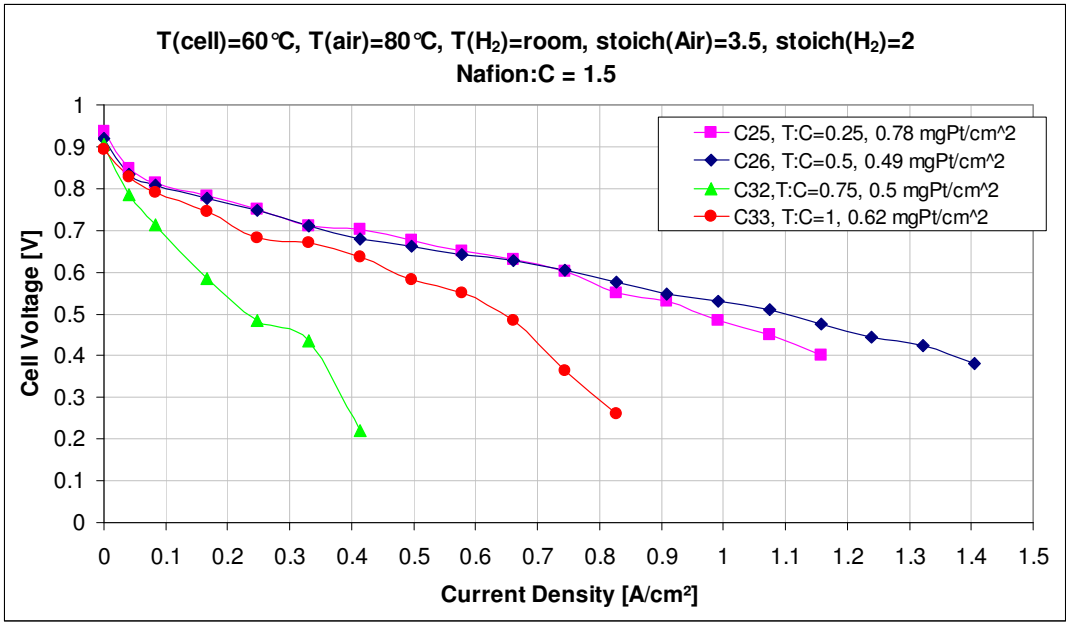

Figure 3.3.4-1. Polarization curves of varying Teflon® content at Nafion®:C = 1.5

The catalyst samples with Nafion®:C = 1.5 follow the overall performance trend from earlier. The optimal Teflon® content at Teflon®:C = 0.5 is higher than before and starts decreasing rapidly by adding more Teflon®.

As for Nafion®:C = 1.25 high Teflon® amounts don't only show mass transfer limitation problems at lower current densities but also an high increase of ohmic resistances. Sample C33 shows surprisingly better performance than sample C32, which can not be explained by the above reasoning. For proper validation one would have to repeat both cases.

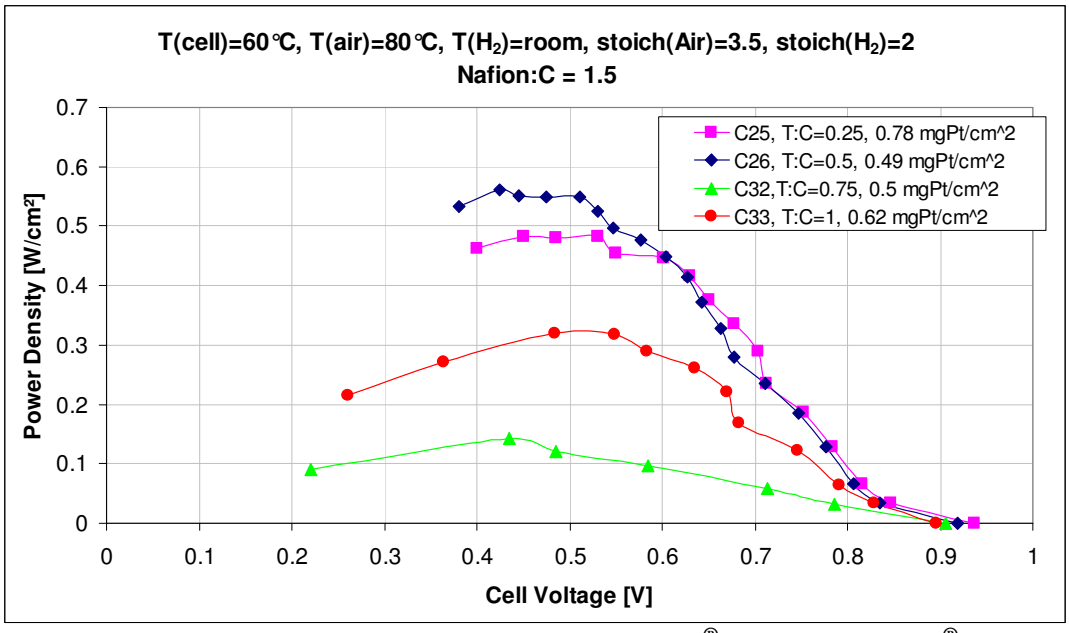

Figure 3.3.4-2. Power density curves of varying Teflon® content at Nafion®:C = 1.5

In general the effect of Teflon® at this Nafion® content is very strong, as expected before. The high Nafion® loadings create, as before, only very little void spaces between the agglomerates, so that the disturbing effect of too much Teflon® overrides the benefit of high ionomer content. As for Nafion®:C = 1.25 too much Teflon® could cause particle separation and isolation and bad electrical connectivity and conductivity. But one can not only regard Nafion® or Teflon® separately, but the combined effect of both electronically insulating materials. Samples C22, C31, Figure 3.3.3-1) C32 and C33 all display the same effect of extensive loadings of both

Nafion® and Teflon®. Overall a too high solid content in general leads to a disruption of the electronic pathways within the CL and the performance of the fuel cell becomes very variable and decreases rapidly.

One problem that arises when comparing the last two sections is that the best performing catalyst at Nafion®:C = 1.25 contains less Teflon® than the one of the Nafion®:C = 1.5-set. According to earlier reasoning at higher Nafion® loadings Teflon® should affect the catalyst structure sooner, i.e. one should require less Teflon® for good performance. However, a closer look at the sample pair C24/C21 and C25/C26 shows, that in both cases the better performing catalysts have a loading close to 0.5 mg Pt/cm². Since sample C21 has a 25% higher loading than sample C24, the effects of the CL thickness might play a role and the composition of sample C21 might actually perform better than sample C24 if the loading was lower. The same reasoning applies for sample C25 which has even a 56% higher loading than sample C26. Then the best performance of a catalyst with highest Nafion® loadings would be with the lowest Teflon® content. However, a validation of this hypothesis has yet to be made experimentally.

3.3.5 Exploratory Comparison Study

Figure 3.3.5-1 shows the summary of all peak powers of the different cathode catalyst layer compositions. One can see the descriptions from above in a cleared form in this graph. In general, there are regions of high and low peak power, depending strongly on the CL composition. For high peak powers the graph shows again that at low Nafion® loadings more Teflon® is needed and vice versa.

For both components there are of course variation limits beyond which the ionomer and electronic networks start getting discontinuous or active catalyst sites being blocked. Hence regions with Nafion®:C = 1.25 or higher show a major performance drop for Teflon®:C = 0.75 or higher, which is attributed to the fact of too much total solid in the CL. The positive effects of Nafion® and Teflon® can not develop

anymore, because the electronic network is becoming disrupted. Therefore it is very suggestive to avoid those regions, since one can not expect good fuel cell performance.

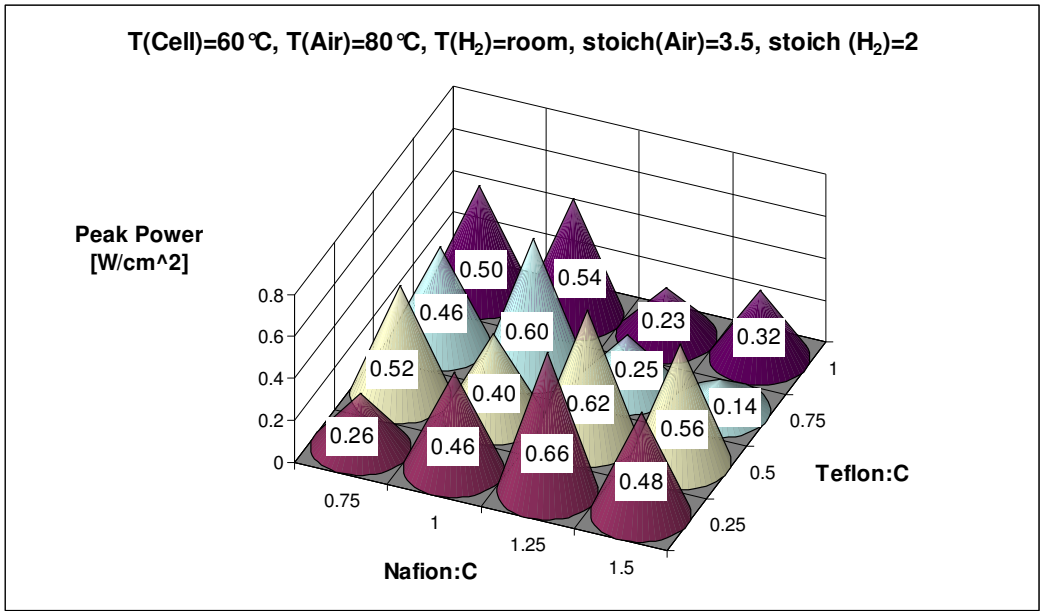

Figure 3.3.5-1. Peak power of various formulations at basic operating conditions

On the other hand however one can find composition regions that are highly desired to work in. For compositions in those regions performance is not too sensitive to Teflon® and Nafion® variations. Catalyst powder, Nafion® and Teflon® form a CL produced by a 2-step preparation method, that leads to good fuel cell performance and excellent structural characteristics for ionomer and electronic conductivity, gas and water transport. Figure 3.3.5-1 suggests 2 regions that were tested in the following. By hypothesis catalysts with a composition of Nafion®:Teflon®:C = 0.875:0.875:1 and with a composition of Nafion®:Teflon®:C = 1.375:0.375:1 should both lead to good CL structures and peak powers of around 0.5 W/cm².

3.3.6 Predicted catalyst layer compositions

In the following the two predicted cathode catalyst layer compositions (Nafion®:Teflon®:C = 0.875:0.875:1 and Nafion®:Teflon®:C = 1.375:0.375:1) are tested and discussed. In Figure 3.3.6-1 one can see the polarization curves and in Figure 3.3.6-2 the power density curves of samples C45 and C49, the catalysts with the 2 optimized compositions.

Both compositions show a good performance in the ohmic region and mass transfer limitations occur at current densities of 1.5 A/cm² or more. Also, as expected, the peak powers of both catalyst samples are at least 0.5 W/cm². That means that the hypothesis drawn from the actual matrix-study is validated and it is indeed suggestive to use catalysts with those compositions.

However, as mentioned earlier in this study, the high air flow rate combined with the interdigitated lead to a very high pressurization of air and thus the concentration at the active sites of the cathode catalyst layer increases. The pressure curves of both samples are plotted in Figure 3.3.6-3.

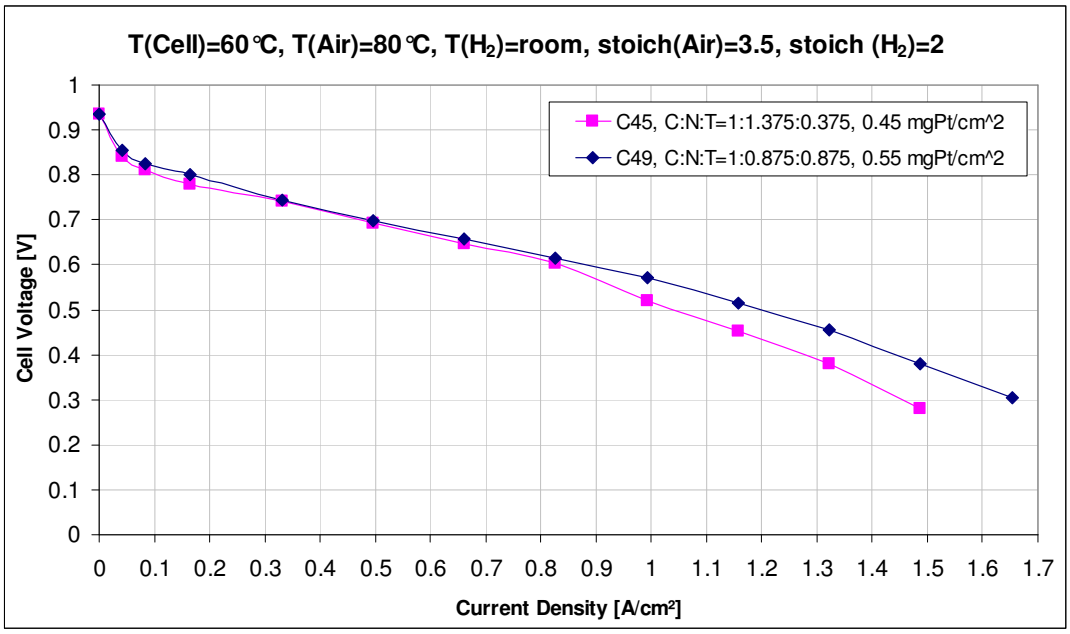

Figure 3.3.6-1. Polarization curves of hypothesized optimized catalyst compositions

The pressure curves show a maximum pressure difference of up to 200 cmH_2O, which equals around 0.21 atm. This means that the pressure within the fuel cell increases by more than 20% from 1 atm to 1.21 atm. According to a model by Kazim et al. [45] a fuel cell running with interdigitated flow fields and pressurized oxygen at 3atm showed a 3 times higher limiting current and 3 times higher peak power than at 1 atm. This is because the gas mole-fraction of oxygen increases with pressure and thus the cell activation over-potential changes.

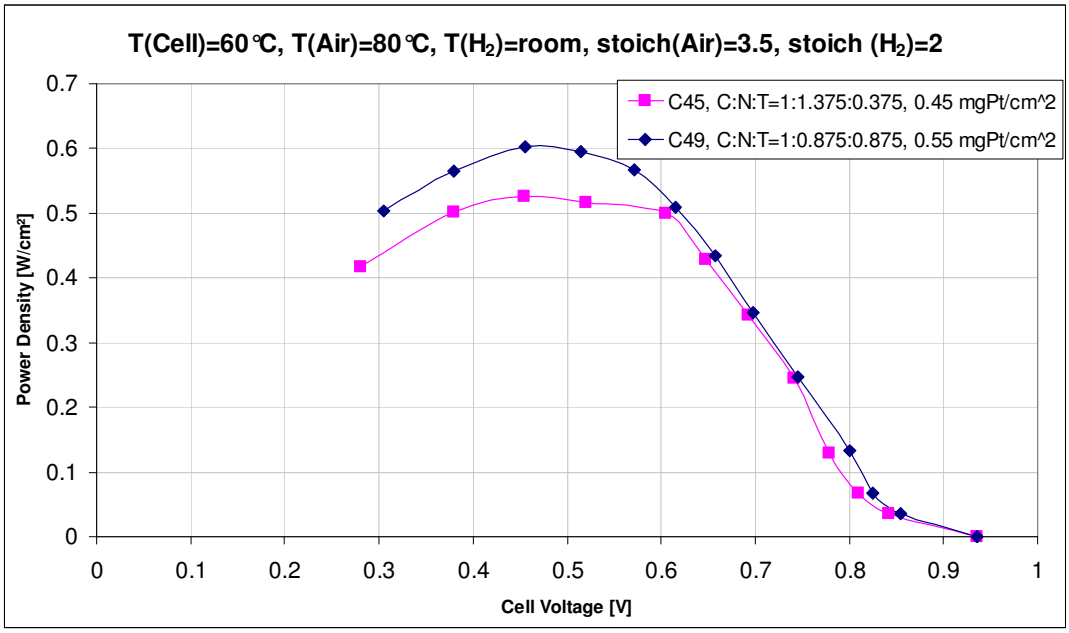

Figure 3.3.6-2. Power density curves of hypothesized optimized catalyst compositions

The same effect might occur in the system of this study although air is used as reactant gas instead of pure oxygen and the degree of pressurization was not as high. To fully understand the phenomena another investigation at lower stoichiometric air flow rates was done.

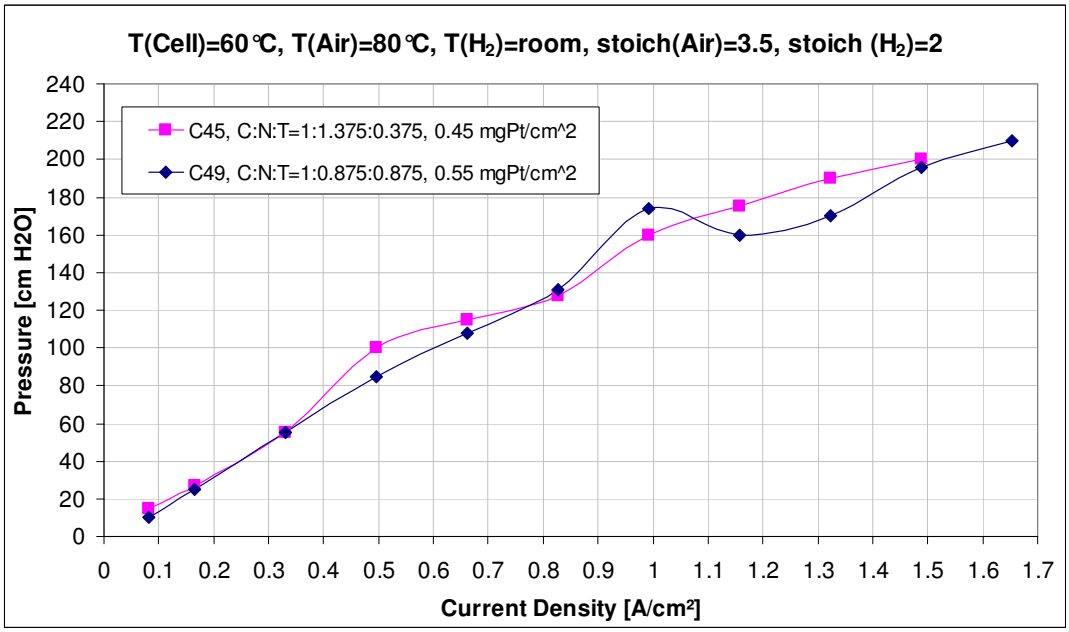

Figure 3.3.6-3. Pressure curves at hypothesized optimized catalyst compositions

3.4 2-step and 1-step catalyst at lower stoichiometric air flow rates

A study at lower stoichiometric air flow rates could show if the same performance advantage of the 2-step prepared catalyst layer can be achieved with lower pressures achieved at air flow rates. Further it might be possible that at high pressures and/or high stoichiometric air flow rates the advantages of a better structure of the 2-step prepared catalyst layer are not significant when comparing it to a regular prepared catalyst layer by simple intermixing of all components. Thus a study with both a 2-step and a 1-step prepared catalyst at a composition of Nafion®:Teflon®:C = 0.875:0.875:0.875:1 and stoichiometric air flow rates of 3.5 and 2 have been made. The results are shown in Figure 3.4-1, Figure 3.4-2.

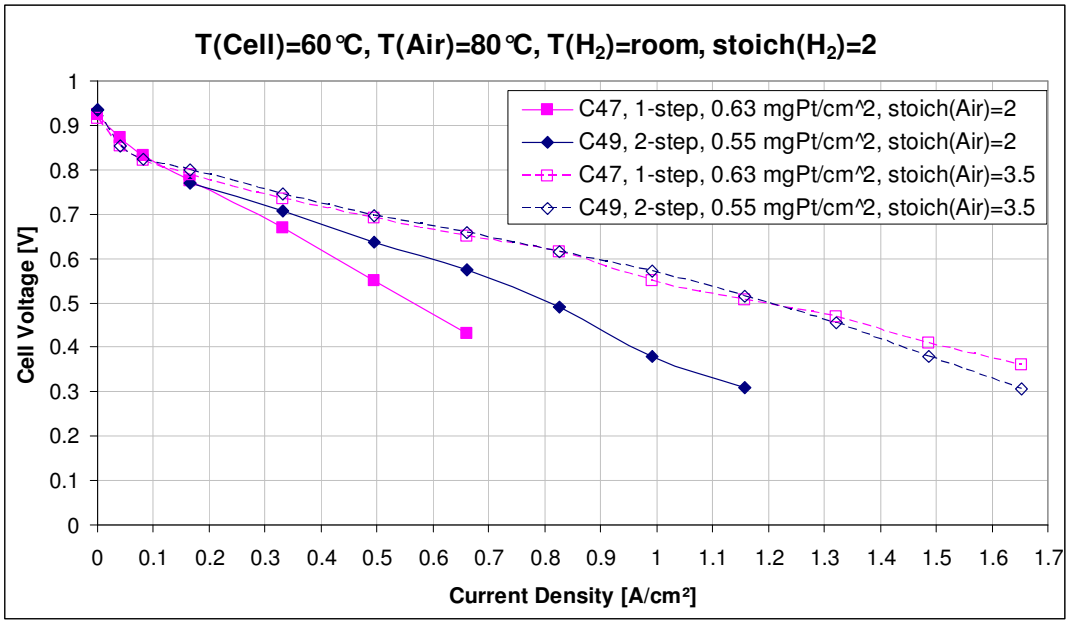

Figure 3.4-1. Polarization curves of a 2-step and 1-step CL with a composition Nafion®:Teflon®:C = 0.875:0.875:0.875:1 at different air flow rates

The graphs clearly show that at lower air flow rates sample C49, prepared with the 2-step method shows better performance than sample C47, which has the same composition, but was prepared without the steam annealing process. Both its limiting current density and the peak power show higher values.

The hypothesis that at high stoichiometric flow rates the advantage of a better structure of sample C49 over sample C47 may not stand out was also validated, since one can see that both catalyst layers lead to almost identical performance. However, from a loading point of view sample C49 is still more desirable than sample C47, since it gives the same performance as sample C47 at a lower loading. However, that would have to be validated in further investigations.

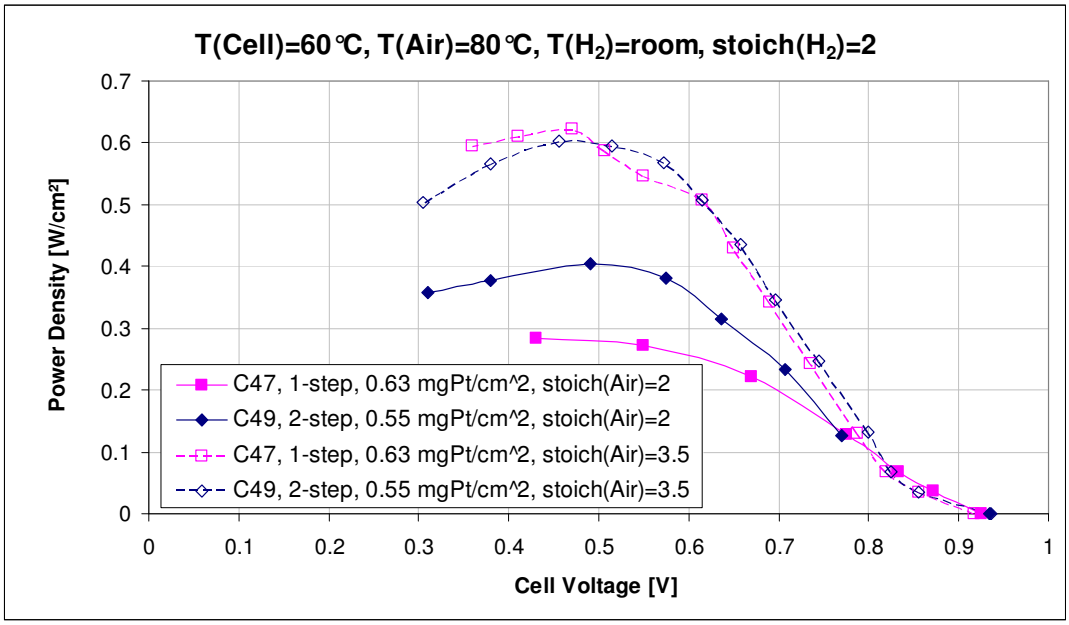

Figure 3.4-2. Power density curves of a 2-step and 1-step CL with a composition Nafion®:Teflon®:C = 0.875:0.875:0.875:1 at different air flow rates

The peak power density of sample C47, the 1-step prepared CL, went down by 50% and that of sample C49, the 2-step prepared CL, was around 33% less when reducing the air flow rate from stoich 3.5 to stoich 2. The limiting current densities of both stoich 2 –cases occur at lower values than at a stoich of 3.5. This was expected, because the lower flow rates resulted in lower concentration of oxygen at the active catalyst sites [45]. There seems to be a structural advantage of the 2-step prepared catalyst layer over the 1-step one, which Nguyen et al. already showed with some sample SEM pictures [39]. Those structural differences seem to show a higher impact on performance at low air flow rates. It makes sense that at low air flow rates a more optimized CL that provides well-structured pathways for gas and liquid transport and since the convective force of the gas flow is not that high, the CL layer itself has to assure for good transport properties. This is in accordance to the observation that the pressurization of sample C47 is higher at higher air flow rates, since the structure is less arranged, so that there is a higher pressure build-up due to structural hindrance.

Chapter 4

Conclusions and Recommendations

4.1 Conclusions

In this work the operating conditions of a PEM fuel cell using interdigitated flow fields, an anode electrode manufactured by TVN Systems with a catalyst coated GDL 35 BC by SGL Carbon and a self-made cathode electrode with the same GDL material, were investigated. It was shown that at a stoichiometric air flow rate of 3.5 and a flow rate of stoich 2 for hydrogen, the fuel cells resulted in good performance. The high flow rate was capable of pushing generated liquid water out of the GDL pores to provide better gas accessibility to the active reaction sites. The fuel cell temperatures were not investigated in-depth but set to a standard temperature of 60°C. Depending on the cell temperature both the cathode and the anode side's humidifier temperatures were examined. The best results were found with asymmetrical temperature settings, i.e. hydrogen entered the cell at room temperature while air was at 80°C. The water carried by the saturated air at this stoichiometric (3.5) flow rate was enough to provide good membrane hydration as well as hydration of the ionic phase in the anode catalyst layer, so that the anode could be fed by dry hydrogen. Back diffusion and permeation from the cathode and anode under these operating conditions were able to sustain membrane and anode catalyst layer hydration while maintaining low flooding condition in the cathode catalyst layer. Flooding at the cathode was minimized by the use of the interdigitated flow field and saturated air at high flow rate. Water vapor carried by air helped to drag liquid water out of the pores in the GDL and gas accessibility was greatly enhanced. The setup with saturated hydrogen and dry air did not work well. The electro-osmotic drag was not able to humidify the membrane and the ionic phase in the cathode, because under these operating conditions ($P_{air} > P_{H2}$ and high flow rate of dry air) the water removal rate from the cathode by evaporation and transport through the cathode GDL and

permeation from the cathode to the anode was too high.

By means of a novel 2-step preparation method a catalyst layer with an optimal structure for electronic, ionic, gas and liquid transport for the cathode of a PEM fuel cell has been made. The catalyst layer consisted of the platinum supported by carbon black catalyst particles, an ionomer phase made of Nafion®, as hydrophilic component, and Teflon®, as hydrophobic component. The first half of Nafion® was steam-annealed onto the catalyst particles in the first step. To achieve a continuous ionomer network and connect the particles, the annealed catalyst agglomerates were cross-linked with additional Nafion® solution in the second step. To create hydrophobic pathways for gas transport in the catalyst layer network, Teflon® was added to the catalyst ink in the second step as well. The steam-annealing in the first step made it possible to incorporate Teflon® without blocking active catalyst sites, but rather placing itself into void spaces created by the catalyst layer structure. Obviously there are limitations for both the amount Nafion® and Teflon® beyond which the catalyst layer becomes electronically non-conductive, since both Nafion® and Teflon® are electronically insulating and an excess would lead to a stretched catalyst layer structure with a disrupted electronic network. Hence a matrix-study with different compositions has been made.

In the first composition study the ratio of Nafion®:C = 0.75 was fixed and Teflon® was increased from Teflon®:C = 0.25 to 1 in 0.25-steps. With increasing Teflon® content the fuel cell performance showed an upward trend. Even at high Teflon® contents the fuel cell showed good performance, so it was concluded that at low Nafion® contents there are sufficient void spaces for Teflon® to be placed and thus the ionomer and electronic network did not become disrupted. It was further shown that a too thick catalyst layer would increase the diffusion resistance for air and thus decrease its concentration at the active catalyst sites resulting in low performance.

The second study was on the fixed ratio Nafion®:C =1 with varying Teflon® likewise from Teflon®:C = 0.25 to 1. It was shown that Teflon® filled up the voids successfully and the performance of the cell increased with Teflon® up to a certain level and then dropped again. Unexpectedly the best performing cell contained more Teflon® than the latter case, although void spaces between agglomerates are smaller. It was further shown that the activation losses were smaller for these cases than the case with less Nafion®. This difference was attributed to the fact that Teflon® was less probable of blocking active catalyst sites, since more Nafion® was annealed onto the catalytic particles.

The third study with Nafion®:C = 1.25 showed clearly that at higher Nafion® contents the effect of Teflon® occurred at lower Teflon® loadings. The best performing catalyst had a Teflon loading of Teflon®:C = 0.25, which was the lowest of all studies made up to then. Those findings supported the reasoning that at higher Nafion® loadings the void volumes between the catalyst particles are smaller and thus less Teflon® can be incorporated. Further it was validated that high Teflon® loadings at high Nafion® loadings result in significant performance loss, since Teflon® placed itself outside of the void spaces and started stretching the ionomer and electronic network.

The last study at a Nafion® content of Nafion®:C = 1.5 showed basically the same as the Nafion®:C = 1.25 – set of data. Again the effects of Teflon® were found to be very strong and a too high content lead to a severe drop in performance, since the total amount of the electronically insulating materials (Nafion® and Teflon®) exceeded a certain limit.

Based on those studies a matrix of peak powers was generated which illustrated clearly compositions regions that are desired or to be avoided. By hypothesis two regions of high peak powers were suggested and two catalyst layers with a composition of (C45) Nafion®:Teflon®:C = 1.375:0.375:1 and (C49) Nafion®:Teflon®:C = 0.875:0.875:1 were prepared. Both catalysts showed peak powers of > 0.5 W/cm², and it was verified that the two hypothetical regions led to

high fuel cell power.

In a last investigation two catalysts at the optimized composition of Nafion®:Teflon®:C = 0.875:0.875:1 were compared. Catalyst C49 was prepared with the 2-step method while the simple single-step intermixing method was used for catalyst C47. It was shown that at a high (3.5) stoichiometric air flow rate the 2-step catalyst didn't show significant advantages over the single-step prepared one. However, at an air flow rate of stoich 2 the peak power of catalyst C47 dropped by 50% while that of catalyst C49 dropped only by 33%. The polarization curve of the 2-step catalyst showed better behavior in the ohmic region as well as a higher limiting current density. Hence it was concluded that at lower air flow rates the structural improvement of the 2-step catalyst played a very significant role. With the 2-step method the optimal arrangement of Nafion® and Teflon® created pathways for good gas and liquid transport.

4.2 Recommendations for Future Works

For a better understanding of the operating conditions future research groups should test all catalyst layers at lower stoichiometric air flow rates and with different flow fields to get an idea whether the 2-step prepared catalyst shows better performance and behavior. Since heat losses of the tubes seemed to be high, heating inlet tubes would yield to more constant saturation of inlet gases and water could not condensate before reaching the fuel cell. Water drag measurements, i.e. measurements of the back diffusion rate and the electro-osmotic drag rate, with neutron imaging and internal cell resistance measurements should be carried out to fully understand temperature and pressure effects on the water transport phenomena in the fuel cell.

However, of bigger importance is to get a better understanding of the phenomena within the catalyst layers. Investigations have to be done on the catalyst structure of the annealed particles. It is surprising that the annealed catalyst particles show a hydrophobic surface, because the annealing takes place in a steam-

environment. Thus one expects the hydrophilic sulfuric groups to place itself towards the water phase and the annealed particles should show a hydrophilic surface. Since the contrary is observed Nafion® seems to polymerize in a way that the hydrophobic CF_2-groups are located at the outside. To fully understand this phenomena the annealed structure should be analyzed. Besides only looking at the surface, the whole annealed agglomerate should be investigated. The distribution of Nafion® and Teflon® in final micro-structure of the catalyst layer should be determined. How does the Nafion® polymerize on the catalyst surface? How does the structure between the agglomerates look? How big are the created void volumes and does Teflon® place itself into the voids? Here one also needs to measure the size of the Teflon® nano-particles in the Teflon® suspension to validate that Teflon® would fit into the voids. The hydrophobic surface of the annealed catalyst could enhance the deposition of Teflon® into the catalytic layer or probably the hydrophobicity is even high enough to leave Teflon® completely out of the catalyst ink. Preliminary studies have already been made with no Teflon®, and all have resulted in good performance.

References

1. http://www.un.org/News/Press/docs//2007/pop952.doc.htm
2. Allen, D.T., and Shonnard, D.R., *Green Engineering: Environmentally Conscious Design of Chemical Processes,* p.11, Table 1.4-1, New Jersey, Prentice Hall PTR (2002)
3. Energy Information Administration (Official Energy Statistics form the U.S. Government), *International Energy Outlook 2007* (2007)
4. William R. Grove, *Philosophical Magazine, Ser. III., XV.* (1839)
5. Hoogers, G., *Fuel Cell Technology Handbook*, p. 1-1 – p.1-2, Boca Raton, CRC Press LLC (2003)
6. Kordesch, K., and Simader, G., *Fuel Cells and Their Applications*, p. 8-11 Weinheim, VCH (1996)
7. http://www.members.tripod.com/trungvannguyen/
8. Nguyen, T. V., *J. Electrochem. Soc.,* **143**, L103 (1996).
9. Hoogers, G., *Fuel Cell Technology Handbook*, p. 3-1 – p.3-12, Boca Raton, CRC Press LLC (2003)
10. Leddy, J., and Fenton J., Proton Exchange Membrane Fuel Cells for Transportation Applications, *ECS Interface Fall 2005* (2005)
11. Gottesfeld, S., and Zawodzinski T., *Advances in Electrochemical Science and Engineering*, Vol. 5, p. 244-249, Weinheim, Wiley-VCH (1997)
12. Kocha, S.S., Principles of MEA preparation, *Handbook of Fuel Cells, Technology and Applications*, Vol. 3,Chapter 43, p. 544-550, John Wiley & Sons (2003)
13. Kordesch, K., and Simader, G., *Fuel Cells and Their Applications*, p. 72-89 Weinheim, VCH (1996)
14. Hoogers, G., *Fuel Cell Technology Handbook*, p. 6-2, Boca Raton, CRC Press LLC (2003)
15. Kordesch, K., and Simader, G., *Fuel Cells and Their Applications*, p. 45-54 Weinheim, VCH (1996)

16. Gottesfeld, S., and Zawodzinski T., *Advances in Electrochemical Science and Engineering*, Vol. 5., p. 198-203, Weinheim, Wiley-VCH (1997)
17. Raistick, I. D., "Proceeding of Symposium on Diagrams, Separators, and Ion Exchanged Membrane," Zee, J. W. V., White, R. E., Kinoshita, K., and Burney, H. S. (Eds.), *The Electrochemical Society, Inc*., Pennington, New York (1986)
18. Srinivasan, S , Ticianelli, E. A., Derouin, C. R., and Redondo, A., *J. Power Sources.*, **22**, 359 (1988)
19. Wilson, M.S., and Gottesfeld, S., *J. Appl. Electrochem.*, **22**, 1 (1992)
20. Wilson, M. S. and Gottesfeld S., *J. Electrochem. Soc.*, **139**, L28 (1992)
21. Poltarzewski, Z., Staiti, P., Alderucci, V., Wieczorek W., and Giordano, N., *J. Electrochem. Soc.*, **139**, 761 (1992)
22. Uchida, M., Aoyama, Y., Eda, N., and Ohta, A., *J. Electrochem. Soc.*, **142**, 4143 (1995)
23. Passalacqua, E., Lufrano, F., Squadrito, G., Patti, A., and Giorgi, L., *Electrochim. Acta*, **43**, 3665 (1998)
24. Lee, S. J., McBreen, J., Rho, Y. W., and Lee, T. H., *Electrochim. Acta*, **43**, 3693 (1998)
25. Cheng, X., Yi, B., Han, M., Zhang, J., Qiao, Y., and Yu, J., *J. Power Sources.*, **79**, 75 (1999)
26. Antolini, E., Giorgi, L., Pozio, A., and Passalacqua, E., *J. Power Sources.*, **77**, 136 (1999)
27. Passalacqua, E., Lufrano, F., Squadrito, G., Patti, A., and Giorgi, L., *Electrochim. Acta*, **46**, 799 (2001)
28. Qi, Z., and Kaufman, A., *J. Power Sources.*, **113**, 37 (2003)
29. Gode, P., Jaouen, F., Lindbergh, G., Lundblad, A., and Sundholm, G., *Electrochim. Acta*, **48**, 4175 (2003)
30. Uchida, M., Aoyama, Y., Eda, N., and Ohta, A., *J. Electrochem. Soc.*, **142**, 463 (1995)

31. Shin, S., Lee, J., Ha, H., Hong, S., Chun, H., and Oh, I., *J. Power Sources.*, **79**, 75 (2002)
32. Wang, Q., Eikerling, Q., Song, D., and Liu, Z., *J. Electroanalytical Chemistry*, **573**, 61 (2004)
33. Wang, Q., Eikerling, M., Song, D., Liu, Z., Navessin, T., Xie, Z., and Holdcroft, S., *J. Electrochem. Soc.*, **151**, 950 (2004)
34. Xie, Z., Navessin, T., Shi, K., Chow, R., Wang, Q., Song, D., Andreaus, B., Eikerling, M., Liu, Z., and Holdcroft, S., *J. Electrochem. Soc.*, **152**, 1171 (2005)
35. Song, D., Wang, Q., Liu, Z., Eikerling, M., Xie, Z., Navessin, T., and Holdcroft, S., *Electrochim. Acta*, **50**, 3347 (2005)
36. Song, D., Wang, Q., Liu, Z., Navessin, T., Eikerling, M., and Holdcroft, S., *J. Power Sources.*, **126**, 104 (2004)
37. Cheng, C., Lin, H., and Lai, G., *J. Power Sources.*, **164**, 730 (2007)
38. Eikerling, M., *J. Electrochem. Soc.*, **153**, 58 (2006)
39. Nguyen, T. V., Natarajan, D., and Jain, R., *ECS Transactions*, **1**, 501 (2006)
40. Litster, S., Buie, C., Fabian, T., Eaton, J., and Santiago, J., *J. Electrochem. Soc.*, **154**, 1049 (2007)
41. Weber, A., and Newman, J., *J. Electrochem. Soc.*, **152**, 677 (2005)
42. Nguyen, Trung Van, private communication
43. Pau Ying Chong, private communication
44. He, W., Lin, G., and Nguyen, T. V., "A Diagnostic Tool to Determine Electrode Flooding in PEM Fuel Cells Using Interdigitated Flow Fields", submitted to *AICHE J.,* (August, 2002)
45. Kazim, A., Forges, P., and Liu, H., *International J. Energy Research*, **27**, 401 (2003)
46. Nguyen, T. V., and White, R., *J. Electrochem. Soc.*, **140**, 2178 (1993)
47. Yan, Q., Toghiani, H., and Wu, J., , *J. Power Sources.*, **158**, 316 (2006)
48. Saleh, M., Okajima, T., Hayase, M., Kitamura, F., and Ohsaka, T., *J. Power Sources.*, **164**, 503 (2007)

A Appendix A

Calculation of catalyst ink preparation with a 2-step method

As a an example a catalyst ink has to be prepared with the following catalyst and ratios

	% of solution/dispersion	ratio C to x
Carbon	1-0.46 = 0.54	
Platinum	0.46	1.1739
Nafion® solution	0.15 = X_{Nafion}	1
Teflon® (dispersed)	0.1 = X_{Teflon}	1

Table A-1. Sample catalyst composition

As you can see a Nafion® solution of 15 wt-% Nafion® in a 80/20 water/IPA solution was used. As Teflon® dispersion a 10 wt-% Teflon® in deionized water was used. Hence one has to differentiate very carefully between Nafion® solution and dry weight of Nafion®. The ratio *r1* of Carbon (C) to platinum (Pt) is obviously fixed by the catalyst powder being used and is calculated by

$$r1\left(\frac{Carbon}{Pt}\right) = \frac{0.54}{0.46} = 1.1739 \qquad (1)$$

Hence all ratios were based on the amount of Carbon in the catalyst (Cat). The ratios *r2* of Carbon/Nafion® (Naf) and *r3* Carbon/Teflon® (Tef) can be varied by adding more or less ionomer solution or Teflon® dispersion. In this example both ratios were set to unity. Based on the used mass of catalyst the total amounts of Nafion® solution and Teflon® dispersion to be used are calculated. For a given mass m(Cat) = 1g, i.e. m(C) = 0.54g and m(Pt) = 0.46g.

$$m(Naf\ \ solution) = \frac{m(C)}{X_{Naf} \cdot r2\left(\frac{C}{Naf}\right)} = \frac{0.54g}{0.15 \cdot 1} = 3.6g \qquad (2)$$

$$m(Tef\ \ dispersion) = \frac{m(C)}{X_{Tef} \cdot r3\left(\frac{C}{Tef}\right)} = \frac{0.54g}{0.1 \cdot 1} = 5.4g \qquad (3)$$

For the 2-step method used in this study, the amount of Nafion® was split to 50:50, i.e. 3.6g/2 = 1.8g Nafion® solution was used per step. Since the preparation of the catalyst ink was being done by hand one has to account for the inexactness of components. Thus we assume that in the first step the added amount of Nafion® solution was

$$m_{1,actual}(Naf\ \ solution) = 1.7g$$

After the heat treatment in the 1st step of the catalyst ink all solvents are evaporated and the only product left is the annealed catalyst containing C, Pt and Nafion®. The 1.7g Nafion® solution contained

$$m_{1,actual}(Naf) = m_{1,actual}(Naf\ \ solution) \cdot X_{Naf} = 1.7g \cdot 0.15 = 0.255g \qquad (4)$$

Hence the total mass of catalyst including the annealed ionomer after the 1st step is

$$m_1(Cat_{annealed}) = m(Cat) + m_{1,actual}(Naf) = 1g + 0.255g = 1.255g \qquad (5)$$

Since the annealed catalyst is placed into a mortar to grind it and then back into a glass vial, one has to account for the mass loss coming along with this operation. Thus the annealed and grinded $Cat_{annealed}$ which is placed back into the vial is weighed. In this example the determined weight was

$$m_{1,actual}(Cat_{annealed}) = 1.2g$$

A new ratio *r3* is defined as

$$r3 = \frac{m_{1,actual}(Cat_{annealed})}{m_1(Cat_{annealed})} = \frac{1.2g}{1.255g} = 0.9562 \quad (6)$$

The catalyst being used now ($m_{1,actual}(Cat_{annealed})$) has still the same ratios *r1*of C/Pt and *r2* of C/Naf, but the total mass is reduced and the calculations for the second step have to consider the decreased mass. The masses of the single components are thus

$$m_{2,actual}(C) = r3 \cdot m(C) = 0.9562 \cdot 0.54g = 0.5163g \quad (7)$$
$$m_{2,actual}(Pt) = r3 \cdot m(Pt) = 0.9562 \cdot 0.46g = 0.4398g \quad (8)$$
$$m_{2,actual}(Naf) = r3 \cdot m_{1,actual}(Naf) = 0.9562 \cdot 0.255g = 0.2438g \quad (9)$$

The amounts of Nafion® and Teflon® to be added in the 2nd step are

$$m_2(Naf\ solution) = r3 \cdot \left(m(Naf\ solution) - m_{1,actual}(Naf\ solution)\right)$$
$$= 0.9562 \cdot (3.6g - 1.7g) = 1.8167g \quad (10)$$
$$m_2(Tef\ dispersion) = r3 \cdot m(Tef\ dispersion) = 0.9562 \cdot 5.4g = 5.1633g \quad (11)$$

Again there has been some inaccuracy when adding the species and the actual masses being added were

$$m_{2,actual}(Naf\ solution) = 1.8g$$
$$m_{2,actual}(Tef\ dispersion) = 5.4g$$

And thus

$$m_{2,actual\ added}(Naf) = X_{Naf} \cdot m_{2,actual}(Naf\ solution) = 0.15 \cdot 1.8g = 0.27g \quad (12)$$
$$m_{2,actual\ added}(Tef) = X_{Tef} \cdot m_{2,actual}(Tef\ dispersion) = 0.1 \cdot 5.4g = 0.54g \quad (13)$$

The total amounts of all components are

$$m_{total}(C) = m_{2,actual}(C) = 0.5163g \quad (14)$$

$$m_{total}(Pt) = m_{2,actual}(Pt) = 0.4398g \quad (15)$$

$$m_{total}(Naf) = m_{2,actual}(Naf) + m_{2,actual\ added}(Naf) = 0.5163g$$

$$= 0.2438g + 0.27g = 0.5138g \quad (16)$$

$$m_{total}(Tef) = m_{2,actual\ added}(Tef) = 0.54g \quad (17)$$

Now the real ratios of the prepared catalyst ink can be calculated. The ratios are normalized with respect to $m_{total}(C)$, which is set to be *normalizer = 1*. Throughout the process *r1* stayed constant at *r1 = 1.1739*.

$$r2_{actual}\left(\frac{C}{Naf}\right) = normalizer \cdot \frac{m_{total}(C)}{m_{total}(Naf)} = 1 \cdot \frac{0.5163g}{0.5138g} = 1.0049 \quad (18)$$

$$r3_{actual}\left(\frac{C}{Tef}\right) = normalizer \cdot \frac{m_{total}(C)}{m_{total}(Tef)} = 1 \cdot \frac{0.5163g}{0.54g} = 0.9562 \quad (19)$$

The prepared catalyst has a composition of

$$C : Pt : Naf : Tef = 1 : \frac{1}{r1} : \frac{1}{r2_{actual}} : \frac{1}{r3_{actual}} \quad (20)$$

$$= 1 : \frac{1}{1.1739} : \frac{1}{1.0049} : \frac{1}{0.9562} = 1 : 0.8519 : 0.9951 : 1.0458$$

Now the GDL can be coated with the prepared catalyst ink. The desired loading is set to *loading = 0.5 mgPt/cm²*. At first the weight of the GDL ((2.7 x 5.2) cm²) is determined. In this sample the mass and the area density of the dry GDL were

$$m_{dry}(GDL) = 0.1615g$$

$$\delta_{area,dry} = \frac{m_{dry}(GDL)}{A_{GDL}} = \frac{0.1615g}{2.7 \cdot 5.2\ cm^2} = 0.115\frac{g}{cm^2} \quad (21)$$

The mass of platinum per gram of the catalyst is

$$x_{Pt} = \frac{1}{r1} \cdot \left(1 + \frac{1}{r1} + \frac{1}{r2_{actual}} + \frac{1}{r3_{actual}}\right)^{-1} = 0.2188\frac{g\ Pt}{g\ Cat} \quad (22)$$

Thus the mass of catalyst which is needed and the total weight of the coated GDL after evaporation of the solvent can be calculated

$$m_{need}(Cat) = \frac{1}{x_{Pt}} loading \cdot A_{GDL} \quad (23)$$

$$= \frac{1}{0.2188\frac{g\ Pt}{g\ Cat}} \cdot 0.0005\frac{g\ Pt}{cm^2} \cdot 14.04\ cm^2 = 0.0321\ g\ Cat$$

$$m_{need}(GDL) = m_{dry}(GDL) + m_{need}(Cat) = 0.1615g + 0.0321g = 0.1936g \quad (24)$$

Since with the brush coating the amount applied onto the GDL can not be determined very precisely, it is unlikely to achieve the desired loading. Thus after having dried the coated GDL is weighed again and the actual loading is calculated

$$m_{actual}(coated\ GDL) = 0.2041g$$

$$m_{actual}(Cat) = m_{actual}(coated\ GDL) - m_{dry}(coated\ GDL) = 0.0426g \quad (25)$$

$$loading_{actual} = \frac{m_{actual}(Cat) \cdot x_{Pt}}{A_{GDL}} = 0.000664\frac{g\ Pt}{cm^2} = 0.664\frac{mg\ Pt}{cm^2} \quad (26)$$

B Appendix B

Calculation of the stoichiometric gas flow rates

In order to operate a fuel cell the stoichiometric flow rates have to be adjusted based on the current drawn from the cell. Since the gas flow rates are adjusted before the gases enter the humidification bottles, the densities of hydrogen, oxygen and air were based on the ideal gas law at *T = 298.15K* and *p = 101 325 Pa*. It was assumed that air consisted of 21% oxygen, i.e. $x_{O_2} = 0.21$. The electrons transported by the gas molecules are

$$n_{e^-}(H_2) = 2$$
$$n_{e^-}(O_2) = 4$$

The stoichiometric flow rates are calculated by

$$F = stoich \cdot \frac{I}{n_{e^-} \cdot Faraday} \left[\frac{mol}{s}\right] \quad (1)$$

With the current I [A] and Faraday constant = 96485.3415 C / mole of electrons.

$$F(H_2) = stoich \cdot \frac{I}{2 \cdot Faraday} \quad (2)$$
$$F(O_2) = stoich \cdot \frac{I}{4 \cdot Faraday} \quad (3)$$
$$F(Air) = \frac{F(O_2)}{x_{O_2}} \quad (4)$$

Since the flow rate controllers have units of cm³/min, Equation (1) needs to be converted with $\Re = 8.314 \frac{J}{mol - K}$ assuming the ideal gas law into

$$F_{controller} = \frac{F \cdot \Re \cdot T \cdot 10^6 cm^3}{p \cdot \frac{1}{60}\ [\text{min}]} \quad (5)$$

I [A]	F(Air) [mol/s]	F(Air) [cm^3/min]	F(Hydrogen) [mol/s]	F(Hydrogen) [cm^3/*min]
0.2	8.64E-06	12.68	2.07E-06	3.04
0.4	1.73E-05	25.36	4.15E-06	6.09
0.6	2.59E-05	38.03	6.22E-06	9.13
0.8	3.45E-05	50.71	8.29E-06	12.17
1	4.32E-05	63.39	1.04E-05	15.21
1.2	5.18E-05	76.07	1.24E-05	18.26
1.4	6.05E-05	88.74	1.45E-05	21.30
1.6	6.91E-05	101.42	1.66E-05	24.34
1.8	7.77E-05	114.10	1.87E-05	27.38
2	8.64E-05	126.78	2.07E-05	30.43
2.2	9.50E-05	139.45	2.28E-05	33.47
2.4	1.04E-04	152.13	2.49E-05	36.51
2.6	1.12E-04	164.81	2.69E-05	39.55
2.8	1.21E-04	177.49	2.90E-05	42.60
3	1.30E-04	190.16	3.11E-05	45.64
3.2	1.38E-04	202.84	3.32E-05	48.68
3.4	1.47E-04	215.52	3.52E-05	51.72
3.6	1.55E-04	228.20	3.73E-05	54.77
3.8	1.64E-04	240.87	3.94E-05	57.81
4	1.73E-04	253.55	4.15E-05	60.85
4.2	1.81E-04	266.23	4.35E-05	63.90
4.4	1.90E-04	278.91	4.56E-05	66.94
4.6	1.99E-04	291.58	4.77E-05	69.98
4.8	2.07E-04	304.26	4.97E-05	73.02
5	2.16E-04	316.94	5.18E-05	76.07
5.2	2.25E-04	329.62	5.39E-05	79.11
5.4	2.33E-04	342.30	5.60E-05	82.15
5.6	2.42E-04	354.97	5.80E-05	85.19
5.8	2.50E-04	367.65	6.01E-05	88.24
6	2.59E-04	380.33	6.22E-05	91.28
6.2	2.68E-04	393.01	6.43E-05	94.32
6.4	2.76E-04	405.68	6.63E-05	97.36
6.6	2.85E-04	418.36	6.84E-05	100.41
6.8	2.94E-04	431.04	7.05E-05	103.45
7	3.02E-04	443.72	7.25E-05	106.49
7.2	3.11E-04	456.39	7.46E-05	109.53
7.4	3.20E-04	469.07	7.67E-05	112.58
7.6	3.28E-04	481.75	7.88E-05	115.62
7.8	3.37E-04	494.43	8.08E-05	118.66
8	3.45E-04	507.10	8.29E-05	121.70
8.2	3.54E-04	519.78	8.50E-05	124.75
8.4	3.63E-04	532.46	8.71E-05	127.79
8.6	3.71E-04	545.14	8.91E-05	130.83
8.8	3.80E-04	557.81	9.12E-05	133.88

9	3.89E-04	570.49	9.33E-05	136.92
9.2	3.97E-04	583.17	9.54E-05	139.96
9.4	4.06E-04	595.85	9.74E-05	143.00
9.6	4.15E-04	608.52	9.95E-05	146.05
9.8	4.23E-04	621.20	1.02E-04	149.09
10	4.32E-04	633.88	1.04E-04	152.13

Table B-1. Flow rates of stoich(Air) = 3.5 and stoich(Hydrogen) = 2

C Appendix C

Raw Data

C.1 Nafion®:C = 0.75

C.1.1 Teflon®:C = 0.25, Catalyst C27

Real ratio: C:Pt:Nafion®:Teflon® = 1:0.86:0.73:0.25.

Loading: 0.51 mg Pt/ cm².

T(Cell) = 60°C

T(Air) = 80°C

Stoich(Air) = 3.5

Stoich(Hydrogen) = 2

I [A]	i [A/cm2]	U [V]	p [W/cm²]	dp [cmH2O]
0	0.000	0.932	0.000	
0.2	0.041	0.834	0.034	
0.4	0.083	0.804	0.066	10
0.6	0.124			
0.8	0.165	0.762	0.126	16
1	0.207			
1.2	0.248	0.727	0.180	21
1.4	0.289			
1.6	0.331	0.690	0.228	31
1.8	0.372			
2	0.413	0.610	0.252	43
2.2	0.455			
2.4	0.496	0.520	0.258	52
2.6	0.537			
2.8	0.579	0.440	0.255	60
3	0.620			
3.2	0.661	0.365	0.241	70

Table C.1.1-1. C27 at T(Air) = 80°C and T(Hydrogen) = room

I [A]	i [A/cm2]	U [V]	p [W/cm²]	dp [cmH2O]
0	0.000	0.935	0.000	
0.2	0.041	0.835	0.035	
0.4	0.083	0.790	0.065	7
0.6	0.124			
0.8	0.165	0.750	0.124	21
1	0.207			

1.2	0.248	0.700	0.174	32
1.4	0.289			
1.6	0.331			
1.8	0.372			
2	0.413	0.630	0.260	52
2.2	0.455			
2.4	0.496			
2.6	0.537			
2.8	0.579	0.440	0.255	65

Table C.1.1-2. C27 at T(Air) = 80°C and T(Hydrogen) = 65°C

C.1.2 Teflon®:C = 0. 5, Catalyst C28

Real ratio: C:Pt:Nafion®:Teflon® = 1:0.86:0.77:0.49.

Loading: 0.55 mg Pt/ cm².

T(Cell) = 60°C

Stoich(Air) = 3.5

Stoich(Hydrogen) = 2

I [A]	i [A/cm2]	U [V]	p [W/cm²]	dp [cmH2O]
0	0.000	0.920	0.000	
0.2	0.041	0.841	0.035	
0.4	0.083	0.806	0.067	7
0.6	0.124			
0.8	0.165	0.779	0.129	16
1	0.207			
1.2	0.248	0.751	0.186	32
1.4	0.289			
1.6	0.331	0.724	0.239	44
1.8	0.372			
2	0.413	0.692	0.286	67
2.2	0.455			
2.4	0.496	0.669	0.332	70
2.6	0.537			
2.8	0.579	0.657	0.380	80
3	0.620			
3.2	0.661	0.633	0.419	82
3.4	0.702			
3.6	0.744	0.605	0.450	93

3.8	0.785			
4	0.826	0.580	0.479	102
4.2	0.868			
4.4	0.909	0.557	0.506	112
4.6	0.950			
4.8	0.992	0.520	0.516	123
5	1.033			
5.2	1.074	0.488	0.524	122
5.4	1.116			
5.6	1.157	0.453	0.524	124
5.8	1.198			
6	1.240	0.410	0.508	134
6.2	1.281			
6.4	1.322	0.372	0.492	138

Table C.1.2-1. C28 at T(Air) = 80°C and T(Hydrogen) = room

I [A]	**i [A/cm2]**	**U [V]**	**p [W/cm²]**	**dp [cmH2O]**
0	0.000	0.925	0.000	
0.2	0.041	0.855	0.035	
0.4	0.083	0.815	0.067	8
0.6	0.124			
0.8	0.165	0.783	0.129	
1	0.207			
1.2	0.248			
1.4	0.289			
1.6	0.331	0.732	0.242	34
1.8	0.372			
2	0.413			
2.2	0.455			
2.4	0.496	0.675	0.335	60
2.6	0.537			
2.8	0.579			
3	0.620			
3.2	0.661	0.624	0.413	78
3.4	0.702			
3.6	0.744			
3.8	0.785			
4	0.826	0.590	0.488	110
4.2	0.868			
4.4	0.909			
4.6	0.950			
4.8	0.992	0.530	0.526	120
5	1.033			
5.2	1.074			
5.4	1.116			

5.6	1.157	0.455	0.526	

Table C.1.2-2. C28 at T(Air) = 80°C and T(Hydrogen) = 65°C

I [A]	i [A/cm2]	U [V]	p [W/cm²]	dp [cmH2O]
0	0.000	0.924	0.000	
0.2	0.041	0.831	0.034	
0.4	0.083	0.799	0.066	8
0.6	0.124			
0.8	0.165	0.772	0.128	12
1	0.207			
1.2	0.248			
1.4	0.289			
1.6	0.331	0.710	0.235	18
1.8	0.372			
2	0.413			
2.2	0.455			
2.4	0.496	0.645	0.320	28
2.6	0.537			
2.8	0.579			
3	0.620			
3.2	0.661	0.555	0.367	33
3.4	0.702			
3.6	0.744			
3.8	0.785			
4	0.826	0.350	0.289	40

Table C.1.2-3. C28 at T(Air) = room and T(Hydrogen) = 65°C

C.1.3 Teflon®:C = 0.75, Catalyst C29_2

Real ratio: C:Pt:Nafion®:Teflon® = 1:0.86:0.75:0.74.

Loading: 0.65 mg Pt/ cm².

T(Cell) = 60°C

T(Air) = 80°C

T(Hydrogen) = room

Stoich(Air) = 3.5

Stoich(Hydrogen) = 2

I [A]	i [A/cm2]	U [V]	p [W/cm²]	dp [cmH2O]
0	0.000	0.925	0.000	
0.2	0.041	0.829	0.034	
0.4	0.083	0.795	0.066	
0.6	0.124			
0.8	0.165	0.773	0.128	
1	0.207			
1.2	0.248	0.742	0.184	
1.4	0.289			
1.6	0.331	0.712	0.235	
1.8	0.372			
2	0.413	0.682	0.282	
2.2	0.455			
2.4	0.496	0.657	0.326	
2.6	0.537			
2.8	0.579	0.620	0.359	
3	0.620			
3.2	0.661	0.585	0.387	
3.4	0.702			
3.6	0.744	0.547	0.407	
3.8	0.785			
4	0.826	0.500	0.413	
4.2	0.868			
4.4	0.909	0.475	0.432	
4.6	0.950			
4.8	0.992	0.463	0.459	
5	1.033			
5.2	1.074	0.410	0.440	
5.4	1.116			
5.6	1.157	0.355	0.411	

Table C.1.3-1. C29_2 at T(Air) = 80°C and T(Hydrogen) = room

C.1.4 Teflon®:C = 1, Catalyst C30

Real ratio: C:Pt:Nafion®:Teflon® = 1:0.86:0.77:1.00.

Loading: 0.48 mg Pt/ cm².

T(Cell) = 60°C

Stoich(Hydrogen) = 2

I [A]	i [A/cm2]	U [V]	p [W/cm²]	dp [cmH2O]
0	0.000	0.920	0.000	
0.2	0.041	0.850	0.035	
0.4	0.083	0.815	0.067	12
0.6	0.124			
0.8	0.165	0.782	0.129	24
1	0.207			
1.2	0.248	0.758	0.188	32
1.4	0.289			
1.6	0.331	0.730	0.241	55
1.8	0.372			
2	0.413	0.708	0.293	76
2.2	0.455			
2.4	0.496	0.682	0.338	93
2.6	0.537			
2.8	0.579	0.660	0.382	100
3	0.620			
3.2	0.661	0.642	0.424	110
3.4	0.702			
3.6	0.744	0.616	0.458	120
3.8	0.785			
4	0.826	0.567	0.469	128
4.2	0.868			
4.4	0.909	0.540	0.491	133
4.6	0.950			
4.8	0.992	0.507	0.503	140
5	1.033			
5.2	1.074	0.460	0.494	150
5.4	1.116			
5.6	1.157	0.425	0.492	150
5.8	1.198			
6	1.240			
6.2	1.281	0.300	0.384	

Table C.1.4-1. C30 at T(Air) = 80°C, stoich(Air)=3.5 and T(Hydrogen) = room

I [A]	i [A/cm2]	U [V]	p [W/cm²]	dp [cmH2O]
0	0.000	0.920	0.000	
0.2	0.041	0.846	0.035	
0.4	0.083	0.811	0.067	13
0.6	0.124			
0.8	0.165	0.782	0.129	23
1	0.207			
1.2	0.248			
1.4	0.289			
1.6	0.331	0.726	0.240	44

1.8	0.372			
2	0.413			
2.2	0.455			
2.4	0.496	0.678	0.336	60
2.6	0.537			
2.8	0.579			
3	0.620			
3.2	0.661	0.626	0.414	101
3.4	0.702			
3.6	0.744			
3.8	0.785			
4	0.826	0.563	0.465	120
4.2	0.868			
4.4	0.909			
4.6	0.950			
4.8	0.992	0.488	0.484	

Table C.1.4-2. C30 at T(Air) = 80°C, stoich(Air)=3.5 and T(Hydrogen) = 65°C

I [A]	i [A/cm2]	U [V]	p [W/cm²]	dp [cmH2O]
0	0.000	0.926	0.000	
0.2	0.041	0.830	0.034	
0.4	0.083	0.795	0.066	7
0.6	0.124			
0.8	0.165	0.765	0.126	14
1	0.207			
1.2	0.248			
1.4	0.289			
1.6	0.331	0.694	0.229	21
1.8	0.372			
2	0.413			
2.2	0.455			
2.4	0.496	0.615	0.305	31
2.6	0.537			
2.8	0.579			
3	0.620			
3.2	0.661	0.516	0.341	43
3.4	0.702			
3.6	0.744			
3.8	0.785			
4	0.826	0.430	0.355	47

Table C.1.4-3. C30 at T(Air) = room, stoich(Air)=3.5 and T(Hydrogen) = 65°C

I [A]	i [A/cm2]	U [V]	p [W/cm²]	dp [cmH2O]
0	0.000			
0.2	0.041			
0.4	0.083			
0.6	0.124			
0.8	0.165	0.765	0.126	17
1	0.207			
1.2	0.248			
1.4	0.289			
1.6	0.331	0.695	0.230	40
1.8	0.372			
2	0.413			
2.2	0.455			
2.4	0.496	0.635	0.315	
2.6	0.537			
2.8	0.579			
3	0.620			
3.2	0.661	0.565	0.374	63
3.4	0.702			
3.6	0.744			
3.8	0.785			
4	0.826	0.466	0.385	86
4.2	0.868			
4.4	0.909			
4.6	0.950			
4.8	0.992	0.380	0.377	100
5	1.033			
5.2	1.074			
5.4	1.116			
5.6	1.157	0.270	0.312	115

Table C.1.4-4. C30 at T(Air) = 80°C, stoich(Air)=2 and T(Hydrogen) = room

C.2 Nafion®:C = 1

C.2.1 Teflon®:C = 0.25, Catalyst C37

Real ratio: C:Pt:Nafion®:Teflon® = 1:0.96:1.04:0.26.

Loading: 0.55 mg Pt/ cm².

T(Cell) = 60°C

T(Air) = 80°C

T(Hydrogen) = room

Stoich(Air) = 3.5

Stoich(Hydrogen) = 2

I [A]	i [A/cm2]	U [V]	p [W/cm²]	dp [cmH2O]
0	0.000	0.931	0.000	
0.2	0.041	0.869	0.036	
0.4	0.083	0.828	0.068	9
0.6	0.124			
0.8	0.165	0.800	0.132	23
1	0.207			
1.2	0.248			
1.4	0.289			
1.6	0.331	0.740	0.245	40
1.8	0.372			
2	0.413			
2.2	0.455			
2.4	0.496	0.683	0.339	65
2.6	0.537			
2.8	0.579			
3	0.620			
3.2	0.661	0.623	0.412	83
3.4	0.702			
3.6	0.744			
3.8	0.785			
4	0.826	0.560	0.463	118
4.2	0.868			
4.4	0.909			
4.6	0.950			
4.8	0.992	0.455	0.451	120
5	1.033			
5.2	1.074			
5.4	1.116			
5.6	1.157	0.362	0.419	140

Table C.2.1-1. C37 at T(Air) = 80°C and T(Hydrogen) = room

C.2.2 Teflon®:C = 0.25, Catalyst C11

Real ratio: C:Pt:Nafion®:Teflon® = 1:0.86:1.04:0.28.

Loading: 0.55 mg Pt/ cm².

T(Cell) = 50°C

Stoich(Hydrogen) = 2

T(Air) [°C]	room	room	room	40	60	80	80
Stoich(Air)	3.5	2.5	3.5	3.5	3.5	3.5	3.5
T(H2) [°C]	70	70	55	55	55	55	70
U [V]	i [A]	i [A]	i [A]	i [A]	i [A]	i [A]	i [A]
0.4	3.22	2.43	2.91	2.88	4.43	4.65	4.67
0.5	2.99	2.2	2.52	2.38	3.64	3.85	3.94
0.6	2.27	1.87	2.04	1.93	2.69	2.94	3.07

Table C.2.2-1. C11 at various operating conditions

C.2.3 Teflon®:C = 0. 5, Catalyst C38

Real ratio: C:Pt:Nafion®:Teflon® = 1:0.96:0.98:0.50.

Loading: 0.59 mg Pt/ cm².

T(Cell) = 60°C

T(Air) = 80°C

Stoich(Air) = 3.5

Stoich(Hydrogen) = 2

I [A]	i [A/cm2]	U [V]	p [W/cm²]	dp [cmH2O]
0	0.000	0.945	0.000	
0.2	0.041	0.849	0.035	
0.4	0.083	0.820	0.068	13
0.6	0.124			
0.8	0.165	0.790	0.131	27
1	0.207			
1.2	0.248			
1.4	0.289			
1.6	0.331	0.715	0.236	64
1.8	0.372			
2	0.413			
2.2	0.455			
2.4	0.496	0.633	0.314	108

2.6	0.537			
2.8	0.579			
3	0.620			
3.2	0.661	0.560	0.370	122
3.4	0.702			
3.6	0.744			
3.8	0.785			
4	0.826	0.480	0.397	140
4.2	0.868			
4.4	0.909			
4.6	0.950			
4.8	0.992	0.380	0.377	180
5	1.033			
5.2	1.074			
5.4	1.116			
5.6	1.157	0.280	0.324	190

Table C.2.3-1. C38 at T(Air) = 80°C and T(Hydrogen) = room

I [A]	i [A/cm2]	U [V]	p [W/cm²]	dp [cmH2O]
0	0.000	0.942	0.000	
0.2	0.041	0.857	0.035	
0.4	0.083	0.830	0.069	21
0.6	0.124			
0.8	0.165			
1	0.207			
1.2	0.248			
1.4	0.289			
1.6	0.331	0.680	0.225	60
1.8	0.372			
2	0.413			
2.2	0.455			
2.4	0.496	0.624	0.309	90
2.6	0.537			
2.8	0.579			
3	0.620			
3.2	0.661	0.559	0.370	112
3.4	0.702			
3.6	0.744			
3.8	0.785			
4	0.826	0.450	0.372	150
4.2	0.868			
4.4	0.909			
4.6	0.950			
4.8	0.992	0.370	0.367	170
5	1.033			

5.2	1.074			
5.4	1.116			
5.6	1.157	0.000	0.000	

Table C.2.3-2. C38 at T(Air) = 80°C and T(Hydrogen) = 65°C

C.2.4 Teflon®:C = 0. 5, Catalyst C19

Real ratio: C:Pt:Nafion®:Teflon® = 1:0.86:1.07:0.56.

Loading: 0.9 mg Pt/ cm².

T(Cell) = 60°C

T(Air) = room

Stoich(Air) = 3.5

Stoich(Hydrogen) = 2

I [A]	i [A/cm2]	U [V]	p [W/cm²]	dp [cmH2O]
0	0.000	0.962	0.000	
0.2	0.041	0.853	0.035	
0.4	0.083	0.814	0.067	
0.6	0.124			
0.8	0.165	0.789	0.130	
1	0.207			
1.2	0.248	0.755	0.187	
1.4	0.289			
1.6	0.331	0.719	0.238	
1.8	0.372			
2	0.413	0.685	0.283	
2.2	0.455			
2.4	0.496	0.644	0.319	
2.6	0.537			
2.8	0.579	0.604	0.349	
3	0.620			
3.2	0.661	0.553	0.366	
3.4	0.702			
3.6	0.744	0.498	0.370	
3.8	0.785			
4	0.826	0.460	0.380	

Table C.2.4-1. C19 at T(Air) = room and T(Hydrogen) = 70°C

I [A]	i [A/cm2]	U [V]	p [W/cm²]	dp [cmH2O]
0	0.000	0.951	0.000	
0.2	0.041	0.869	0.036	
0.4	0.083	0.830	0.069	
0.6	0.124			
0.8	0.165	0.798	0.132	
1	0.207			
1.2	0.248	0.763	0.189	
1.4	0.289			
1.6	0.331	0.729	0.241	
1.8	0.372			
2	0.413	0.694	0.287	
2.2	0.455			
2.4	0.496	0.654	0.324	
2.6	0.537			
2.8	0.579	0.615	0.356	
3	0.620			
3.2	0.661	0.559	0.370	
3.4	0.702			
3.6	0.744	0.433	0.322	

Table C.2.4-2. C19 at T(Air) = room and T(Hydrogen) = 60°C

C.2.5 Teflon®:C = 0.75, Catalyst C39

Real ratio: C:Pt:Nafion®:Teflon® = 1:0.96:1.00:0.76.

Loading: 0.49 mg Pt/ cm².

T(Cell) = 60°C

T(Air) = 80°C

T(Hydrogen) = room

Stoich(Air) = 3.5

Stoich(Hydrogen) = 2

I [A]	i [A/cm2]	U [V]	p [W/cm²]	dp [cmH2O]
0	0.000	0.937	0.000	
0.2	0.041	0.833	0.034	
0.4	0.083	0.797	0.066	15
0.6	0.124			
0.8	0.165	0.775	0.128	24

1	0.207			
1.2	0.248			
1.4	0.289			
1.6	0.331	0.722	0.239	58
1.8	0.372			
2	0.413			
2.2	0.455			
2.4	0.496	0.683	0.339	110
2.6	0.537			
2.8	0.579			
3	0.620			
3.2	0.661	0.625	0.413	126
3.4	0.702			
3.6	0.744			
3.8	0.785			
4	0.826	0.585	0.483	141
4.2	0.868			
4.4	0.909			
4.6	0.950			
4.8	0.992	0.538	0.534	165
5	1.033			
5.2	1.074			
5.4	1.116			
5.6	1.157	0.514	0.595	200
5.8	1.198			
6	1.240			
6.2	1.281			
6.4	1.322	0.455	0.602	225
6.6	1.364			
6.8	1.405			
7	1.446			
7.2	1.488	0.380	0.565	0.245

Table C.2.5-1. C19_2 at T(Air) = 80°C and T(Hydrogen) = room

C.2.6 Teflon®:C = 1, Catalyst C23

Desired ratio: C:Pt:Nafion®:Teflon® = 1:0.86:1.00:1.00

Real ratio: Data lost.

Loading: 0.58 mg Pt/ cm².

T(Cell) = 60°C

T(Air) = 80°C

T(Hydrogen) = room

Stoich(Air) = 3.5

Stoich(Hydrogen) = 2

I [A]	i [A/cm2]	U [V]	p [W/cm²]	dp [cmH2O]
0	0.000	0.917	0.000	
0.2	0.041	0.850	0.035	
0.4	0.083	0.820	0.068	10
0.6	0.124			
0.8	0.165	0.791	0.131	14
1	0.207			
1.2	0.248	0.765	0.190	
1.4	0.289			
1.6	0.331			
1.8	0.372			
2	0.413	0.722	0.298	35
2.2	0.455			
2.4	0.496			
2.6	0.537			
2.8	0.579	0.678	0.392	85
3	0.620			
3.2	0.661			
3.4	0.702			
3.6	0.744	0.619	0.460	112
3.8	0.785			
4	0.826			
4.2	0.868			
4.4	0.909	0.565	0.514	115
4.6	0.950			
4.8	0.992			
5	1.033			
5.2	1.074	0.505	0.543	130
5.4	1.116			
5.6	1.157			
5.8	1.198			
6	1.240	0.428	0.531	155

Table C.2.6-1. C23 at T(Air) = 80°C and T(Hydrogen) = room

C.3 Nafion®:C = 1.25

C.3.1 Teflon®:C = 0.25, Catalyst C24

Real ratio: C:Pt:Nafion®:Teflon® = 1:0.86:1.28:0.24.

Loading: 0.56 mg Pt/ cm².

T(Cell) = 60°C

T(Air) = 80°C

T(Hydrogen) = room

Stoich(Air) = 3.5

Stoich(Hydrogen) = 2

I [A]	i [A/cm2]	U [V]	p [W/cm²]	dp [cmH2O]
0	0.000	0.933	0.000	
0.2	0.041	0.843	0.035	
0.4	0.083	0.811	0.067	9
0.6	0.124			
0.8	0.165	0.785	0.130	16
1	0.207			
1.2	0.248			
1.4	0.289			
1.6	0.331	0.741	0.245	52
1.8	0.372			
2	0.413			
2.2	0.455			
2.4	0.496	0.697	0.346	80
2.6	0.537			
2.8	0.579			
3	0.620			
3.2	0.661	0.659	0.436	125
3.4	0.702			
3.6	0.744			
3.8	0.785			
4	0.826	0.622	0.514	148
4.2	0.868			
4.4	0.909			
4.6	0.950			
4.8	0.992	0.583	0.578	171
5	1.033			

5.2	1.074			
5.4	1.116			
5.6	1.157	0.538	0.622	194
5.8	1.198			
6	1.240			
6.2	1.281			
6.4	1.322	0.495	0.655	215
6.6	1.364			
6.8	1.405			
7	1.446			
7.2	1.488	0.445	0.662	230
7.4	1.529			
7.6	1.570	0.421	0.661	237
7.8	1.612			
8	1.653	0.383	0.633	243

Table C.3.1-1. C24 at T(Air) = 80°C and T(Hydrogen) = room

C.3.2 Teflon®:C = 0. 5, Catalyst 21

Real ratio: C:Pt:Nafion®:Teflon® = 1:0.86:1.23:0.49.

Loading: 0.70 mg Pt/ cm².

T(Cell) = 60°C

T(Air) = 80°C

Stoich(Air) = 3.5

Stoich(Hydrogen) = 2

I [A]	i [A/cm2]	U [V]	p [W/cm²]	dp [cmH2O]
0	0.000	0.926	0.000	
0.2	0.041	0.840	0.035	7
0.4	0.083	0.805	0.067	7
0.6	0.124			
0.8	0.165	0.792	0.131	17
1	0.207			
1.2	0.248	0.767	0.190	32
1.4	0.289			
1.6	0.331	0.740	0.245	68
1.8	0.372			
2	0.413	0.706	0.292	73

2.2	0.455			
2.4	0.496	0.675	0.335	83
2.6	0.537			
2.8	0.579	0.655	0.379	90
3	0.620			
3.2	0.661	0.645	0.426	115
3.4	0.702			
3.6	0.744	0.607	0.451	
3.8	0.785			
4	0.826	0.600	0.496	127
4.2	0.868			
4.4	0.909	0.575	0.523	
4.6	0.950			
4.8	0.992	0.558	0.553	140
5	1.033			
5.2	1.074	0.545	0.586	152
5.4	1.116			
5.6	1.157	0.525	0.607	167
5.8	1.198			
6	1.240	0.498	0.617	173
6.2	1.281			
6.4	1.322	0.455	0.602	170
6.6	1.364			
6.8	1.405	0.390	0.548	170

Table C.3.2-1. C21 at T(Air) = 80°C and T(Hydrogen) = room

I [A]	**i [A/cm2]**	**U [V]**	**p [W/cm²]**	**dp [cmH2O]**
0	0.000	0.926	0.000	
0.2	0.041	0.835	0.035	7
0.4	0.083	0.800	0.066	7
0.6	0.124		0.000	
0.8	0.165	0.775	0.128	10
1	0.207		0.000	
1.2	0.248	0.715	0.177	25
1.4	0.289		0.000	
1.6	0.331	0.671	0.222	
1.8	0.372		0.000	
2	0.413	0.600	0.248	45
2.2	0.455		0.000	
2.4	0.496	0.550	0.273	45
2.6	0.537		0.000	
2.8	0.579	0.450	0.260	

Table C.3.2-2. C21 at T(Air) = room and T(Hydrogen) = 65°C

C.3.3 Teflon®:C = 0.75, Catalyst C22

Real ratio: C:Pt:Nafion®:Teflon® = 1:0.86:1.25:0.75.

Loading: 0.6 mg Pt/ cm².

T(Cell) = 60°C

T(Air) = 80°C

Stoich(Air) = 3.5

Stoich(Hydrogen) = 2

I [A]	i [A/cm2]	U [V]	p [W/cm²]	dp [cmH2O]
0	0.000	0.930	0.000	
0.2	0.041	0.830	0.034	
0.4	0.083	0.795	0.066	11
0.6	0.124			
0.8	0.165	0.757	0.125	20
1	0.207			
1.2	0.248	0.710	0.176	38
1.4	0.289			
1.6	0.331	0.645	0.213	
1.8	0.372			
2	0.413	0.580	0.240	
2.2	0.455			
2.4	0.496	0.500	0.248	88

Table C.3.3-1. C22 at T(Air) = 80°C and T(Hydrogen) = room

I [A]	i [A/cm2]	U [V]	p [W/cm²]	dp [cmH2O]
0	0.000	0.941	0.000	
0.2	0.041	0.824	0.034	10
0.4	0.083	0.795	0.066	10
0.6	0.124			
0.8	0.165	0.735	0.121	20
1	0.207			
1.2	0.248	0.660	0.164	46
1.4	0.289			
1.6	0.331	0.620	0.205	66
1.8	0.372			
2	0.413	0.595	0.246	84
2.2	0.455			
2.4	0.496	0.550	0.273	90

2.6	0.537			
2.8	0.579	0.500	0.289	110

Table C.3.3-2. C22 at T(Air) = 80°C and T(Hydrogen) = room

C.3.4 Teflon®:C = 1, Catalyst C31

Real ratio: C:Pt:Nafion®:Teflon® = 1:0.86:1.24:0.97.

Loading: 0.52 mg Pt/ cm².

T(Cell) = 60°C

Stoich(Air) = 3.5

Stoich(Hydrogen) = 2

I [A]	i [A/cm2]	U [V]	p [W/cm²]	dp [cmH2O]
0	0.000	0.905	0.000	
0.2	0.041	0.820	0.034	
0.4	0.083	0.778	0.064	9
0.6	0.124			
0.8	0.165	0.731	0.121	18
1	0.207			
1.2	0.248	0.691	0.171	30
1.4	0.289			
1.6	0.331	0.629	0.208	48
1.8	0.372			
2	0.413	0.548	0.226	60
2.2	0.455			
2.4	0.496	0.230	0.114	64

Table C.3.4-1. C31 at T(Air) = 80°C and T(Hydrogen) = room

I [A]	i [A/cm2]	U [V]	p [W/cm²]	dp [cmH2O]
0	0.000	0.900	0.000	
0.2	0.041	0.817	0.034	
0.4	0.083	0.777	0.064	8
0.6	0.124			
0.8	0.165	0.680	0.112	21
1	0.207			
1.2	0.248	0.641	0.159	25
1.4	0.289			
1.6	0.331			41

1.8	0.372			
2	0.413	0.460	0.190	50
2.2	0.455			
2.4	0.496	0.300	0.149	63

Table C.3.4-2. C31 at T(Air) = 80°C and T(Hydrogen) = 65°C

I [A]	i [A/cm2]	U [V]	p [W/cm²]	dp [cmH2O]
0	0.000	0.917	0.000	
0.2	0.041	0.822	0.034	
0.4	0.083	0.786	0.065	6
0.6	0.124			
0.8	0.165	0.757	0.125	11
1	0.207			
1.2	0.248			
1.4	0.289			
1.6	0.331	0.692	0.229	20
1.8	0.372			
2	0.413			
2.2	0.455			
2.4	0.496	0.617	0.306	28
2.6	0.537			
2.8	0.579			
3	0.620			
3.2	0.661	0.512	0.339	40
3.4	0.702			
3.6	0.744			
3.8	0.785			
4	0.826	0.404	0.334	40
4.2	0.868			
4.4	0.909			
4.6	0.950			
4.8	0.992	0.170	0.169	45

Table C.3.4-3. C31 at T(Air) = 80°C and T(Hydrogen) = 65°C

C.4 Nafion®:C = 1.5

C.4.1 Teflon®:C = 0.25, Catalyst C25

Real ratio: C:Pt:Nafion®:Teflon® = 1:0.86:1.48:0.27.

Loading: 0.78 mg Pt/ cm².

T(Cell) = 60°C

Stoich(Air) = 3.5

Stoich(Hydrogen) = 2

I [A]	i [A/cm2]	U [V]	p [W/cm²]	dp [cmH2O]
0	0.000	0.937	0.000	
0.2	0.041	0.847	0.035	
0.4	0.083	0.815	0.067	10.8
0.6	0.124			
0.8	0.165	0.783	0.129	20
1	0.207			
1.2	0.248	0.752	0.186	36
1.4	0.289			
1.6	0.331	0.712	0.235	60
1.8	0.372			
2	0.413	0.703	0.290	85
2.2	0.455			
2.4	0.496	0.677	0.336	100
2.6	0.537			
2.8	0.579	0.650	0.376	115
3	0.620			
3.2	0.661	0.630	0.417	128
3.4	0.702			
3.6	0.744	0.601	0.447	140
3.8	0.785			
4	0.826	0.550	0.455	120
4.2	0.868			
4.4	0.909	0.530	0.482	142
4.6	0.950			
4.8	0.992	0.485	0.481	136
5	1.033			
5.2	1.074	0.450	0.483	150
5.4	1.116			
5.6	1.157	0.400	0.463	163

Table C.4.1-1. C25 at T(Air) = 80°C and T(Hydrogen) = room

I [A]	i [A/cm2]	U [V]	p [W/cm²]	dp [cmH2O]
0	0.000	0.943	0.000	
0.2	0.041	0.847	0.035	
0.4	0.083	0.816	0.067	10
0.6	0.124			
0.8	0.165	0.780	0.129	20
1	0.207			
1.2	0.248	0.752	0.186	34

1.4	0.289			
1.6	0.331	0.705	0.233	55
1.8	0.372			
2	0.413	0.693	0.286	70
2.2	0.455			
2.4	0.496	0.680	0.337	105
2.6	0.537			
2.8	0.579	0.641	0.371	105
3	0.620			
3.2	0.661	0.614	0.406	120
3.4	0.702			
3.6	0.744	0.590	0.439	128
3.8	0.785			
4	0.826	0.550	0.455	130
4.2	0.868			
4.4	0.909	0.513	0.466	103
4.6	0.950			
4.8	0.992	0.462	0.458	127
5	1.033			
5.2	1.074	0.415	0.446	133

Table C.4.1-2. C25 at T(Air) = 80°C and T(Hydrogen) = 65°C

I [A]	**i [A/cm2]**	**U [V]**	**p [W/cm²]**	**dp [cmH2O]**
0	0.000	0.950	0.000	
0.2	0.041	0.852	0.035	
0.4	0.083	0.821	0.068	10
0.6	0.124			
0.8	0.165	0.793	0.131	15.5
1	0.207			
1.2	0.248	0.764	0.189	20
1.4	0.289			
1.6	0.331	0.728	0.241	23
1.8	0.372			
2	0.413	0.663	0.274	26
2.2	0.455			
2.4	0.496	0.594	0.295	32
2.6	0.537			
2.8	0.579	0.572	0.331	38
3	0.620			
3.2	0.661	0.462	0.305	41
3.4	0.702			
3.6	0.744	0.325	0.242	45

Table C.4.1-3. C25 at T(Air) = room and T(Hydrogen) = 65°C

C.4.2 Teflon®:C = 0.5, Catalyst C26

Real ratio: C:Pt:Nafion®:Teflon® = 1:0.86:1.53:0.51.

Loading: 0.49 mg Pt/ cm².

T(Cell) = 60°C

Stoich(Air) = 3.5

Stoich(Hydrogen) = 2

I [A]	i [A/cm2]	U [V]	p [W/cm²]	dp [cmH2O]
0	0.000	0.919	0.000	
0.2	0.041	0.835	0.035	
0.4	0.083	0.807	0.067	11
0.6	0.124			
0.8	0.165	0.777	0.128	25
1	0.207			
1.2	0.248	0.747	0.185	42
1.4	0.289			
1.6	0.331	0.711	0.235	67
1.8	0.372			
2	0.413	0.678	0.280	86
2.2	0.455			
2.4	0.496	0.663	0.329	100
2.6	0.537			
2.8	0.579	0.642	0.371	112
3	0.620			
3.2	0.661	0.627	0.415	122
3.4	0.702			
3.6	0.744	0.604	0.449	135
3.8	0.785			
4	0.826	0.577	0.477	143
4.2	0.868			
4.4	0.909	0.547	0.497	157
4.6	0.950			
4.8	0.992	0.530	0.526	160
5	1.033			
5.2	1.074	0.511	0.549	174
5.4	1.116			
5.6	1.157	0.475	0.550	185
5.8	1.198			
6	1.240	0.445	0.552	185
6.2	1.281			

6.4	1.322	0.425	0.562	205
6.6	1.364			
6.8	1.405	0.380	0.534	210

Table C.4.2-1. C26 at T(Air) = 80°C and T(Hydrogen) = room

I [A]	i [A/cm2]	U [V]	p [W/cm²]	dp [cmH2O]
0	0.000	0.919	0.000	
0.2	0.041	0.835	0.035	
0.4	0.083	0.806	0.067	9
0.6	0.124			
0.8	0.165			
1	0.207			
1.2	0.248	0.755	0.187	31
1.4	0.289			
1.6	0.331			
1.8	0.372			
2	0.413	0.697	0.288	75
2.2	0.455			
2.4	0.496			
2.6	0.537			
2.8	0.579	0.654	0.378	117
3	0.620			
3.2	0.661			
3.4	0.702			
3.6	0.744	0.608	0.452	137
3.8	0.785			
4	0.826			
4.2	0.868			
4.4	0.909	0.555	0.505	154
4.6	0.950			
4.8	0.992			
5	1.033			
5.2	1.074	0.507	0.545	185
5.4	1.116			
5.6	1.157			
5.8	1.198			
6	1.240	0.438	0.543	193

Table C.4.2-2. C26 at T(Air) = 80°C and T(Hydrogen) = 65°C

I [A]	i [A/cm2]	U [V]	p [W/cm²]	dp [cmH2O]
0	0.000	0.930	0.000	
0.2	0.041	0.835	0.035	
0.4	0.083	0.803	0.066	8
0.6	0.124			

0.8	0.165			
1	0.207			
1.2	0.248	0.758	0.188	24
1.4	0.289			
1.6	0.331			
1.8	0.372			
2	0.413	0.708	0.293	34
2.2	0.455			
2.4	0.496			
2.6	0.537			
2.8	0.579	0.613	0.355	43
3	0.620			
3.2	0.661			
3.4	0.702			
3.6	0.744	0.474	0.353	58
3.8	0.785			
4	0.826			
4.2	0.868			
4.4	0.909	0.395	0.359	77

Table C.4.2-3. C26 at T(Air) = room and T(Hydrogen) = 65°C

C.4.3 Teflon®:C = 0.75, Catalyst C32

Real ratio: C:Pt:Nafion®:Teflon® = 1:0.86:1.52:0.74.

Loading: 0.5 mg Pt/ cm².

T(Cell) = 60°C

Stoich(Air) = 3.5

Stoich(Hydrogen) = 2

I [A]	i [A/cm2]	U [V]	p [W/cm²]	dp [cmH2O]
0	0.000	0.906	0.000	
0.2	0.041	0.786	0.032	
0.4	0.083	0.714	0.059	16
0.6	0.124			
0.8	0.165	0.585	0.097	41
1	0.207			
1.2	0.248	0.485	0.120	61
1.4	0.289			
1.6	0.331	0.435	0.144	62

1.8	0.372			
2	0.413	0.220	0.091	80

Table C.4.3-1. C32 at T(Air) = 80°C and T(Hydrogen) = room

I [A]	i [A/cm2]	U [V]	p [W/cm²]	dp [cmH2O]
0	0.000	0.905	0.000	
0.2	0.041	0.795	0.033	
0.4	0.083	0.725	0.060	9
0.6	0.124			
0.8	0.165	0.627	0.104	41
1	0.207			
1.2	0.248	0.510	0.126	58
1.4	0.289			
1.6	0.331	0.300	0.099	66

Table C.4.3-2. C32 at T(Air) = 80°C and T(Hydrogen) = 65°C

I [A]	i [A/cm2]	U [V]	p [W/cm²]	dp [cmH2O]
0	0.000	0.922	0.000	
0.2	0.041	0.815	0.034	
0.4	0.083	0.757	0.063	7
0.6	0.124			
0.8	0.165	0.709	0.117	12
1	0.207			
1.2	0.248	0.636	0.158	16
1.4	0.289			
1.6	0.331	0.528	0.175	22
1.8	0.372			
2	0.413	0.340	0.140	24

Table C.4.3-3. C32 at T(Air) = room and T(Hydrogen) = 65°C

C.4.4 Teflon®:C = 1, Catalyst C33

Real ratio: C:Pt:Nafion®:Teflon® = 1:0.86:1.51:1.00.

Loading: 0.62 mg Pt/ cm².

T(Cell) = 60°C

T(Air) = 80°C

T(Hydrogen) = room

Stoich(Air) = 3.5

Stoich(Hydrogen) = 2

I [A]	i [A/cm2]	U [V]	p [W/cm²]	dp [cmH2O]
0	0.000	0.895	0.000	
0.2	0.041	0.829	0.034	
0.4	0.083	0.791	0.065	17
0.6	0.124			
0.8	0.165	0.746	0.123	30
1	0.207			
1.2	0.248	0.682	0.169	54
1.4	0.289			
1.6	0.331	0.670	0.221	88
1.8	0.372			
2	0.413	0.635	0.262	108
2.2	0.455			
2.4	0.496	0.583	0.289	113
2.6	0.537			
2.8	0.579	0.549	0.318	128
3	0.620			
3.2	0.661	0.484	0.320	138
3.4	0.702			
3.6	0.744	0.364	0.271	140
3.8	0.785			
4	0.826	0.260	0.215	144

Table C.4.4-1. C33 at T(Air) = 80°C and T(Hydrogen) = room

C.5 Nafion®:Teflon®:C = 0.875:0.875:1

C.5.1 Catalyst C49

Real ratio: C:Pt:Nafion®:Teflon® = 1:0.96:0.88:0.88.

Loading: 0.55 mg Pt/ cm².

T(Cell) = 60°C

T(Air) = 80°C

T(Hydrogen) = room

Stoich(Hydrogen) = 2

I [A]	i [A/cm2]	U [V]	p [W/cm²]	dp [cmH2O]
0	0.000	0.936	0.000	
0.2	0.041	0.855	0.035	
0.4	0.083	0.825	0.068	10
0.6	0.124			
0.8	0.165	0.800	0.132	25
1	0.207			
1.2	0.248			
1.4	0.289			
1.6	0.331	0.745	0.246	55
1.8	0.372			
2	0.413			
2.2	0.455			
2.4	0.496	0.697	0.346	85
2.6	0.537			
2.8	0.579			
3	0.620			
3.2	0.661	0.658	0.435	108
3.4	0.702			
3.6	0.744			
3.8	0.785		0.000	
4	0.826	0.615	0.508	131
4.2	0.868			
4.4	0.909			
4.6	0.950			
4.8	0.992	0.572	0.567	174
5	1.033			
5.2	1.074			
5.4	1.116			
5.6	1.157	0.515	0.596	160
5.8	1.198			
6	1.240			
6.2	1.281			
6.4	1.322	0.456	0.603	170
6.6	1.364			
6.8	1.405			
7	1.446			
7.2	1.488	0.380	0.565	196
7.4	1.529			
7.6	1.570			
7.8	1.612			
8	1.653	0.305	0.504	210

Table C.5.1-1. C49 at T(Air) = 80°C, Stoich(Air)=3.5 and T(Hydrogen) = room

I [A]	i [A/cm2]	U [V]	p [W/cm²]	dp [cmH2O]
0	0.000	0.934	0.000	
0.2	0.041		0.000	
0.4	0.083		0.000	13
0.6	0.124		0.000	
0.8	0.165	0.770	0.127	
1	0.207		0.000	
1.2	0.248		0.000	
1.4	0.289		0.000	
1.6	0.331	0.707	0.234	51
1.8	0.372		0.000	
2	0.413		0.000	
2.2	0.455		0.000	
2.4	0.496	0.636	0.315	93
2.6	0.537		0.000	
2.8	0.579		0.000	
3	0.620		0.000	
3.2	0.661	0.575	0.380	120
3.4	0.702		0.000	
3.6	0.744		0.000	
3.8	0.785		0.000	
4	0.826	0.490	0.405	133
4.2	0.868		0.000	
4.4	0.909		0.000	
4.6	0.950		0.000	
4.8	0.992	0.380	0.377	148
5	1.033		0.000	
5.2	1.074		0.000	
5.4	1.116		0.000	
5.6	1.157	0.310	0.359	155

Table C.5.1-2. C49 at T(Air) = 80°C, Stoich(Air)=2 and T(Hydrogen) = room

C.5.2 Catalyst C47, 1-step

Real ratio: C:Pt:Nafion®:Teflon® = 1:0.96:0.87:0.86.

Loading: 0.63 mg Pt/ cm².

T(Cell) = 60°C

T(Air) = 80°C

T(Hydrogen) = room

Stoich(Hydrogen) = 2

I [A]	i [A/cm2]	U [V]	p [W/cm²]	dp [cmH2O]
0	0.000	0.917	0.000	
0.2	0.041	0.855	0.035	
0.4	0.083	0.820	0.068	10
0.6	0.124			
0.8	0.165	0.788	0.130	20
1	0.207			
1.2	0.248			
1.4	0.289			
1.6	0.331	0.735	0.243	60
1.8	0.372			
2	0.413			
2.2	0.455			
2.4	0.496	0.690	0.342	90
2.6	0.537			
2.8	0.579			
3	0.620			
3.2	0.661	0.650	0.430	112
3.4	0.702			
3.6	0.744			
3.8	0.785			
4	0.826	0.615	0.508	137
4.2	0.868			
4.4	0.909			
4.6	0.950			
4.8	0.992	0.550	0.545	165
5	1.033			
5.2	1.074			
5.4	1.116			
5.6	1.157	0.507	0.587	180
5.8	1.198			
6	1.240			
6.2	1.281			
6.4	1.322	0.470	0.621	203
6.6	1.364			
6.8	1.405			
7	1.446			
7.2	1.488	0.410	0.610	210
7.4	1.529			
7.6	1.570			
7.8	1.612			
8	1.653	0.360	0.595	220

Table C.5.2-1. C47 at T(Air) = 80°C, Stoich(Air)=2 and T(Hydrogen) = room

I [A]	i [A/cm2]	U [V]	p [W/cm²]	dp [cmH2O]
0	0.000	0.917	0.000	
0.2	0.041	0.850	0.035	
0.4	0.083	0.816	0.067	5
0.6	0.124			
0.8	0.165	0.795	0.131	10
1	0.207			
1.2	0.248			
1.4	0.289			
1.6	0.331	0.743	0.246	42
1.8	0.372			
2	0.413			
2.2	0.455			
2.4	0.496	0.705	0.350	90
2.6	0.537			
2.8	0.579			
3	0.620			
3.2	0.661	0.660	0.436	100
3.4	0.702			
3.6	0.744			
3.8	0.785			
4	0.826	0.618	0.511	122
4.2	0.868			
4.4	0.909			
4.6	0.950			
4.8	0.992	0.570	0.565	135
5	1.033			
5.2	1.074			
5.4	1.116			
5.6	1.157	0.508	0.588	136
5.8	1.198			
6	1.240			
6.2	1.281			
6.4	1.322	0.455	0.602	160
6.6	1.364			
6.8	1.405			
7	1.446			
7.2	1.488	0.385	0.573	180
7.4	1.529			
7.6	1.570			
7.8	1.612			
8	1.653	0.315	0.521	195

Table C.5.2-2. C47 at T(Air) = 80°C, Stoich(Air)=2.5 and T(Hydrogen) = room

I [A]	i [A/cm2]	U [V]	p [W/cm²]	dp [cmH2O]
0	0.000	0.925	0.000	
0.2	0.041	0.872	0.036	
0.4	0.083	0.833	0.069	7
0.6	0.124			
0.8	0.165	0.775	0.128	22
1	0.207			
1.2	0.248			
1.4	0.289			
1.6	0.331	0.670	0.221	45
1.8	0.372			
2	0.413			
2.2	0.455			
2.4	0.496	0.550	0.273	66
2.6	0.537			
2.8	0.579			
3	0.620			
3.2	0.661	0.430	0.284	90

Table C.5.2-3. C47 at T(Air) = 80°C, Stoich(Air)=2.5 and T(Hydrogen) = room

C.6 Nafion®:Teflon®:C = 1.375:0.375:1

C.6.1 Catalyst C45

Real ratio: C:Pt:Nafion®:Teflon® = 1:0.96:1.44:0.39.

Loading: 0.45 mg Pt/ cm².

T(Cell) = 60°C

T(Air) = 80°C

T(Hydrogen) = room

Stoich(Air) = 3.5

Stoich(Hydrogen) = 2

I [A]	i [A/cm2]	U [V]	p [W/cm²]	dp [cmH2O]
0	0.000	0.936	0.000	
0.2	0.041	0.842	0.035	
0.4	0.083	0.810	0.067	15
0.6	0.124			

0.8	0.165	0.778	0.129	27
1	0.207			
1.2	0.248			
1.4	0.289			
1.6	0.331	0.741	0.245	55
1.8	0.372			
2	0.413			
2.2	0.455			
2.4	0.496	0.692	0.343	100
2.6	0.537			
2.8	0.579			
3	0.620			
3.2	0.661	0.647	0.428	115
3.4	0.702			
3.6	0.744			
3.8	0.785			
4	0.826	0.605	0.500	128
4.2	0.868			
4.4	0.909			
4.6	0.950			
4.8	0.992	0.520	0.516	160
5	1.033			
5.2	1.074			
5.4	1.116			
5.6	1.157	0.454	0.525	175
5.8	1.198			
6	1.240			
6.2	1.281			
6.4	1.322	0.380	0.502	190
6.6	1.364			
6.8	1.405			
7	1.446			
7.2	1.488	0.280	0.417	200

Table C.6.1-1. C45 at T(Air) = 80°C and T(Hydrogen) = room